UNIVERSITA' DEGLI STUDI DI MILANO

Facoltà di Scienze MM. FF. NN.

Dipartimento di Chimica Fisica ed Elettrochimica

Scuola di Dottorato in Scienze e Tecnologie Chimiche

Dottorato di Ricerca in Chimica Industriale, XXIV ciclo

HIGH TEMPERATURE OXIDATION PHENOMENA' S STUDY OF HIGH ALLOYED MATERIALS FOR POWER GENERATION PLANTS

ING-IND/23 ING-IND/21 CHIM/02

Tutor: Prof. Enrico SIVIERI

Co-tutor: Dott. Stefano TRASATTI

Coordinator: Prof. Dominique ROBERTO

Mirko RIZZI
I.D. R08297

A.Y. 2010/2011

INDEX

ABSTRACT

The aim of the doctorate project is the study of the corrosion and oxidation behavior of some commercial and more recent SS and Ni based alloys for high temperature applications in order to verify their possible use either at operative conditions higher than conventional (temperature up to 900°C) or in different environment (oxygen, air, carburizing atmospheres).

During the first year, the following aspects were investigated:

- Microstructural characterization of solution annealed AISI 310N, 347HFG and 304 HCu (the latter supplied also in the shoot peened condition) was carried out. An homogeneous austenitic fine grain structure accompanied with Nb segregation was observed for 347HFG and 304HCu. In the case of 310N the grains were coarser and the presence of Si segregation were randomly detected beside Nb.
- Microhardness profiles (HV_{50}) were conducted to evaluate the penetration effects of shoot peening treatment at depths as high as 150-200 μm.
- Discontinuous oxidation testing were performed at temperatures in the range of 700-900°C under 15 Nm^3/h flowing moist air atmosphere for 7 days. The preliminary results seem to confirm an oxidation susceptibility in the following order: 310N<347HFG<304HCu.

During the second year, the following activities have been carried out:

- Oxidation kinetic study (thermogravimetric tests) of as received AISI 310N, 347HFG, 304HCu and Alloy 617 in oxygen atmosphere at 900°C; 310N, 347HFG and Alloy 617 show a protective oxidation kinetic, while 304HCu suffers from spalling.
- Investigation of grown oxide layer nature of all SS by microscopic techniques revealed an average oxide thickness in the range of 5 – 15 μm for 347HFG; about 5 μm until spallation for 304HCu and less than 5 μm for 310N. In the case of 347HFG a three layer oxide was clearly detected consisting of a first layer of Cr oxides followed by a mixed Fe and Cr oxide and finally an external layer of FeO_x. For 310N only a Cr oxide layer was detectable; for 304HCu the layer being essentially Fe-Cr oxides. Result confirmed also by GDOES.
- Study of the electrochemical behaviour of as received and oxidized SS specimens by means of polarization curves. All “as received” specimens exhibit a similar passive behaviour in terms of both potentials and current densities, apart the point corresponding at the critical passive current (i_{cr}). For oxidized specimens a statistical approach should be followed.

During the third year, in addition to the accomplishment of the previous topics, new electrochemical approaches were tested during a period spent by the candidate following Dr. Digby Macdonald's research labs at The Pennsylvania State University. Activities were focused on the passivity study

of 347HFG stainless steel. Starting from the results of the potentiodynamic studies, an electrochemical impedance spectroscopy procedure was setted up; results were optimized by applying the “point defect model” developed by the same Dr. Macdonald revealing kinetic parameters of the passive layer and is semiconductive nature that is essentially n-type for all anodic potential values except near the breakdown in which assume a p-type character.

INTRODUCTION

Under most conditions of use, metals are thermodynamically unstable with respect to the surrounding environment. Depending on their composition and conditions, they can react to form oxides, sulphides, carbides, nitrides etc. At low temperatures, an oxidant environment may not be dangerous for many metals because oxidation rates are low but these rates increase rapidly with temperature increasing.

Looking to the following reaction, it seems that oxidation of metals passes trough a simple reaction; however reaction path and oxidation behaviour depend on a variety of factors and could involve several mechanisms.

$$aM + \frac{b}{2}O_2 \rightarrow M_aO_b$$

If the starting point is a clean metallic surface, the initial step in a metal-oxygen reaction involves adsorption of gas on metal surface, oxygen diffusion in the first atomic layers, then oxide is formed on the surface either as film or separated zones. First attack sites are not random but function of surface orientation, crystal defects at the surface, surface preparation and impurities in both metal and environment.

When a continuous oxide film covers the surface, the reaction can proceed only by solid state diffusion of reactants through the film; driving force of that process could be the electric field across the film in the case of thin films or the chemical potential gradient if the film is thick or is a scale [2]. Metals can also form porous oxides.

In addition, at high temperatures, oxides can be also liquid or volatile.

Considering the previous reaction, the standard free Gibbs energy of formation of the M_aO_b oxide is a function of temperature and oxygen pressure according to the following equation:

$$\Delta G_f^0 = -\frac{b}{2}RT \ln p_{O_2}$$

$\Delta G°_f$ values of oxide formation as a function of temperature are summarized in the well-known Ellingham-Richardson diagrams (*figure 1*) where along the ordinates are plotted values for oxides $\Delta G°$ and temperature is plotted along the abscissa. Values of $\Delta G°$ are referred to the formation of oxide per O_2 mole and its temperature function can be approximated as $\Delta G° = A+CT$ [2].

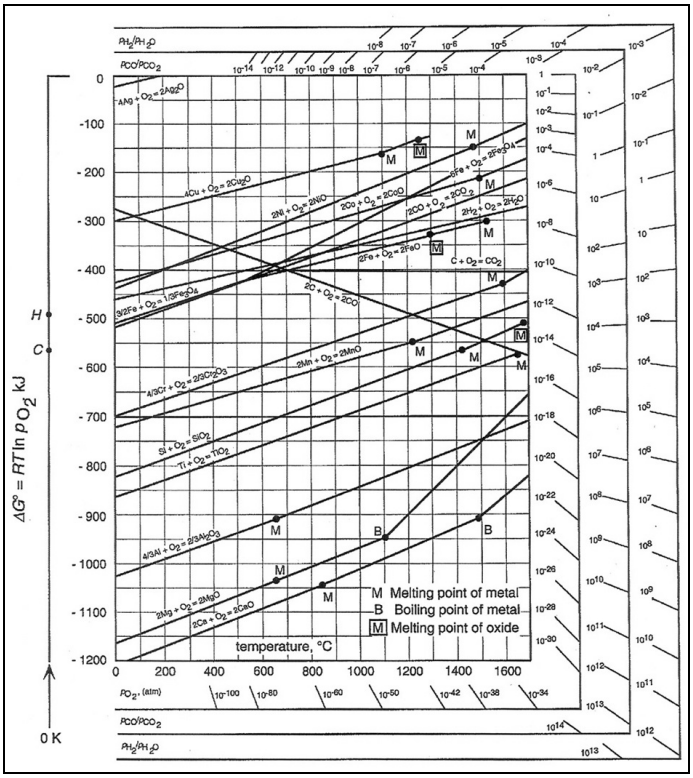

Figure 1: Ellingham-Richardson diagram for some oxide of importance in high temperature oxidation of metal alloys [2]

So, the most stable oxide, have the largest negative $\Delta G°_f$ value. Lines of constant partial pressure of oxygen can be drawn by use the following equation of the oxygen partial molar free energy:

$$\Delta \overline{G}_{O_2} = RT \ln pO_2$$

Ellingham-Richardson diagrams reports also the ratios p_{CO2}/p_{CO} and p_{H2}/p_{H2O} to be considered to evaluate the oxygen partial pressure using CO_2 + CO and H_2O + H_2 gas mixtures. Oxygen partial pressure could be obtained from the following equilibriums:

$$CO_2 = CO + \tfrac{1}{2} O_2$$
$$H_2O = H_2 + \tfrac{1}{2} O_2$$

so

$$p_{O_2} = \left(K_1 \frac{p_{CO_2}}{p_{CO}} \right)^2$$
$$p_{O_2} = \left(K_2 \frac{p_{H_2O}}{p_{H_2}} \right)^2$$

where K_1 and K_2 are the equilibrium constants.

On the diagram, to obtain the line corresponding to $\Delta\overline{G}_{O_2}$ and $\Delta G°$ of the CO_2-CO and H_2O-H_2 equilibriums, is sufficient to draw a line starting respectively from the point O, C and H to the corresponding partial pressure ratio.

In the same way, a number of Ellingham-Richardson diagrams were obtained for different oxidants, the most useful are sulphides and carbides.

To predict the thermodynamically stable oxidation products as a function of temperature and oxygen concentration, phase diagrams have to be considered.

The iron-oxygen phase diagram is shown in *figure 2* where the system contains three oxide phases: wustite, $Fe_{1-y}O$, magnetite, Fe_3O_4 and haematite, Fe_2O_3.

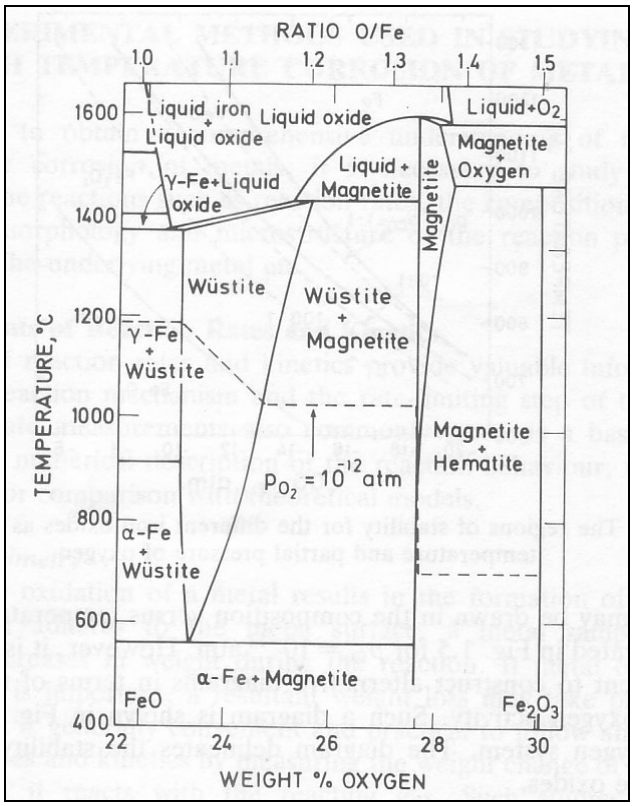

Figure 2: Iron-Oxygen phase diagram [2]

Wustite, nominally written as FeO, is a metal-deficient oxide and is unstable below 570°C where it disproportionates to Fe and magnetite.

Oxidation of iron in air above 570°C give a three layered scale: wustite next to the metal, magnetite intermediate and haematite next to the gas phase. Wustite is the thicker layer as diffusional transport is much faster than in the other phases.

When reaction mechanisms are considered, it is useful to have information about oxygen activity through the scale and to know oxygen activity trough the phase boundaries. So, lines of constant

oxygen activity has to be drawn in the phase diagram (as reported in *figure 1* for $p_{O2}=10^{-20}$ atm). However is more convenient to draw alternative diagrams in terms of temperature vs O_2 activity as reported in *figure 3* for the iron-oxygen system showing stability regions for the three oxides.

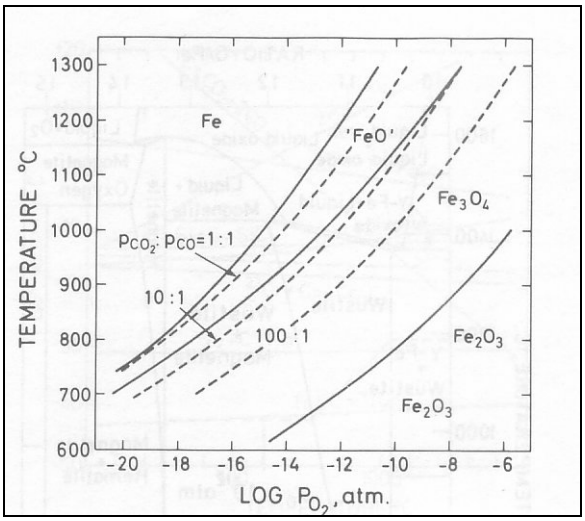

Figure 3: Stability regions forthe different iron oxides as a function of temperature and oxygen partial pressure [2]

Knowledge of thermodynamics of oxidations is not sufficient to interpret metal-oxygen reactions because, first of all, there's no indication on the reaction rates that are dependent to the reaction mechanism. Furthermore, thermodynamics suggest the probable composition of the reaction products but relative amounts are function of formation rates.

Studies of reaction rates provide valuable information about reaction mechanisms and rate determining step of the total reaction.

When metal oxidation results in formation of a solid oxide which adheres to the metal surface, a metal sample increase in weight during the reaction; if metal or oxide evaporation is important, a resultant weight loss may take place. In such cases, is generally convenient and practical to follow and study the oxidation rates and kinetics by measuring the weight change of a metal specimen as it reacts with a gas at a known temperature. Such studies should be done preferably in continuous way. For this purposes, different types of balances may be employed; generally a sensitivity of 10^{-5} -10^{-6} g/cm^2 is adequate.

In practice sensitivity and reproducibility are limited by factors as convective movements, vibrations etc.

Balance system are also often connected with devices for continuous automatic recording of weight changes.

Alternative methods are the following of oxygen consumption by volumetric methods, ellipsometry and electrical conductivity to follow oxide increase during oxidation, metallographic measurements of scale thickness etc.

To identify and characterize reaction products, several techniques can be used such as X-ray and electron diffraction to determine nature and crystal structures, metallographic techniques supported by optical and scanning electron microscopy for morphology with the aim of probe microanalysis to identify elemental distributions. Mass spectroscopy is also used to identify nature of volatile oxides.

As discussed above, knowledge of reaction rates and kinetics is an important basis for investigate reaction mechanisms. Reaction rates and corresponding rate equations for the oxidation of a metal depend on a number of factors such as temperature, oxygen partial pressure, elapsed time of reaction, surface preparation and metal pretreatment.

There are several rate equations that can be encountered each one related with a reaction mechanism but the first stages are common for all mechanisms.

Initial oxidation stage can be subdivided in three parts:

- Adsorption of oxygen on the metal surface
- Formation of individual oxide nuclei which grow laterally to form a continuous oxide film
- Further growth of the oxide film normal to the surface

To reveal these fast first stages, oxidation can be conducted in very reduced oxygen partial pressure and detected by surface techniques like XPS.

To explain metal oxidation after that initial stage, several theories were proposed, the most important one was proposed by Wagner based on lattice diffusion of the reacting atoms or ions or transport of electrons through the scale determining in the overall oxidation reaction.

Lattice diffusion is supposed to take place because of the presence of point defects (vacancies, interstitials, electrons and holes) which are assumed to migrate independently on each other.

Diffusion through the scale is taken as rate determining step. Reactions at the phase boundaries are considered to be rapid; the driving energy of the whole process is the free energy associated with the formation of the metal oxide. Correspondingly a gradient of oxygen through the scale exist from the partial pressure at the outer oxide surface to the partial pressure of oxygen at the metal-oxide interface.

For such reaction mechanism, oxide growth profile is parabolic with time and the integrated form of the rate equation is

$$x^2 = kt + A$$

where x can be the thickness of oxide film, the weight change normalized to the surface area, the amount of consumed oxygen normalized to the surface area etc; k is the rate constant, t the elapsed time and A the integration constant.

In addition to parabolic mechanism, other are common such as logarithmics and linear. They represent only ideal cases, deviations and intermediate rate equations are often obtained.

Logarithmic rate is quite common for a large variety of metals at medium low temperature (generally below 400°C); oxidation is initially rapid and then drops off to low or negligible rates. This can be described by a logarithmic rate equation that could be direct logarithmic or inverse logarithmic:

$$direct: \quad x = k\log(t + t_0) + A$$

$$inverse: \quad \frac{1}{x} = B - k\log t$$

where A and B are integration constants.

A number of theories based on various rate determining mechanisms have been proposed, the different logarithmic rate equations are also difficult to distinguish and also parameters in them contained are difficult to be evaluated using independent measurements and this make difficult to prove validity and correctness of proposed mechanisms. It is taken by known […] that this mechanisms involve too thin films in the case of inverse and cavities into the scale for direct logarithmic.

Linear oxidation kinetic may easily described by the following integrated equation:

$$x = kt + A$$

Here oxidation rate is constant with time and is independent to the amount of oxidant and metal previously consumed by the reaction. The rate determining step may involve the adsorption of gases at the surface or diffusion trough a constant thickness layer. On the practical point of view is common for non protective scales.

In *figure 4*, a schematic representation of these mechanisms is reported considering the x value of previous equations as the net weight gain.

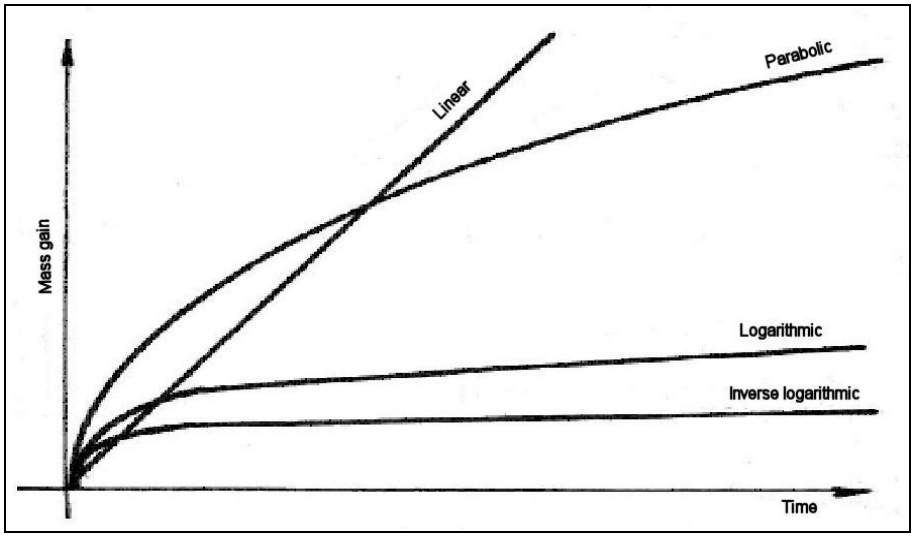

Figure 4: Most common theoretical kinetic trends occuring during hot oxidation [3]

Last two main points to be considered, concerning metal oxidation are temperature and oxygen pressure dependence.

At constant oxygen partial pressure, temperature interferes on the oxidation rate constant obeying to an Arrhenius-like equation:

$$k = k_0 \exp\left(-Q/RT\right)$$

where Q is the activation energy, R the gas constant and T the absolute temperature.

The affection of oxygen pressure on rate constants is related to which one is the rate determining factor of the oxidation process. If it is related to oxygen adsorption, system exhibits a large dependence to oxygen partial pressure; except for very low oxygen pressure, is reported [2] that oxidation rates are proportional to the square root of p_{O2} that suggest oxygen absorption is dissociative ($O_2 = 2\ O_{ads}$).

When oxidation is controlled by solid state diffusion processes, the rate of supply or adsorbed oxygen is not limitative so interface reaction may be compared with the diffusion rates.

Modification of oxidation properties in terms of resistance and grown oxides are expected as function of alloy composition.

Considering a ferritic steel, oxidation behaviour are independent from Cr content for concentrations between 2 and 9% if temperature is below 600°C but becomes marked at 650°C [4], significant improvement on the oxidation resistance is obtained with a 12% of Cr.

Chromium is so important because is one of the key element for a protective layer, is quite common for Cr containing steel to have a bi-layered thermal oxide constituted by an inner layer of Cr and an outer of Fe oxides.

Silicon is reported to have beneficial effect against oxidation because tends to segregate promoting Cr rich scale growth [5] but this content has to be balanced because Si concentrations higher than 0,4% starts to be a problem for mechanical creep strength.

Effect similar to Silicon is given by sulphur in low content, up to 0,01%, which react with chromium forming chromium sulphides that acts similarly to silicon segregates [4].

Manganese, molybdenum and boron were also found to significantly improve the protectiveness of oxide scales.

Grain size is also important, a fine grain is searched because the finer is the grain size, the higher is diffusion of species. This is in contrast with mechanical properties so a balance between oxidation and mechanical resistance has to be considered [4].

Mechanical treatments to reduce local grain size are well used, the most important one is the shoot peening that is a sort of blasting that lower surface grain size improving chromium diffusivity in a such amount that may be possible to have a change of the oxidation rate law (e.g. from parabolic to logarithmic).

Many authors report that common high temperature austenitic stainless steels have a better oxidation resistance if compared with ferritic stainless steel giving a thinner oxide layer if exposed at the same conditions; higher Cr content and finer grain size are also important.

Ni-based alloys give much better performance than austenitic steels but, being a different matrix, correlation between Cr content and mass gain is not so simple like steels.

For an austenitic steel exposed to an oxidant environment, oxide scale grows generally according to a parabolic law and if the chromium content is up to 25%, the layer adherent to the metal surface is constituted by protective Cr_2O_3 followed by other Fe containing layers while for higher Cr content is essentially Cr_2O_3 [6]. Also for Ni based alloys, an higher chromium content is beneficial [7].

About alloying elements; Cr, Mn, Mo and W have a beneficial effect to improve oxidation resistance of austenitic stainless steels and Ni-based alloys while Co is deleterious.

There are essentially two types of oxides that can develop on high alloyed steels, one is basically Cr_2O_3 with excellent protective properties, Fe_3O_4 that is porous and not so protective. There's also a third oxide, that constitute an intermediate layer between internal Cr_2O_3 and external Fe_3O_4; it is a mixed oxide (spinel) of the two with the general formula of $(Fe,Cr)_3O_4$ [8].

In summary, scale compositions changes from Fe_3O_4/Fe_2O_3 in simple low alloyed steels to $(Fe,Cr)_3O_4/ Fe_3O_4$ in low chromium steels to $Cr_2O_3/(Fe,Cr)_3O_4/Fe_3O_4$ for high alloyed austenitic stainless steels.

That kind of oxides may be subjected to exfoliation (or spalling) phenomenon that is associated with stresses into the scale. It is expected that oxide growing produces itself stresses into the scale; in addition there's also the effect of difference in thermal expansion between bulk metal and oxide layer. Influence of alloy composition on exfoliation properties is appreciable and is strictly related to creep (plastic deformation) resistance; as general rule, the higher is the creep resistance, the lower is susceptibility to exfoliation [9].

So, selection of materials for high temperature application is governed by a number of factors such as oxidation resistance, creep strength, weldability, fabricability etc.

For boilers application has to be taken in account a distinguish between fireside and steamside of pipes because ambients are completely different; at fireside there's a dry and oxidant atmosphere due to the combustion chamber and at steamside there's liquid water as input and pressurized steam as output.

To set upper limits for use of materials, boiler designers use to take look to mechanical properties (creep strength first of all) and fireside corrosion.

Steamside corrosion is of primarily interest only from a longevity point of view [viess].

Weld problems are overtaken by adopting seamless tubes.

In the present work, three well used austenitic stainless steels and a novel nickel alloy have been studied focusing on hot oxidation properties in terms of oxidation kinetic and oxide composition and morphology. Furthermore, an electrochemical approach to study and model passivity films and oxide scale has been proposed.

EXPERIMENTAL

The project was carried out by focusing on three main topics:

- Characterization of furnished materials with the aid of optical microscopy (OM), scanning electron microscope (SEM) coupled with EDS microprobe and microhardness measurements on peened tubes.

- Continuous thermogravimetric tests in atmosphere of oxygen and characterization of thermal oxides by SEM-EDS and GDOES (where possible).

- Electrochemical characterization of as received and oxidized specimens by means of electrochemical polarization techniques. Electrochemical impedance spectroscopy (EIS) followed by modeling as further investigation starting from polarizations data.

All materials have been supplied by Salzgitter Mannesmann DMV Stainless in the form of solution annealed seamless tubes, whose nominal composition is reported in *table 1*.
304 HCu was also supplied as shoot peened by Salzgitter and by Sumitomo (with the denomination of Super 304 H).
Shoot peening consists in sandblasting the internal surface of a pipe with 2-3 mm long wire pieces, with the aim of emphasizing the Cr availability for the oxide layer restoration as a consequence of a finer grain distribution (Cr diffusion is faster at the grain boundaries).

	Cmax	Cr	Ni	Fe	Mn	N	Si	Others
347 HFG	0,1	18,5	11,0	Bal.	2,0max	-	0,75max	Ti+Nb>8C<1,0
310 N	0,1	25,0	20,0	Bal.	2,0max	0,20	0,75max	Nb 0,40
304 HCu, S304H	0,13	18,5	9,5	Bal.	1,0max	0,10	0,30max	Cu 3,0; Nb 0,50
Alloy 617	0,08	22,0	55,0	3,0max	0,5max	-	0,5max	Mo 9,0, Co 12; Al; Ti

Table 1: Composition of investigated alloys

Characterization of furnished materials by OM, SEM-EDS and microhardness

Transversal and longitudinal microstructure was examined by OM and SEM, on opportune cross-sections for each tube sample.

Cross sectioned specimens were embedded into glass fiber resin, polished up to 1200 grit then with 1 μm diamond paste.

Metallographic attack of stainless steels was carried out electrochemically in 60% HNO_3 at +0,8V while, for the alloy 617, a chemical attack with a mixture of 15 volume parts HCl 37%, 10 volume parts of glacial CH_3COOH and 10 volume parts of HNO_3 65% was preferred. In some cases, oxalic acid was also used.

Average grain size was determined from optical micrographies at 100 and 400 X using ASTM standard count method (*appendix 1*).

SEM examination (secondary and backscattered electrons) was used to confirm the nature of secondary phases. EDS analysis was employed to obtain informations about the mean chemical composition.

The optical microscope was a Reichert and the SEM was a LEO 1430 coupled with an INCA EDS microprobe.

The penetration effect of shoot peening treatment was evaluated by microhardness measurements. The measurements were carried out on mirror-like samples by using a Vickers microdurometer (Leitz Durimet) with an applied weight of 50g.

Thermogravimetric tests

Thermogravimetric tests were performed to evaluate alloy oxidation susceptibility by recording loss/gain weight vs time. Experiments were conducted in a continuous mode by using an experimental thermobalance instrumentation as reported in *figure 5*.

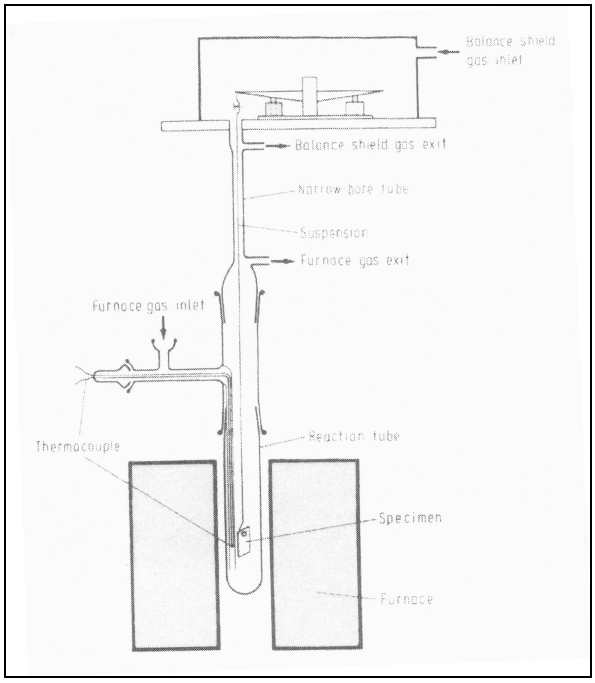

Figure 5: Schematic representation of a thermobalance

15 x 15 mm specimens were taken from a tube piece and tested under oxygen flow at 900°C 7 days. Alloy 617 was tested for 10 days.

In order to optimize gas consumption, different flow rates were used while testing 347HFG SS.

Nature and composition of oxides were investigated by SEM-EDS examination on cross sections of oxidized SS specimens. For that purpose, oxidations were carried out in discontinuous way using a tubular oven at 900°C (700°C for 304HCu) with an oxygen flow rate of 5 NL/h and duration time of 7 days. After each experiment, specimens were embedded in glass fiber resin and polished up to 0,3 μm alumina suspension.

GDOES was tried on a variety of SS samples oxidized for different times; only in some lucky cases, appreciable output data were obtained because of problems due to geometry of GDOES probe in our use.

Electrochemical tests

Potentiodynamic polarization curves of each SS were collected for both as received and oxidized specimens.

Samples had the same dimensions and were oxidized following the same procedures as described at different treatment times (1 to 7 days).

The adopted cell was a modified three electrode o-ring cell suitable for curved surfaces responding to the scheme reported in *figure 6* where the working electrode was located on the cell bottom with a working area of 1 cm^2; reference electrode, saturated calomel electrode (SCE), was inserted in a Luggin tube and a Pt spiral was used as a counter electrode.

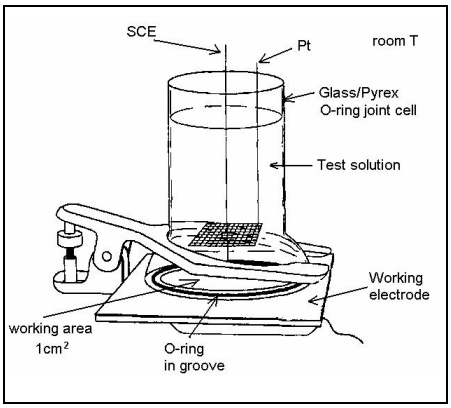

Figure 6: Schematic representation of the adopted electrochemical cell

Polarization curves were recorded after an equilibration time of 30 min, starting from the open circuit potential down to the transpassive region using an EG&G PAR mod. 273A potentiostat/galvanostat.

In order to chose the appropriate electrolyte, preliminary experiments were carried out. Finally, a 3M H_2SO_4 + 0,7M NaCl solution with N_2 bubbling was chosen.

Electrochemical Impedance spectra were recorded using the same cell and electrolyte.

The equilibration period was variable, according to the reaching of steady state conditions. Amplitude of the perturbing potential was 20 mV and spectra were collected starting from 10KHz to 0,01Hz. The instrument used was an EG&G PAR mod. 273 potentiostat/galvanostat coupled with a frequency response analyzer Solartron mod.1250.

Output data were optimized, after definition of an equivalent circuit, on the basis of “Point Defect Model” using a commercial data fitting software IGOR © (see *appendix 2 and 3*).

RESULTS AND DISCUSSION

Characterization of furnished materials by OM, SEM-EDS and microhardness

Looking at the following figures in which metallographic attacks are reported, it can be seen that matrix results clean without precipitates at grain boundaries or secondary phases, confirming the effectiveness of the solution annealing treatment.

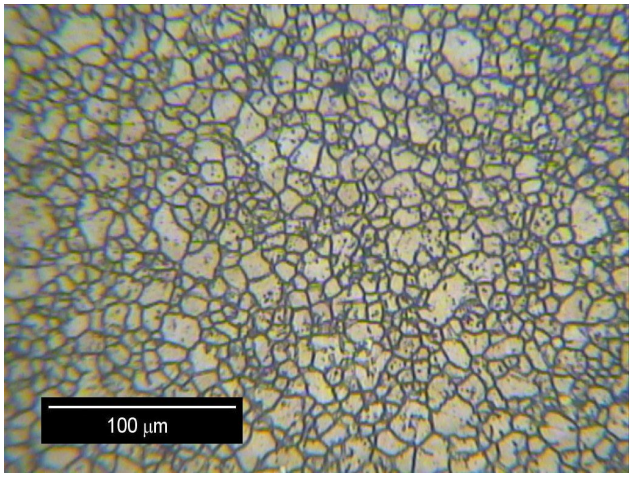

Figure 7: OM micrography of 347HFG SS after nitric etching (400x)

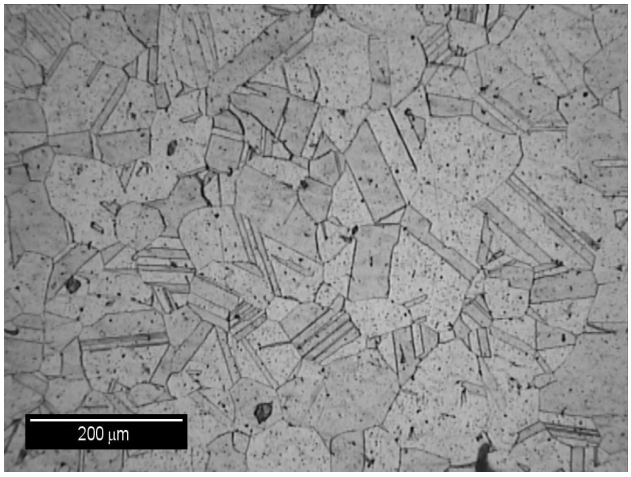

Figure 8: OM micrography of 310N SS oxalic etching (400x)

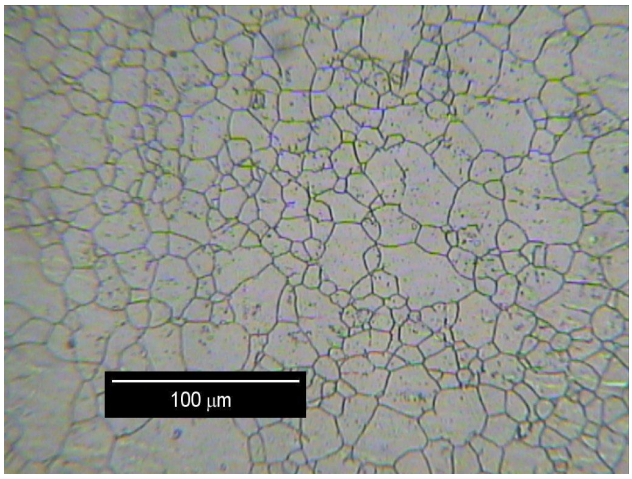

Figure 9:OM micrography of 304HCu SS after nitric etching (400x)

Figure 10: OM micrography of alloy 617 after nitric-hydrochloric-acetic etching (600x)

According to the ASTM E112 standard (*Appendix 1*), the average grain size for AISI 347HFG, 304HCu, 310N and alloy 617 are respectively 7, 8-9, 5 and 5.

Small Nb carbides precipitates should be expected for the three stainless steels. With that aim, SEM-EDS technique were applied.

SEM photos of the 347HFG SS etched area, obtained by secondary electrons confirmed the nature of the microstructure and revealed the presence of a few dark spots and bright zones. The dark spots are probably simple etching holes, while the others are salt filled holes.

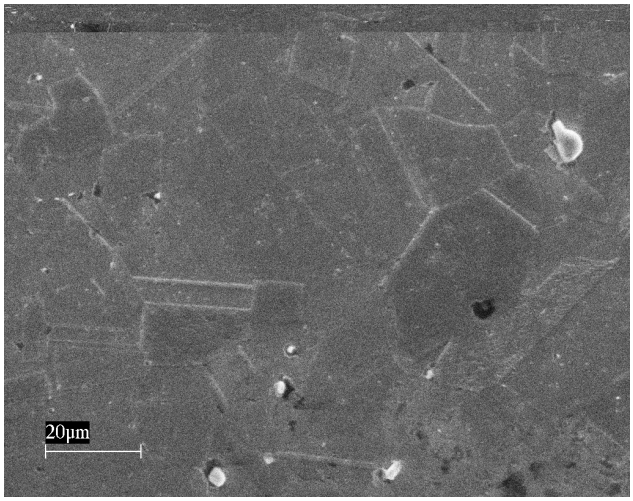

Figure 11: SEM micrography (SE) of 347HFG SS after nitric etching (2000x)

By observing the unetched zone using BSE electrons, some bright island are detectable (*figure 12*), EDS analysis (*figure 13*) confirms that are Nb rich zones, most probabily in form of carbides even than, C is not clearly detectable by EDS.

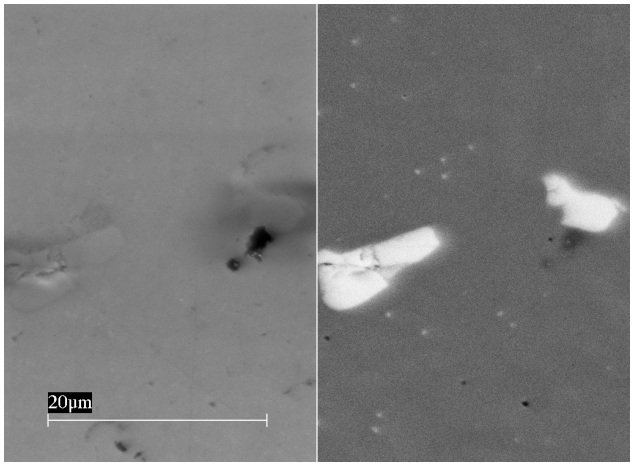

Figure 12: Splitted SEM micrography (SE/BSE) on 347HFG SS, unetched zone (4000x)

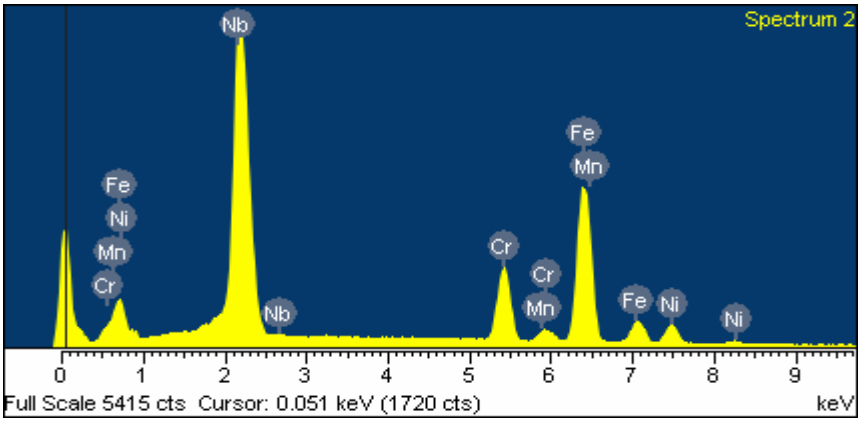

Figure 13: EDS analysis of bright region by BSE reported in figure 11

EDS analysis of the bulk material confirms the chemical composition of the alloy.
SEM micrographies on etched 310N SS doesn't reveal any inclusion

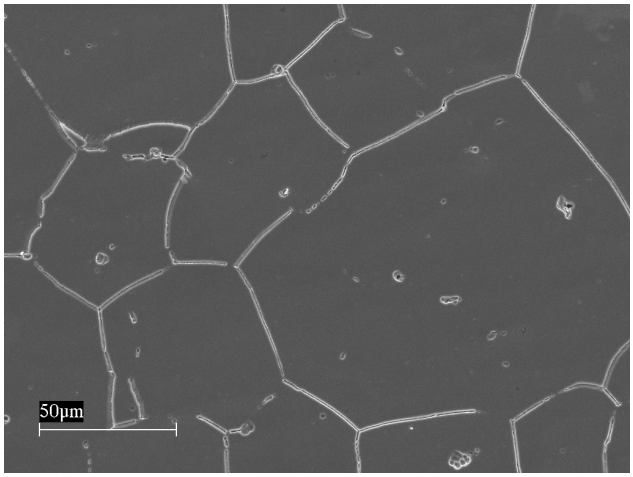

Figure 14: SEM micrography (SE) of 310N SS after nitric etching (2000x)

SEM (BSE) micrography on unetched metal reveal the presence of black and white spots, as reported in *figure 15.* EDS analysis confirm that are respectively Si and Nb segregates (*figures 16 and 17).*

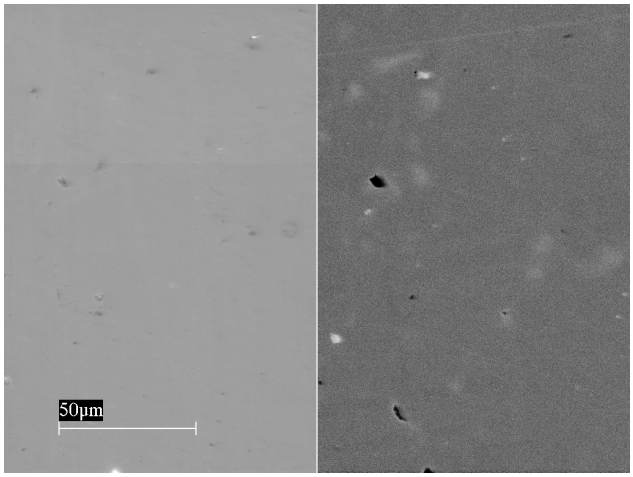

Figure 15: Splitted SEM micrography (SE/BSE) on 310N SS, unetched zone (4000x)

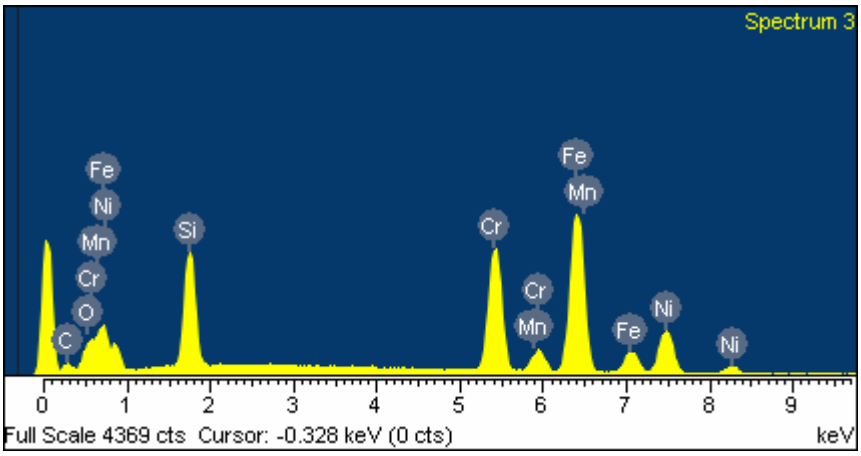

Figure 16: EDS analysis of dark region by BSE reported in figure 14

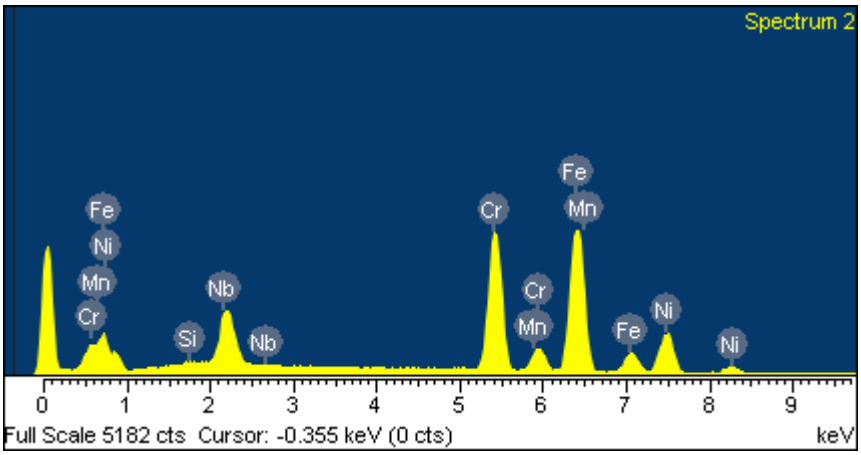

Figure 17: EDS analysis of bright region by BSE reported in figure 14

SEM micrographies on etched 304Hcu SS reveal the presence of some inclusions, EDS analysis confirms that are Nb rich island withstanding the etching process.

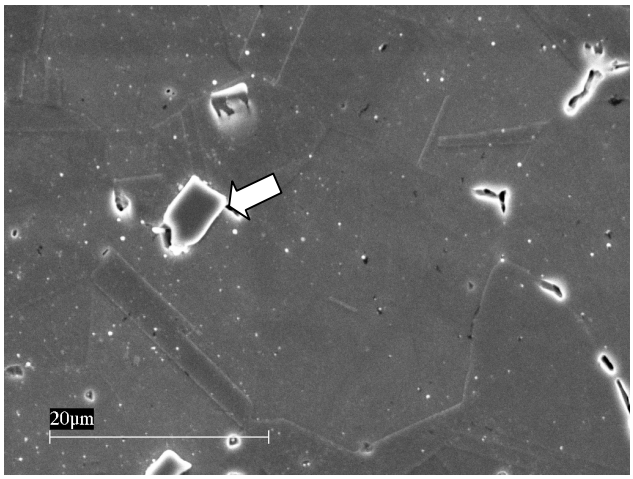

Figure 18: SEM micrography (SE) of 310N SS after nitric etching (2000x)

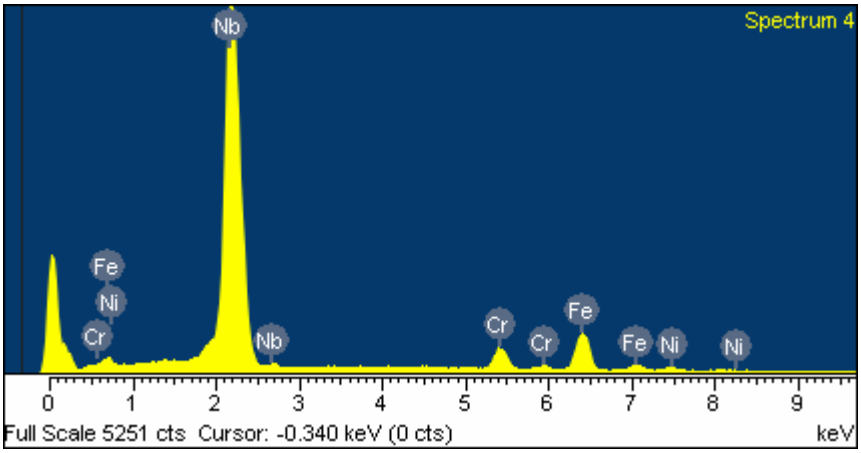

Figure 19: EDS analysis of bright inclusion indicate by the arrow in figure 17

Splitted SE-BSE images and EDS analysis on unetched 304HCu SS surface confirm the presence of Nb rich particles. Furthermore, EDS analysis confirm that Cu is present into the solid solution matrix.

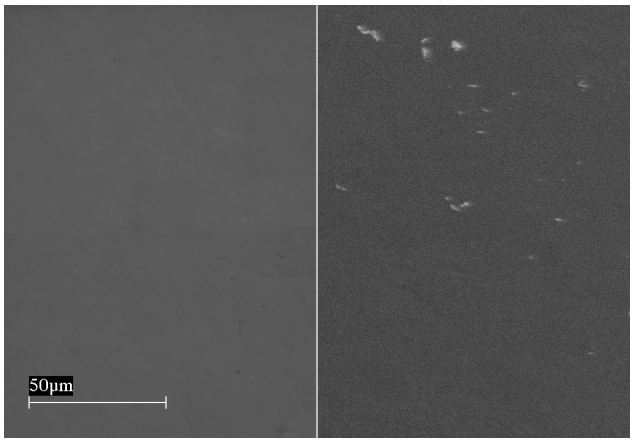

Figure 20: Splitted SEM micrography (SE/BSE) on 304Hu SS, unetched zone (4000x)

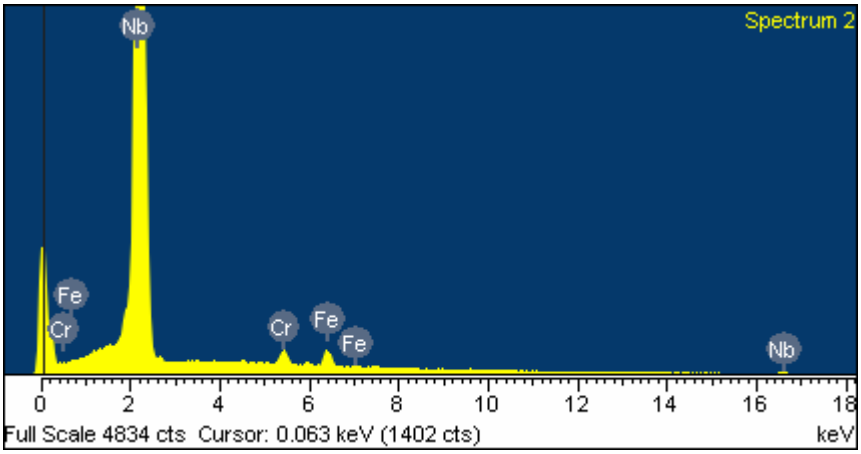

Figure 21: EDS analysis of bright region by BSE reported in figure 19

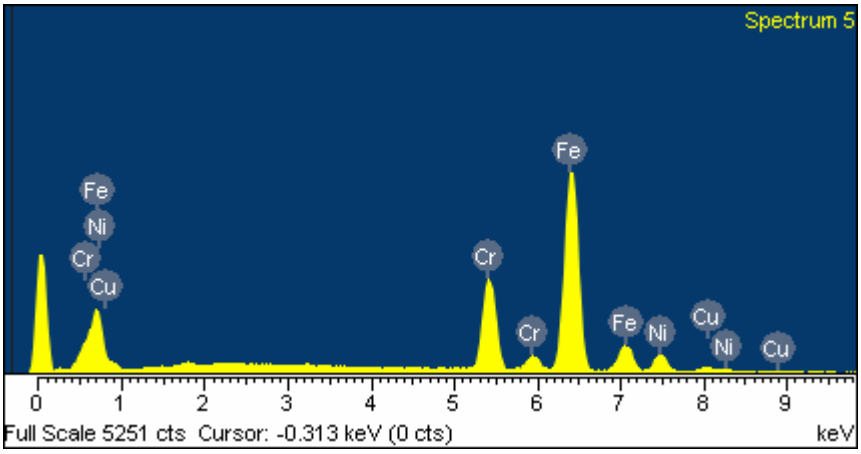

Figure 22: Bulk EDS analysis of 304HCu SS

When considering shoot peened tubes (304 HCu and Super 304H), the bulk microstructure is the same of a conventional 304HCu.

A good way to check the effects of the shoot peening process is by metallographic examination of sectioned specimen. Cross section micrographies of both SS are shown in *figure 23*. Grain size had a standard grade 8 (ASTM E112) for both.

Surface deformation (grain size lowering) due to the shoot peening treatment is well visible.

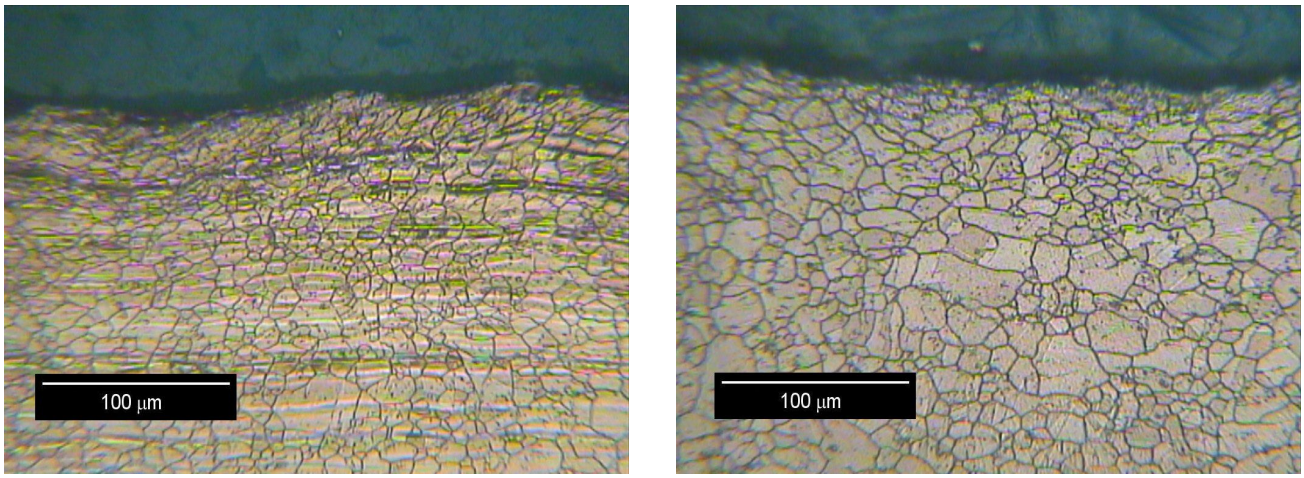

Figure 23: Cross section OM micrographies (400x) of 304HCu (left) and S304H (right) near shoot peened surface

A second way to appreciate the mechanical effect of the peening treatment is by means of microhardness measurement as profiles of a cross section.

In *figures 24 and 25*, microhardness profiles for the two considered steels are plotted.

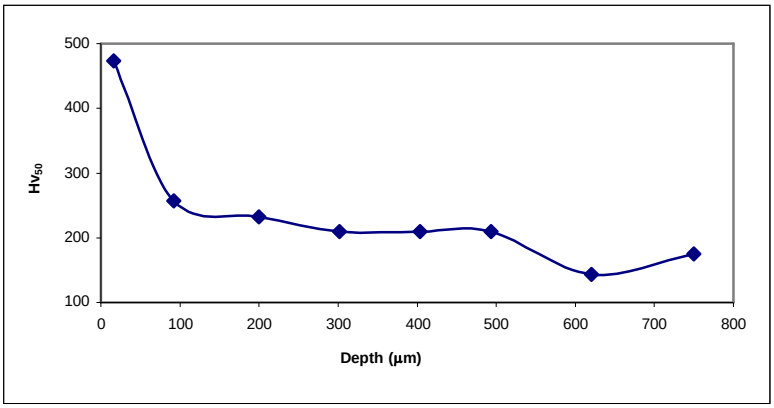

Figure 24: Hardness profiles for shoot peened 304HCu

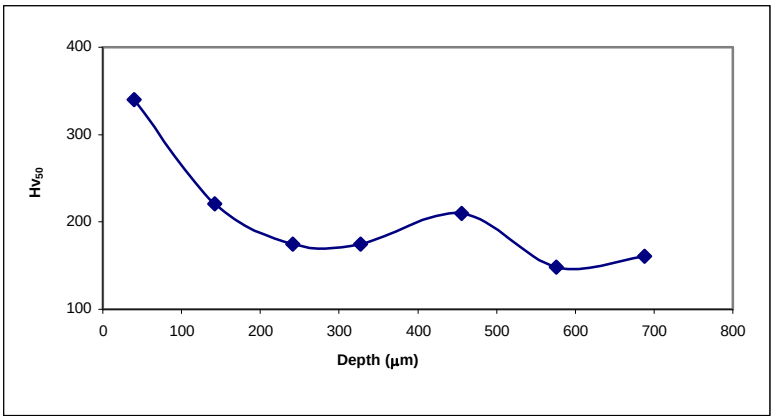

Figure 25:Hardness profiles for shoot peened S304H

Mean values of the bulk hardness were 170 HV_{50} for 304 Hcu SS and 150 HV_{50} for Super 304H SS. The hardness behavior is very similar for the two metals according to the same composition and same heat treatment (but being made by two different companies).
The bulk hardness for both alloys is around 200 HV_{50}.

Thermogravimetric tests

The first step of the thermogravimetric analysis was to define a setup for the experiments on the basis of literature. A temperature of 900°C was chosen in order to speed up tests with the chosen pure oxygen environment. Anther parameter to be defined is the gas flow rate that has to be not so low to win the instrumental pressure drops and to give an appreciable signal but also not so high to save input gas. In *figure 26.* thermogravimetric curves of 347HFG obtained at 900°C in pure oxygen for different fluxes, are shown. As can be seen, gas flux has effects on the effective mass

gain but not on the oxidation kinetic mechanism; on the basis of that results, a 15 Nl/h flux was finally chosen.

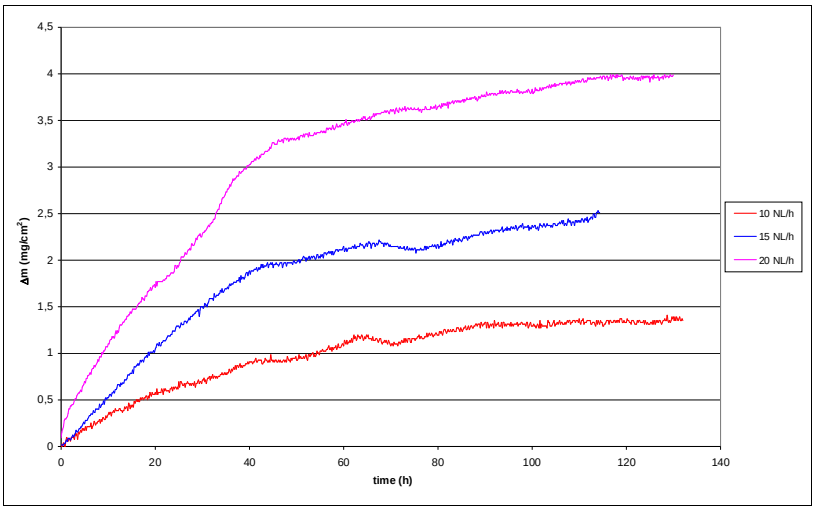

Figure 26: Thermograms of 347HFG SS at 900°C. O2 atmosphere for different flow rates

Linearizing the curve obtained at 15 NL/h, it appears that oxidation follows a parabolic kinetic for the first stages becoming an in between parabolic-logaritmic for higher treatment times indicating that in the considered conditions, the thermal oxide is protective.

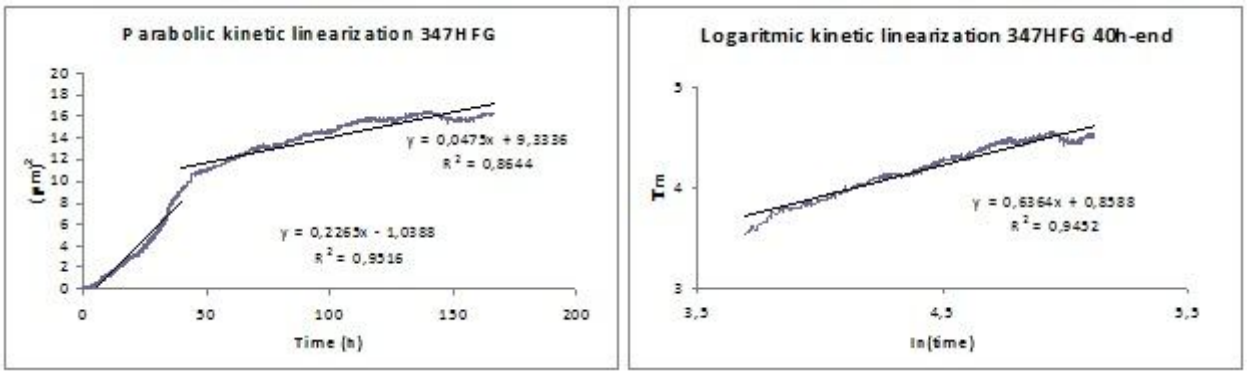

Figures 27: Parabolic (left) and logharitmic (right) linearizations of growth kinetic on 347HFG SS

304HCu SS thermogram collected the same conditions at 15 Nl/h, shows different behaviour: no plateau are reached.

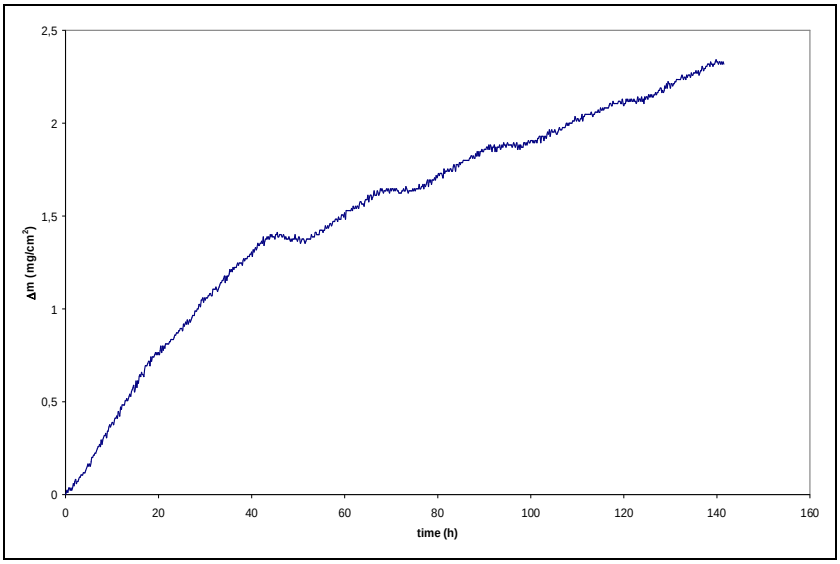

Figure 28: Thermogram of 304HCu SS at 900°C. O2 atmosphere and 15 NL/h flow rate

By linearizing the profile (*figures 29*), the first oxidation stage can be explained both by a parabolic and a linear kinetics where for longer time, a good fitting with a linear kinetics is obtained. That should be good only as a first approximation because by enlarging the curves appears clear that the output signal is constituted by a succession of small parabolas. This means that 340HCu in that condition suffer of spalling, confirmed also by visual examination.

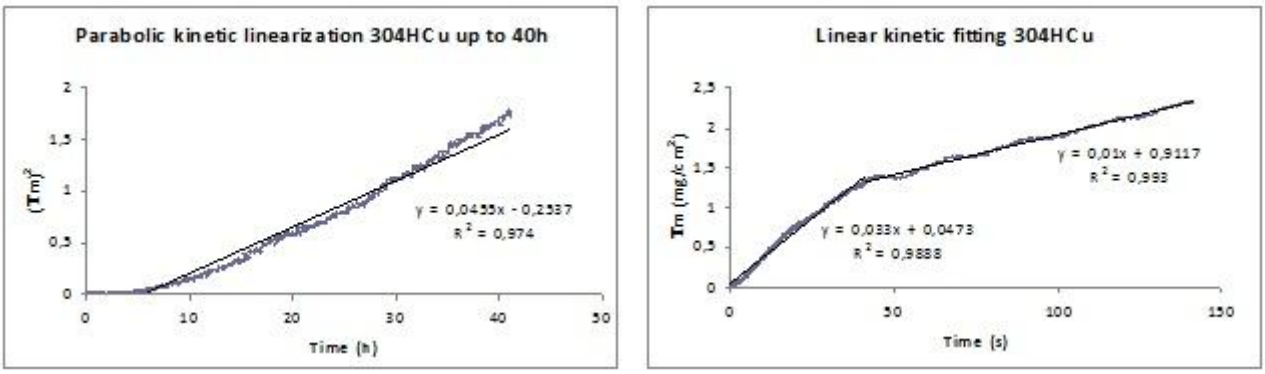

Figure 29: Parabolic linearization (left) and linear fitting (right) of growth kinetic on 304HCu SS

310N SS confirms to be the noblest of the considered steels showing a parabolic oxidation kinetics with a clear plateau after 70 hours treatment. Oscillations that can be seen in the thermogram reported in *figure 30* are reconductable to instrumental oscillations due to the calibration source of the analytical balance included in our instrument.

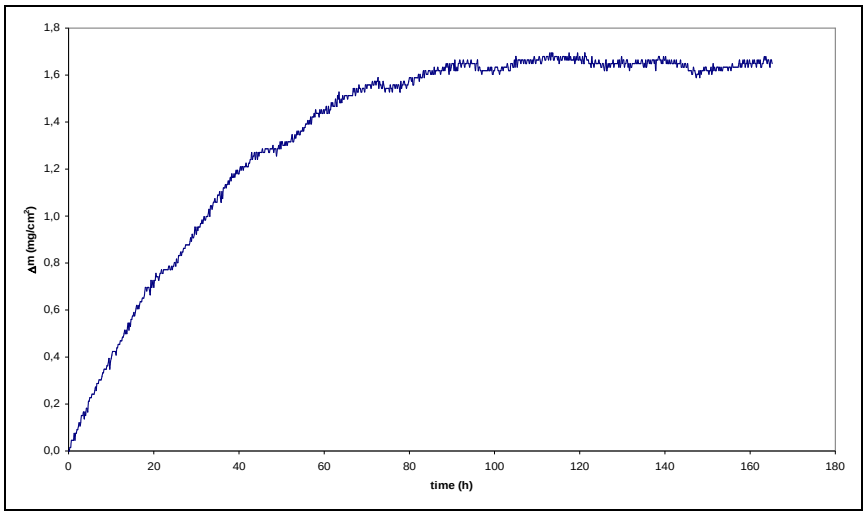

Figure 30: Thermogram of 310N SS at 900°C. O2 atmosphere and 15 NL/h flow rate

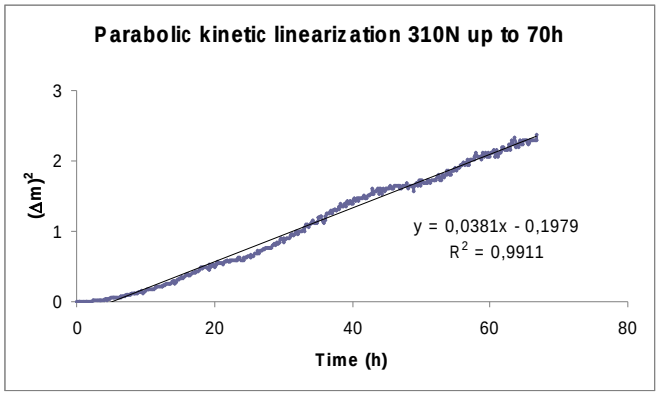

Figure 31: Parabolic linearization of growth kinetic on 310N SS

Same considerations are valid for alloy 617 that shows a parabolic oxidation kinetics with a clear plateau disturbed by some instrumental fluctuation. Looking at the effective mass gain, here it is higher than the one obtained in the case of 310N SS. This doesn't mean that oxide is less protective because of its different nature: 617 is a nickel alloy, 310N SS an iron based one.

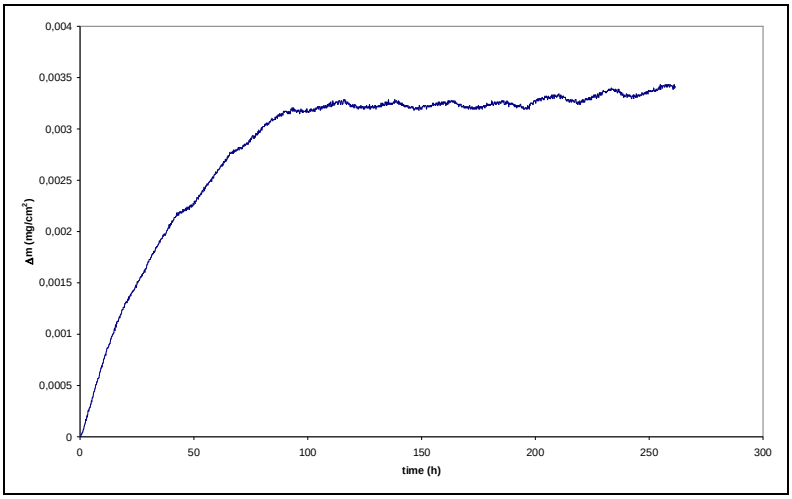

Figure 32: Thermogram of the alloy 617 at 900°C. O2 atmosphere and 15 NL/h flow rate

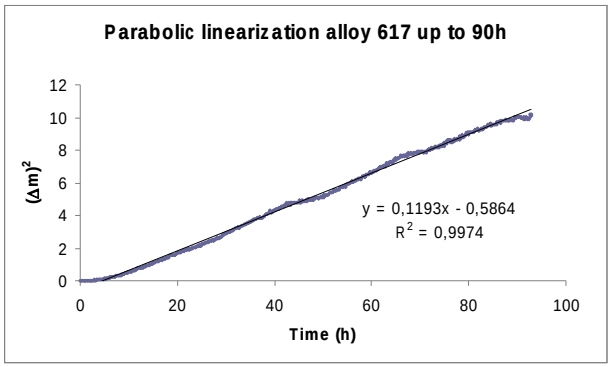

Figure 33: Parabolic linearization of growth kinetic the alloy 617

Oxide layer nature

Combining SEM examinations with EDS spectra of the three oxidized steels, we obtain indications about thickness and oxide composition.

In the following figures, SEM micrographies of the three 7 days oxidized SS are reported. As can be seen, for the 347HFG SS, the oxide thickness is in the range 5 – 15 μm (*figure a*); for 304HCu SS is about 5 μm (*figure b*, spalling is evident) while 310N SS shows the presence of an adherent oxide with an average thickness lower than 5 μm (*figure c*).

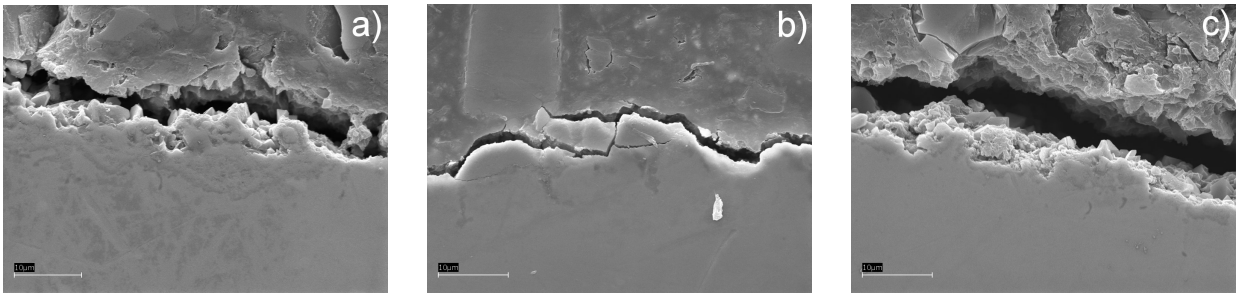

Figure 34:SEM micrographies (2000x) of cross sectioned oxidized SS: a) 347HFG, b) 304HCu, c) 310N

EDS maps of cross sectioned samples give indications about oxide composition and nature.

In the case of 347HFG, the film consists of three different layers: the first one is constituted by Cr-Mn oxides, followed by a mixed Cr-Fe-Mn oxide, probably in a spinel structure and finally a Fe-Mn external oxide layer. Ni is also present in small quantities. Mn presence is beneficial for protective properties of the oxides [4].

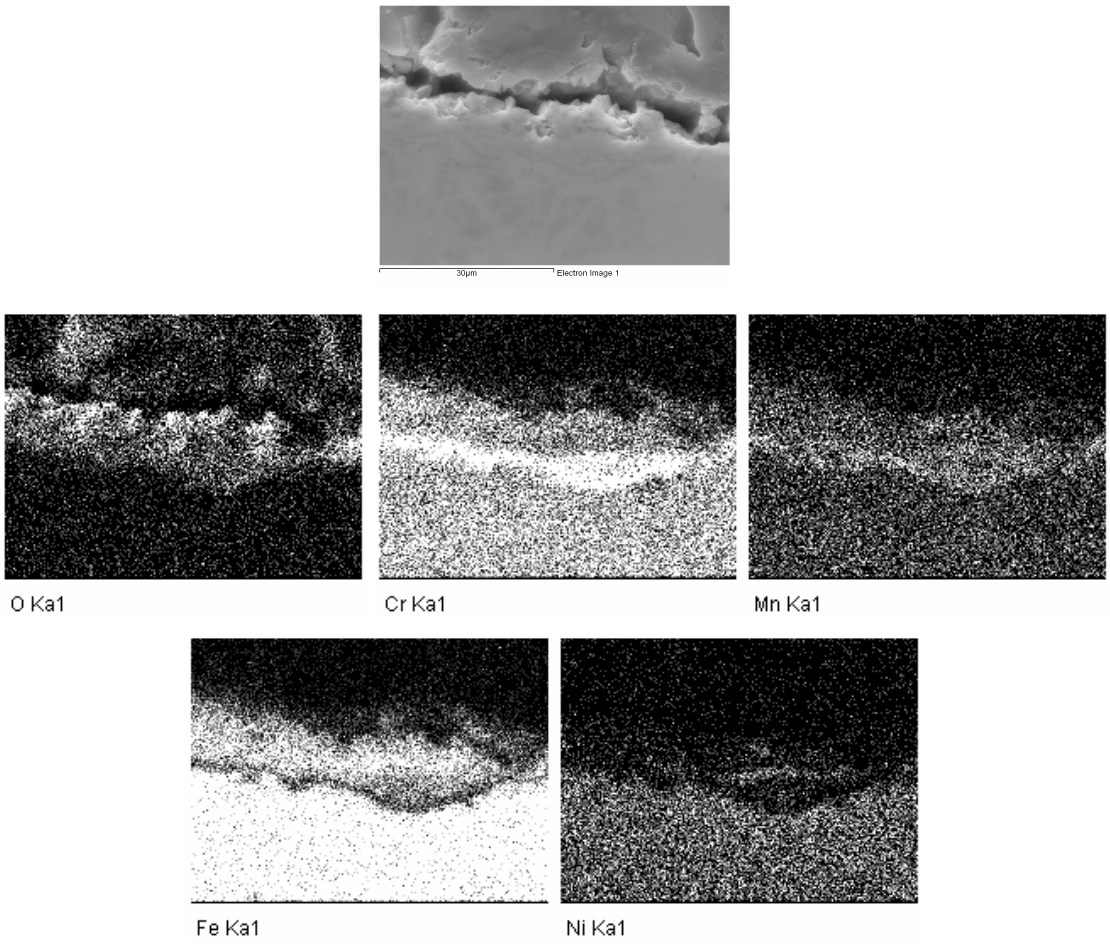

Figure 35: SEM micrography (3000x) and relative EDS maps of cross sectioned oxidized 347HFG SS

In the case of 304HCu (*figure 36*), several islands of Cr-Mn-Ni oxides are detected over the surface, covered by the mixed Cr-Fe-Mn(-Ni) oxides.

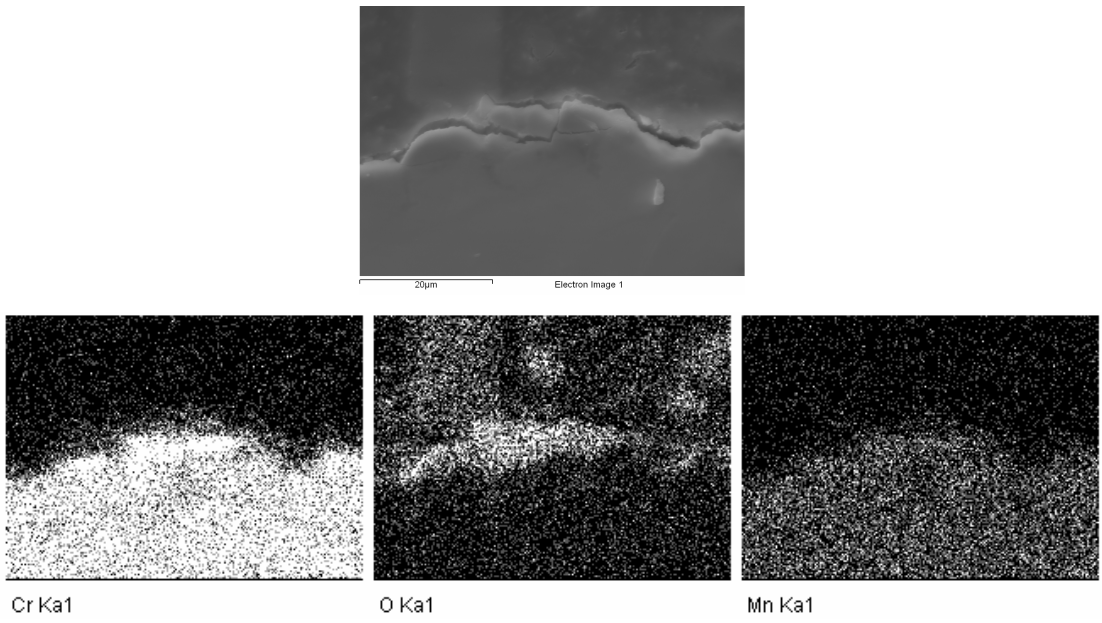

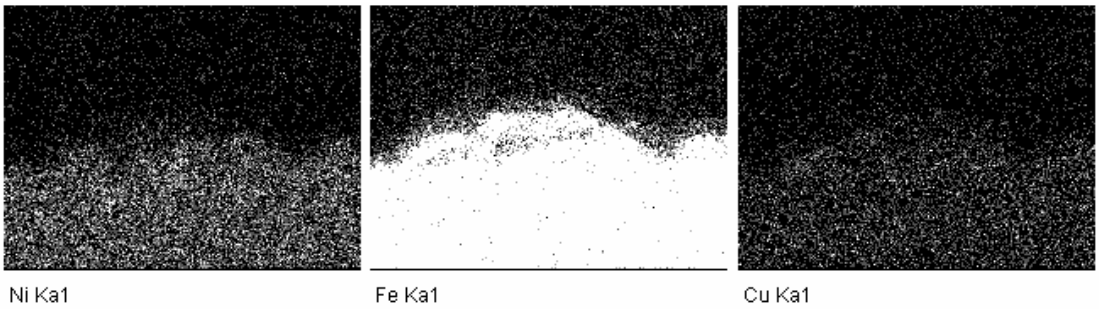

Figure 36: SEM micrography (3000x) and relative EDS maps of cross sectioned oxidized 304HCu SS

310N confirms to be the less susceptible towards oxidation since the oxide layer appears to be constituted only by Cr-Mn oxide (*figure 37*).

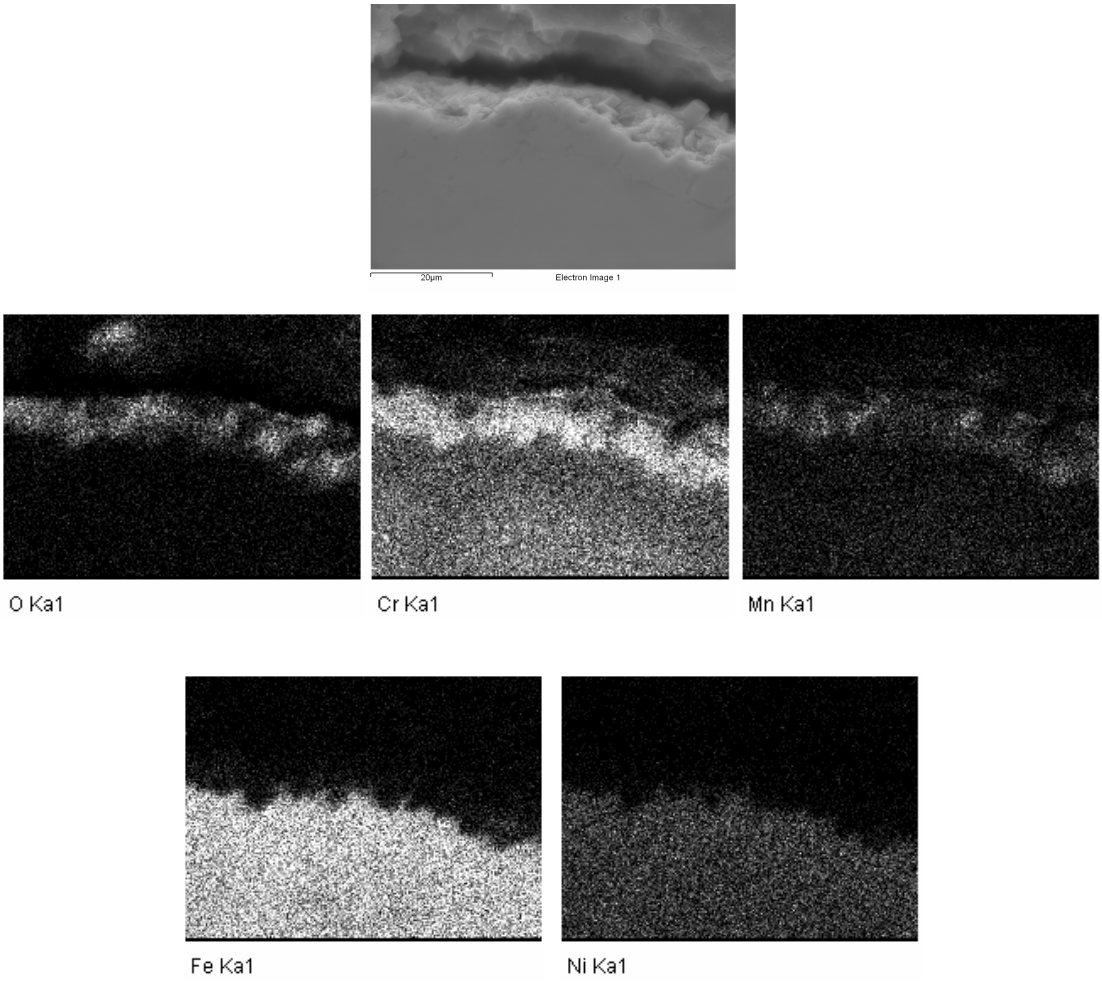

Figure 37: SEM micrography (3000x) and relative EDS maps of cross sectioned oxidized 310N SS

GDOES spectra were obtained only in few cases but only the one related to 347HFG SS oxidized for 4 days was meaningful and is here reported, confirming results obtained by SEM-EDS. As can be seen in *figures 38 and 39*, a three layered oxide with a global thickness around 8 µm can be

detected; first 3 μm from the surface essentially constituted by Fe-Mn oxides, 3 μm of Cr-Fe-Mn and 2 μm of Cr-Ni oxides.

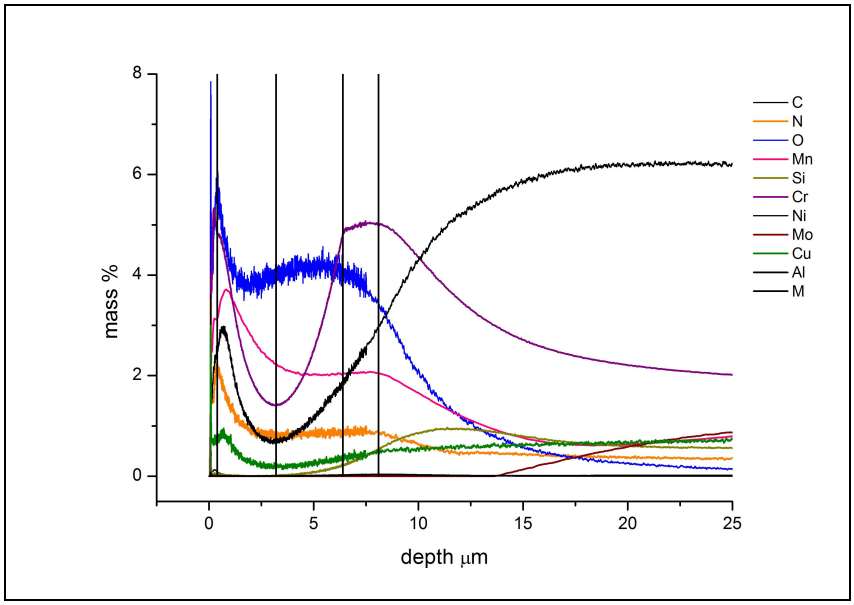

Figure 38: GDOES spectra of 4 days oxidized 347HFG SS in O_2 environment and 900°C temperature

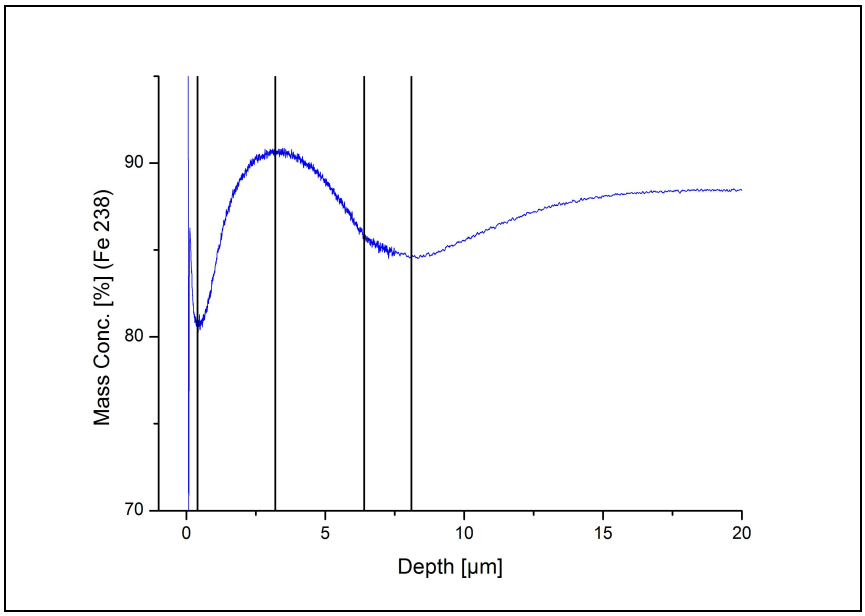

Figure 39: GDOES profile of Fe related to the previous spectrum

Electrochemical tests

Electrochemical potentiodynamic polarizations were conducted on the three considered stainless steels in "as received" and oxidized for different times condition. Typical curves are reported below.

By scrutiny of the curves, it is clear that despite the different compositions, chromium is the key element for the passivity due to the first active-passive transition. Other four secondary active-passive transition, with a very short stability range, are detectable.

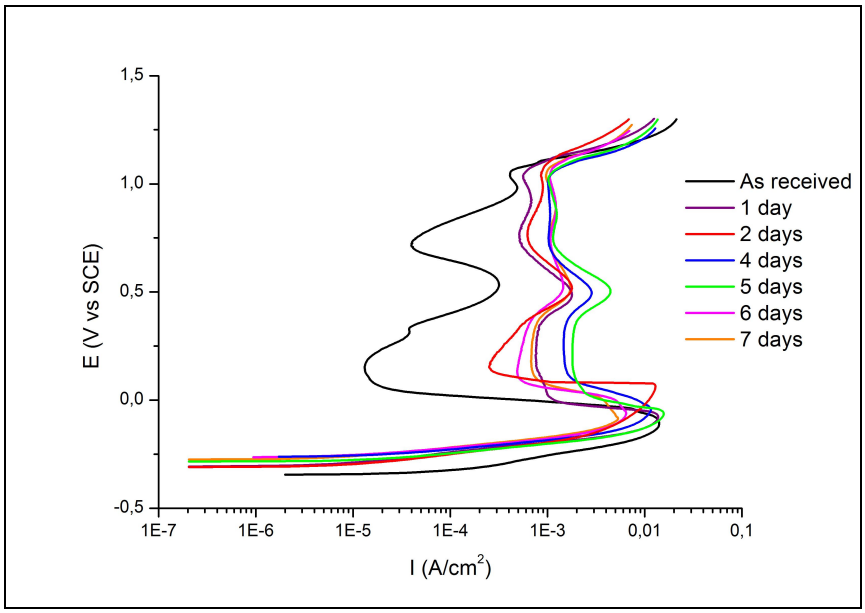

Figure 40: Polarization curves of "as received" and oxidized 347HFG

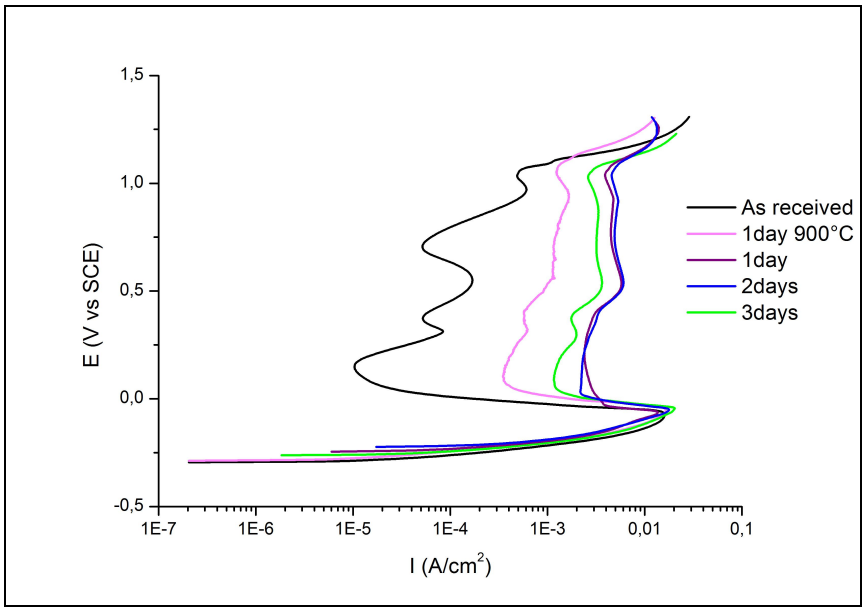

Figure 41: Polarization curves of "as received" and oxidized 304HCu

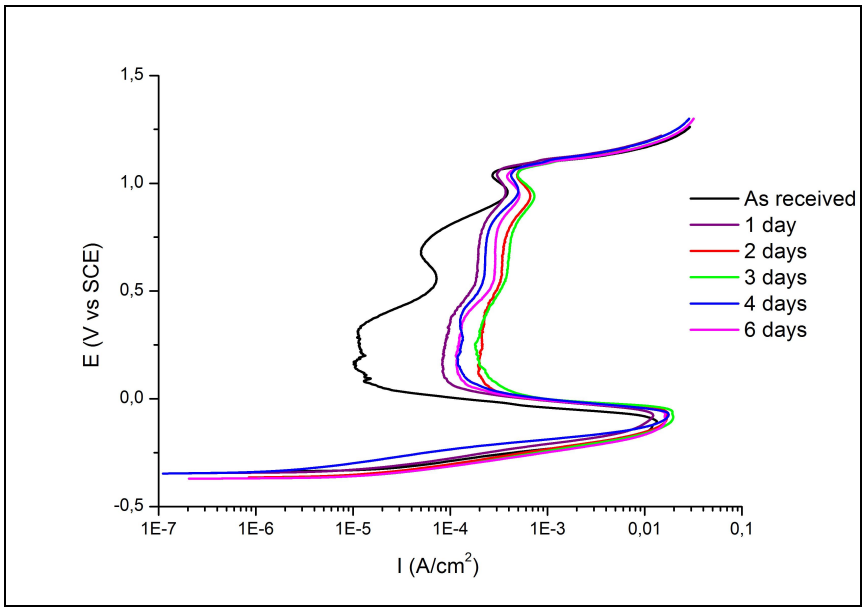

Figure 42: Polarization curves of "as received" and oxidized 310N

Curves of as received materials show four current minimals at a well defined potential value (open circuit potential, +135, +310, +720 and +1050 mV vs SCE); this effect tends to be annihilated with the oxidation time.

This phenomena, regarding that four active-passive transaction were object of the EIS study performed on the 347HFG SS in as received condition.

EIS spectra at the five considered potentials are reported below.

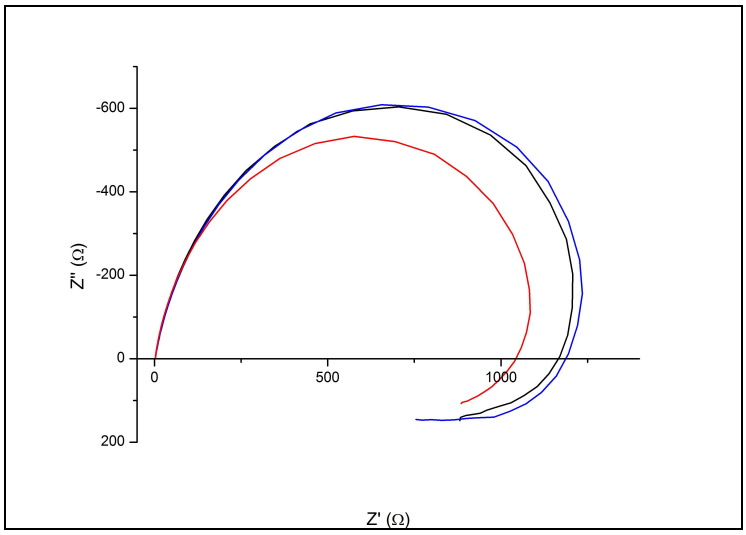

Figure 43: Nyquist plot of "as received" 347HFG SS at open circuit potential

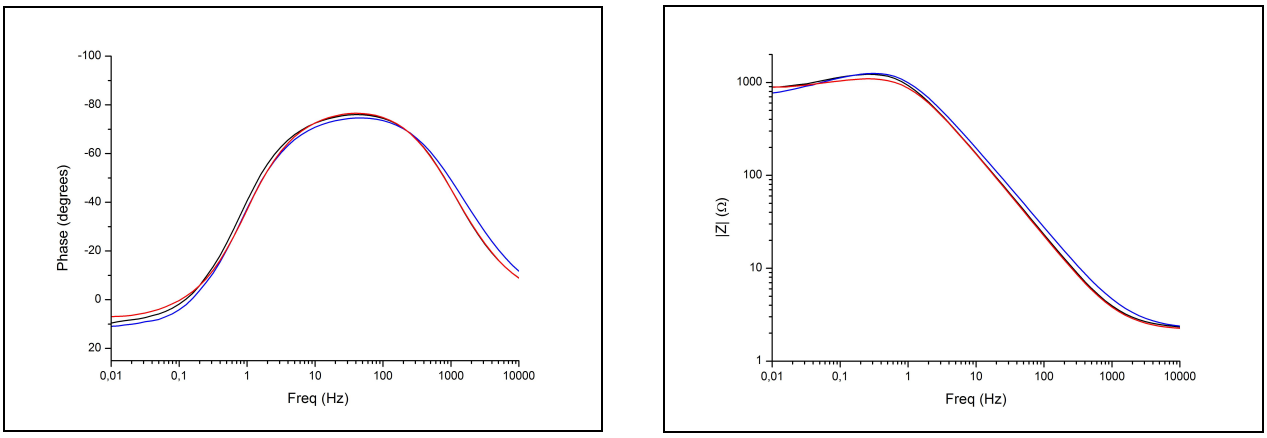

Figure 44: Bode plots of “as received" 347HFG SS at open circuit potential

Starting from Nyquist plot here obtained, an equivalent circuit based on passive elements can be hypothesized and confirmed by data fitting. Having an initial real impedance (Z’) delay followed by a semicircle, the system can be related to a Randles cell as reported in *figure 45*.

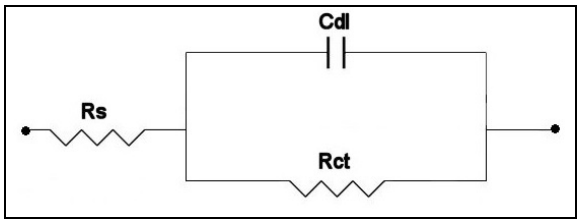

Figure 45: Electrical scheme of a passive Randles cell

On the physical point of view, R_s is the solution resistance between the tip of the luggin probe in the and the working electrode surface, R_{ct} is the charge transfer resistance related to the presence of the passive film and C_{dl} is the capacitance related to his dielectric nature.

This is not enough to completely describe the obtained Nyquist plot because at low frequencies an inductive loop appears. Inductors have not a physical explanation, A lot of authors describe them as an effect that is possible obtain [22] and the only way to find its position into the passive equivalent circuit is by data fitting.

Before fitting procedure, data validation has to be applied. The most useful way for EIS data validation is by applying the Kramers-Kroenig (K-K) transform. It is a complex mathematical algorithm that starting from experimental real impedance, calculates imaginary impedance and from experimental imaginary part, calculates real impedance . As output data, residual, as difference between experimental and calculate, are obtained for both real and imaginary parts of impedance. Nowadays this function is present in most of EIS instrumental software.

Result of K-K transform applied to data obtained at the open circuit potential is reported in *figure 46*.

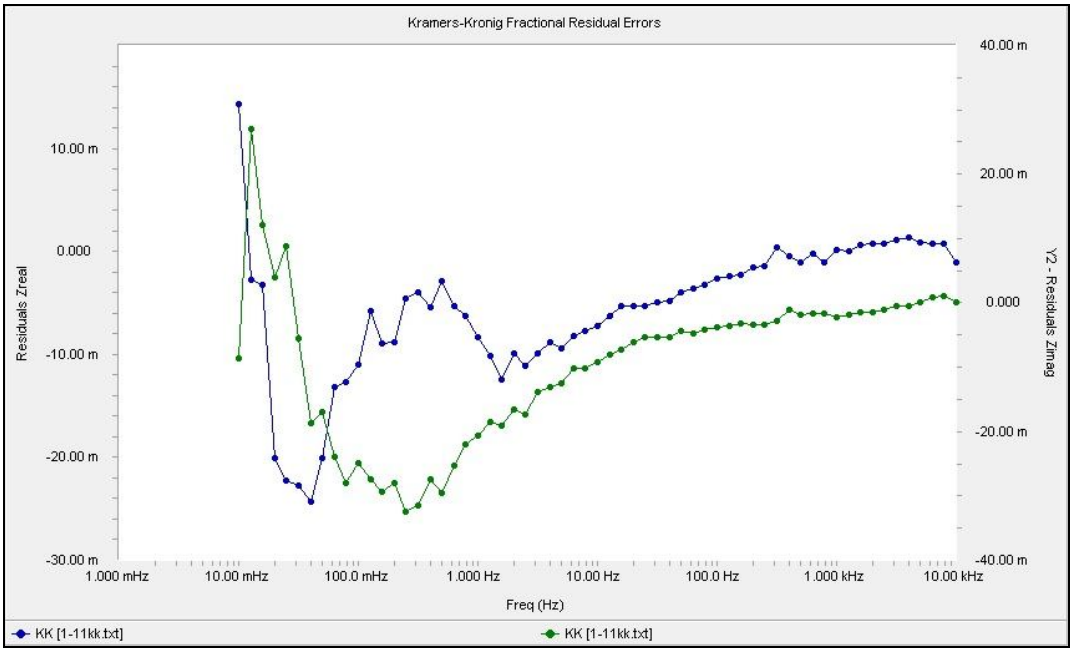

Figure 46: Kramers-Kroenig residual errors from "as received" 347HFG EIS spectra at the OCP

As can be seen, result are pretty good for frequencies higher than 1Hz and completely out of range for frequencies lower than 0,1 Hz. Causes of that fail could be related to system stability, noise or be a peculiarity of the system.

On this basis, dataset was limited to values corresponding to frequencies higher than 0,2 Hz.

Data treatment was conduced on the basis of Point Defect Model (see *appendix 2*) by putting an active element in parallel to the considered Randles passive circuit such as the faradaic impedance (Z_f) that contains all effects due to the movement of charged species in the passive film.

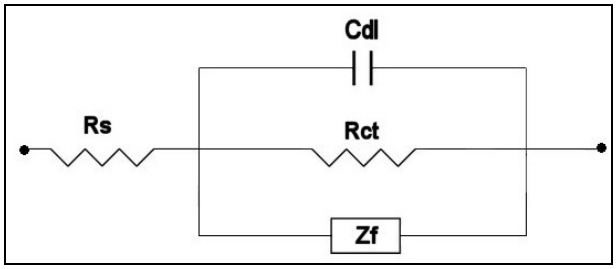

Figure 47:Electrical scheme of a Randles cell including the faradaic impedance

After, equations to describe the total impedance of the circuit were obtained (see *appendix 2* for derivation and explanation of terms). According to the literature, [25] passive film was considered

as an n-type semiconductor so, the final equation able to describe the total impedance of the system was:

$$Z_T = R_s + \frac{EE \cdot GG + DD \cdot FF}{FF^2 + EE^2} + j\frac{FF \cdot GG - EE \cdot DD}{FF^2 + EE^2}$$

where

$$DD = \Omega \cdot (b_3 k_3) \cdot R_{ct}$$

$$EE = \omega\left[1 + C_{dl} \cdot R_{ct} \cdot \Omega \cdot (b_3 k_3) + R_{ct} \cdot I_V\right]$$

$$FF = \Omega \cdot (b_3 k_3) \cdot (1 + R_{ct} I_v) + \Omega \cdot (a_3 k_3 - a_7 k_7 C_H^n) \cdot R_{ct} \cdot I_L - \omega^2 \cdot C_{dl} \cdot R_{ct}$$

$$GG = \omega \cdot R_{ct}$$

A code able to describe this system was written (see *appendix 3*) and using a commercial data fitting software (IGOR©), optimized values of real (Z') and imaginary impedance (Z'') as function of frequency were obtained including rate constants of reactions that govern passivity on the base of PDM.

Fitting software gives also, as output data, the graph of the error trend for both real and imaginary part of impedance, the one obtained in the case of the open circuit potential EIS data fitting is reported in *figure 48*, where frequency is drawn in the abscissa scale and both Z' (red) and Z'' (green) are reported as ordinates; dots are the experimental points and continuous lines are the result of data fitting. The upper part of graph report errors as absolute numbers and as can be seen is low.

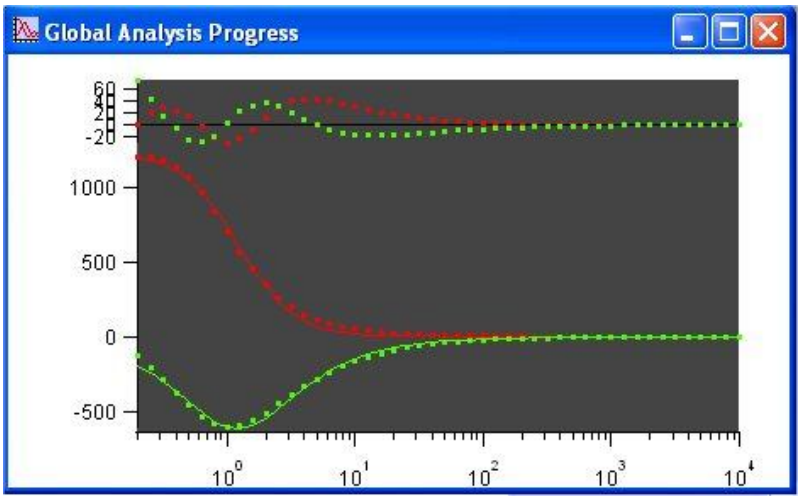

Figure 48: Data fitting and error graph monitor corresponding to the optimization at the open circuit potential

The following Nyquist plot reports results of optimization overlayed to experimental impedances. In *table 2*, values obtained by optimization are reported.

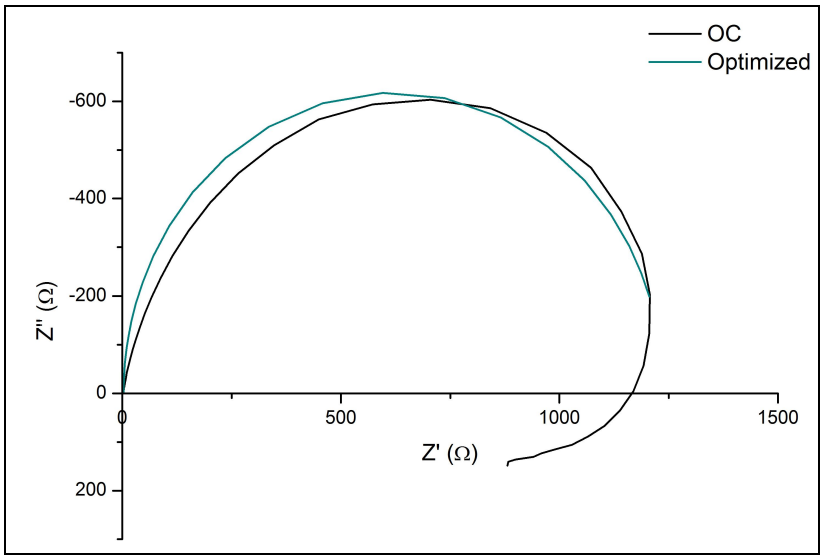

Figure 49: Optimized Nyquist plot for "as received" 347HFG SS at the open circuit potential

Same procedure was adopted for EIS spectra collected at +135, +310, +720 and +1050 mV vs SCE. At +135 mV vs SCE, signal becomes disturbed as the frequency diminishes. This could be explained looking to the polarization curves: that secondary passivity state exist in a too short range of potential.

Parameter	Value	Parameter	Value
R_s (Ω/cm^2)	2,99 (up limit: 3)	k_2^{00} (mol/cm^{2}s)	5,5e-18
R_{ct} (Ω/cm^2)	3,92e16	k_3^{00} (mol/cm^{2}s)	3,75e-19
C_{dl} (F/cm^2)	1,07e-4	k_5^0 (cm/s)	6,28e-8
Thickness (cm)	2,55e-7	k_7^0 (cm/s)	8,03e-16
α	0,724 (fix)	Ω (cm^3/mol)	14,59 (fix)
α_2	0,230	ε (V/cm)	3e6 (fix)
α_3	0,106	ϕ^0	0 (fix)
α_5	0,499	pH	-0,6 (fix)
α_7	0,305	T (K)	298 (fix)
n	0,5 (fix)	V (V vs NHE)	0,08 (fix)
d	3 (fix)	I (A/cm^2)	0 (fix)

χ	3 (fix)	β	-0,01
k_2 (mol/cm^{2}s)	1,17e-26	k_3 (mol/cm^{2}s)	3,50e-23
k_5 (cm/s)	6,28e-8	k_7 (cm/s)	8,03e-16

Table 2: Optimized values for "as received" 347HFG SS at OCP

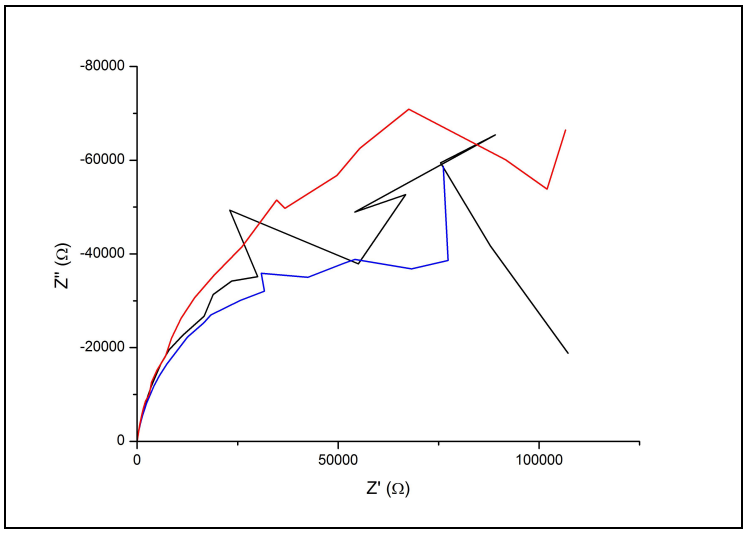

Figure 50: Nyquist plot of "as received" 347HFG SS at +135 mV vs SCE

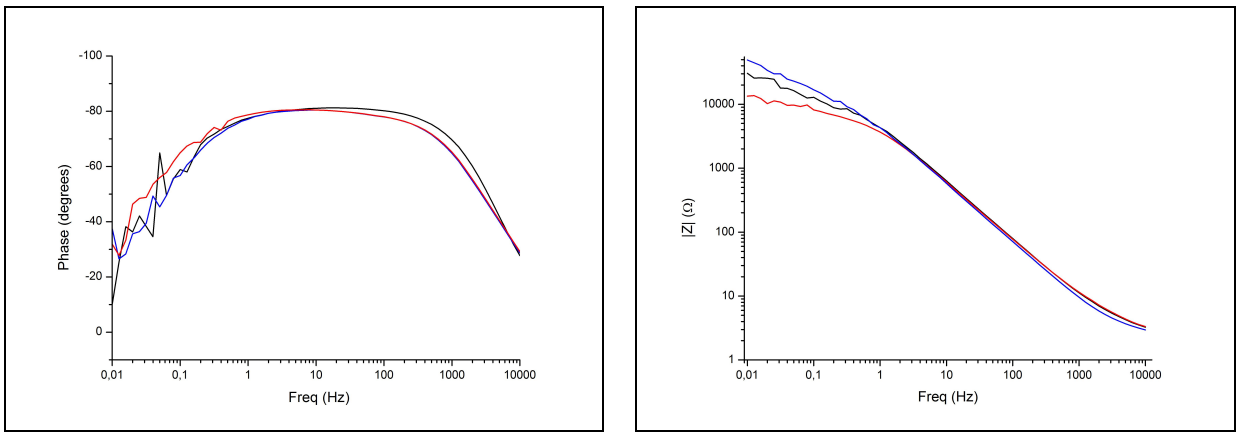

Figure 51: Bode plots of “as received" 347HFG SS at +135 mV vs SCE

The passive equivalent circuit is confirmed to be the same; impedance values are different of some magnitude order.

K-K transform here, validates data for frequencies higher than 1 Hz.

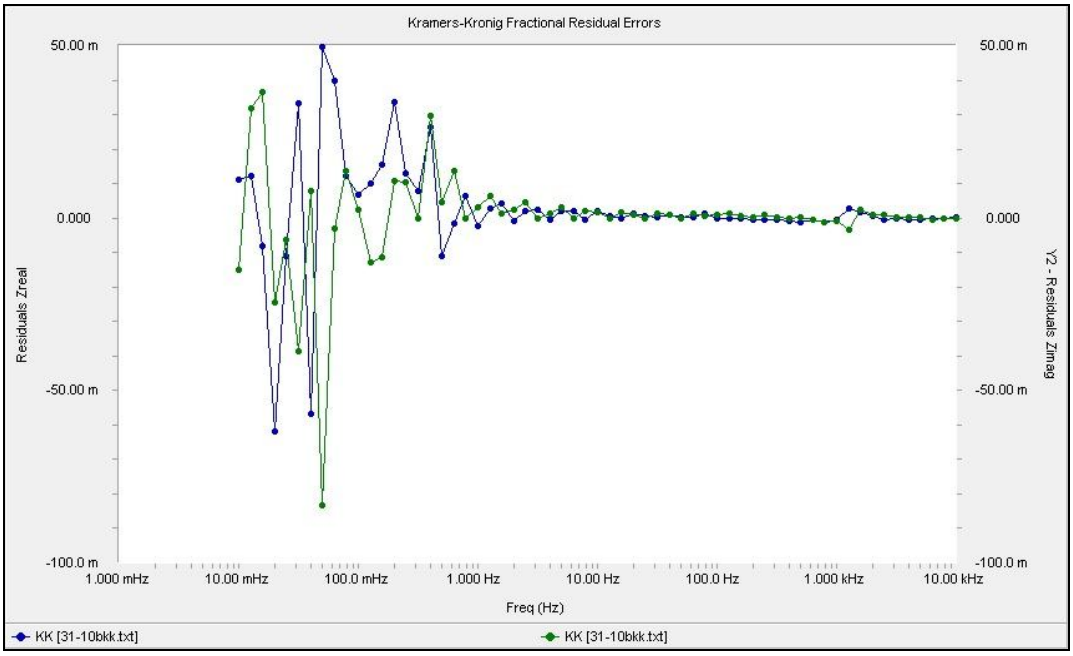

Figure 52: Kramers-Kroenig residual errors from "as received" 347HFG EIS spectra at +135 mV vs SCE

Optimization conducted using the same code gave the following results where the error is still acceptable, the problem was that acceptable input dataset was too restricted (note that ω_{max} in Nyquist plots is obtained at 1 Hz frequency for all potentials).

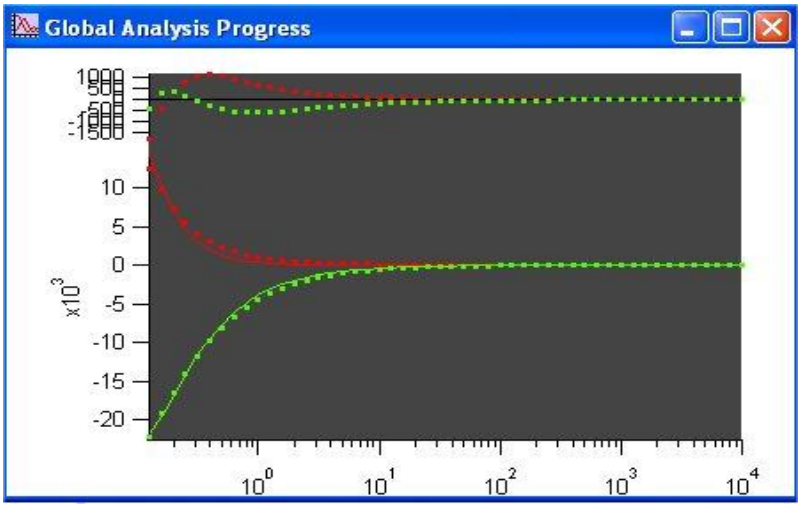

Figure 53:Data fitting and error graph monitor corresponding to the optimization at +135mV vs SCE

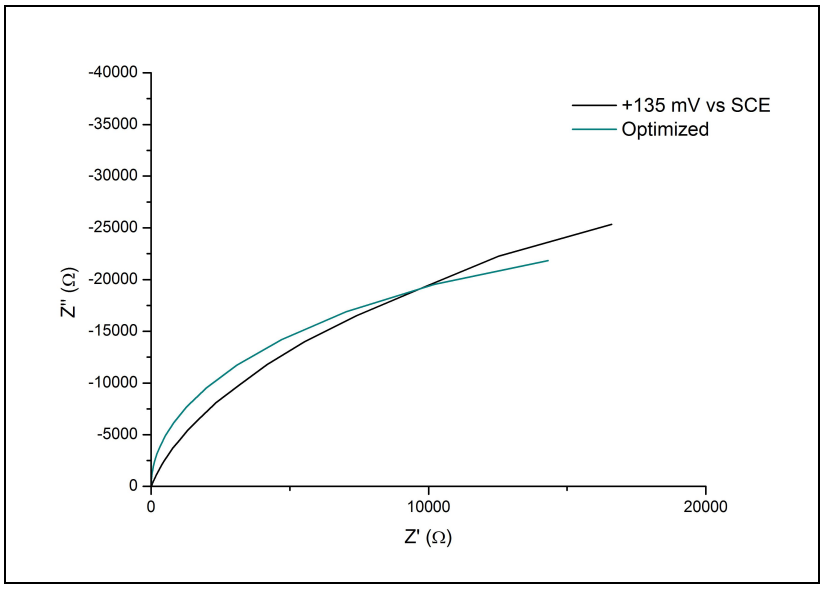

Figure 54: Optimized Nyquist plot for "as received" 347HFG SS at +135mV vs SCE

In *table 3*, optimization results are reported; note that as input impedance are different of some magnitude orders, output rate constant are different too.

Parameter	Value	Parameter	Value
R_s (Ω/cm^2)	2,9 (up limit: 3)	k_2^{00} (mol/cm^{2}s)	3,1e-23
R_{ct} (Ω/cm^2)	5,1e16	k_3^{00} (mol/cm^{2}s)	3,8e-12
C_{dl} (F/cm^2)	4,0e-5	k_5^0 (cm/s)	1,33e-6
Thickness (cm)	4,32e-8	k_7^0 (cm/s)	3,9e-12
α	0,724 (fix)	Ω (cm^3/mol)	14,59 (fix)
α_2	0,074	ε (V/cm)	3e6 (fix)
α_3	0,286	ϕ^0	0 (fix)
α_5	0,416	pH	-0,6 (fix)
α_7	0,779	T (K)	298 (fix)
n	0,5 (fix)	V (V vs NHE)	0,37 (fix)
d	3 (fix)	I (A/cm^2)	0 (fix)
χ	3 (fix)	β	-0,01
k_2 (mol/cm^{2}s)	1,16e-23	k_3 (mol/cm^{2}s)	8,54e-14
k_5 (cm/s)	1,33e-6	k_7 (cm/s)	3,9e-12

Table 3: Optimized values for "as received" 347HFG SS at +135 mV vs SCE

System instability was obtained also for EIS spectra recorded at +310 mV vs SCE.

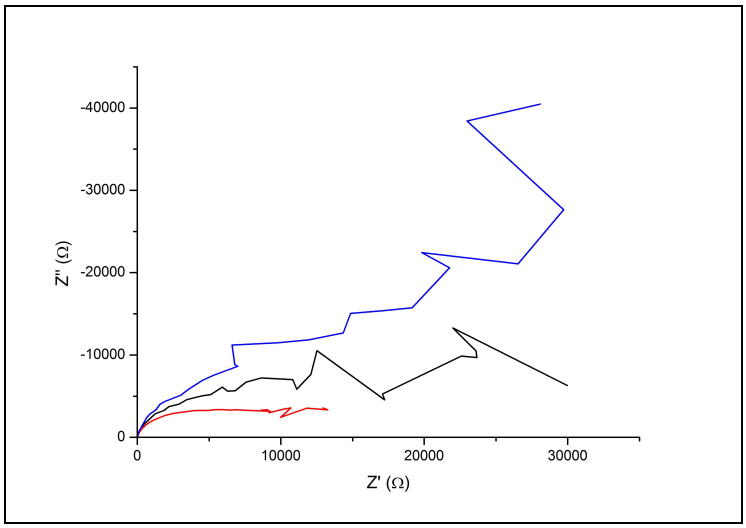

Figure 55: Nyquist plot of "as received" 347HFG SS at +310 mV vs SCE

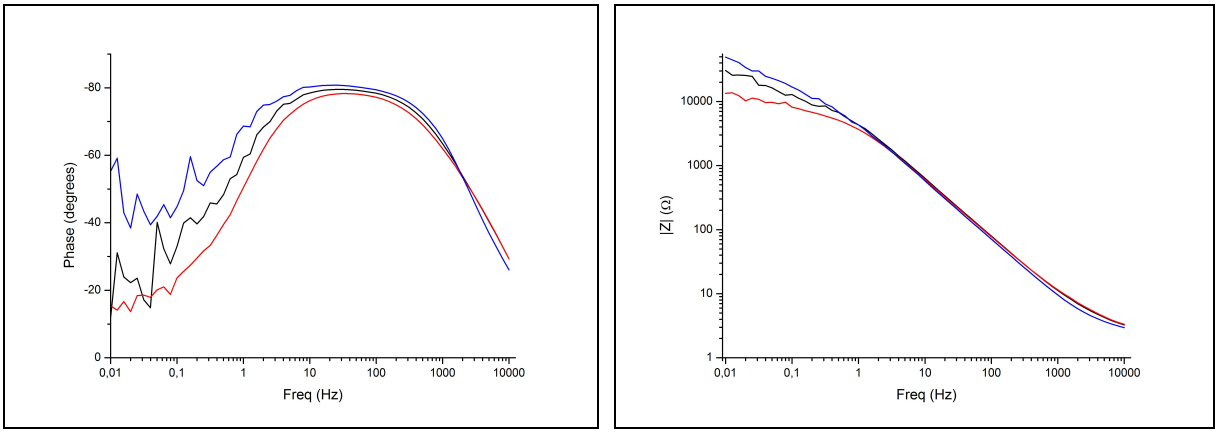

Figure 56: Bode plots of “as received" 347HFG SS at +310 mV vs SCE

K-K transform validates data for frequencies higher than 0,1 Hz.

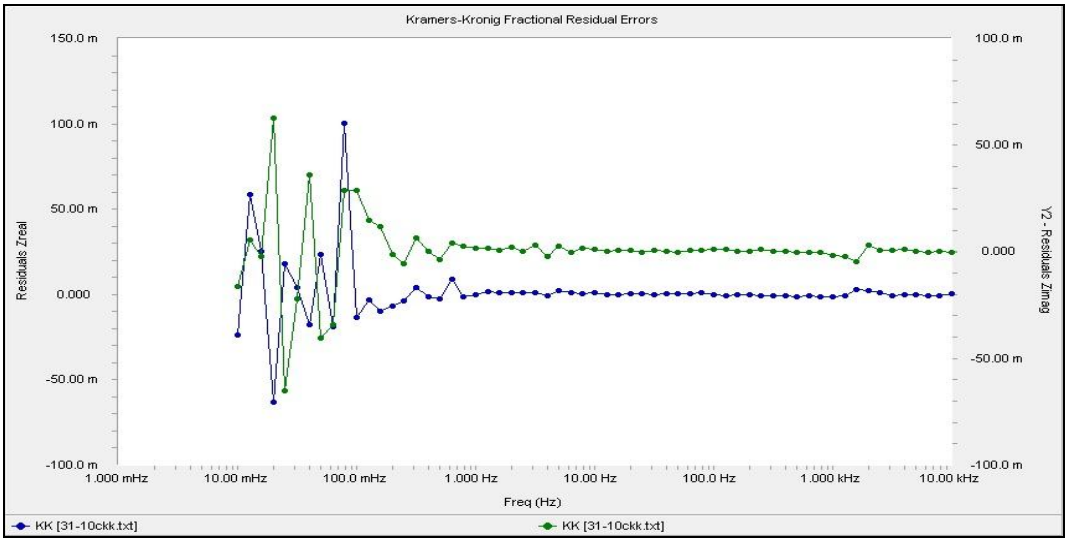

Figure 57: Kramers-Kroenig residual errors from "as received" 347HFG EIS spectra at +310 mV vs SCE

Optimization error (*figure 58*) are acceptable except for the last couple of points for Z''. This error is clearly detectable on the optimized Nyquist plot where ω_{max} is brought forward of a couple of points.

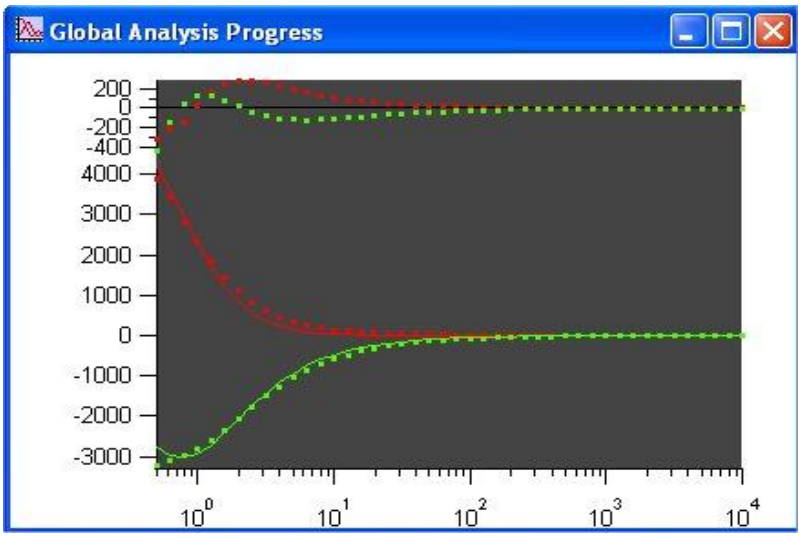

Figure 58: Data fitting and error graph monitor corresponding to the optimization at +310mV vs SCE

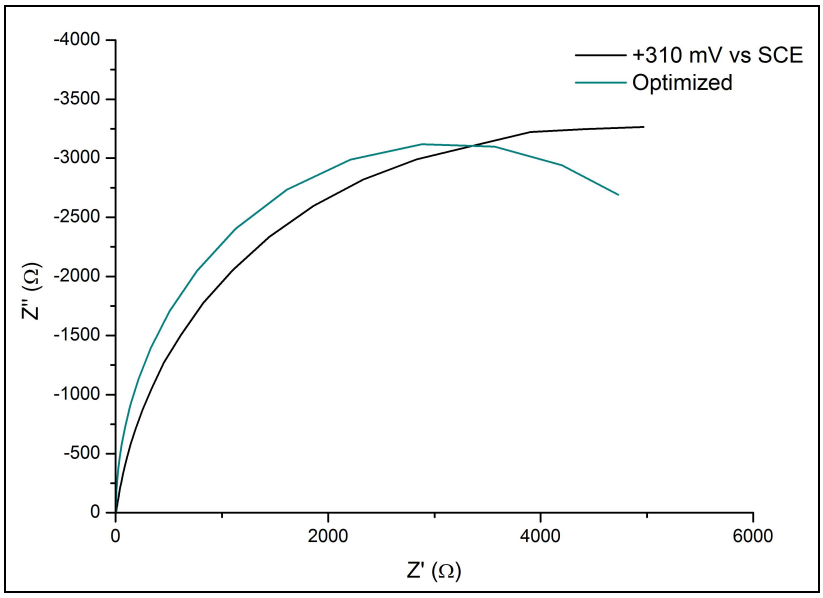

Figure 59: Optimized Nyquist plot for "as received" 347HFG SS at +310mV vs SCE

Optimized data values are reported in *table 4*.

Parameter	Value	Parameter	Value
R_s (Ω/cm^2)	2,99(up limit: 3)	k_2^{00} (mol/cm^{2}s)	1,59e-23
R_{ct} (Ω/cm^2)	5,0e16	k_3^{00} (mol/cm^{2}s)	3,97e-11
C_{dl} (F/cm^2)	3,3e-5	k_5^0 (cm/s)	8,72e-8
Thickness (cm)	7,69e-8	k_7^0 (cm/s)	6,56e-11
α	0,724 (fix)	Ω (cm^3/mol)	14,59 (fix)
α_2	0,135	ε (V/cm)	3e6 (fix)
α_3	0,135	ϕ^0	0 (fix)
α_5	0,836	pH	-0,6 (fix)
α_7	0,660	T (K)	298 (fix)
n	0,5 (fix)	V (V vs NHE)	0,55 (fix)
d	3 (fix)	I (A/cm^2)	0 (fix)
χ	3 (fix)	β	-0,01
k_2 (mol/cm^{2}s)	5,37e-25	k_3 (mol/cm^{2}s)	1,34e-12
k_5 (cm/s)	8,72e-8	k_7 (cm/s)	6,56e-11

Table 4: Optimized values for "as received" 347HFG SS at +310 mV vs SCE

EIS spectra obtained at +720 mV vs SCE shows the same stability problem related to the not steady state condition of the system.

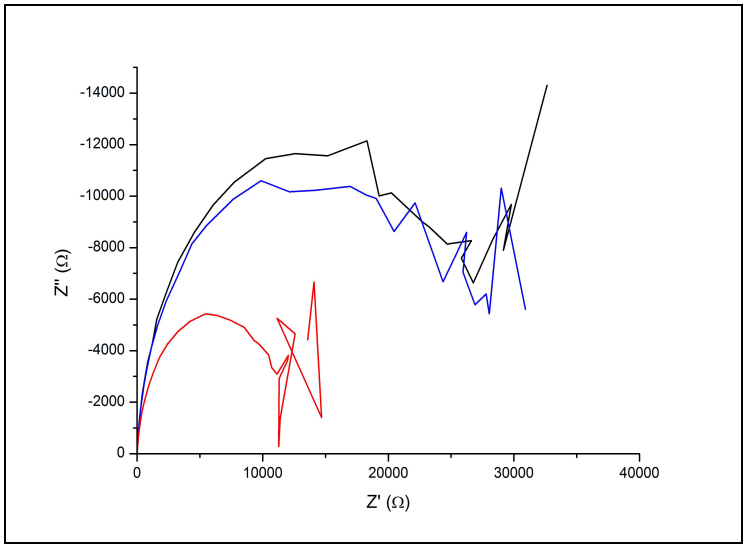

Figure 60: Nyquist plot of "as received" 347HFG SS at +720 mV vs SCE

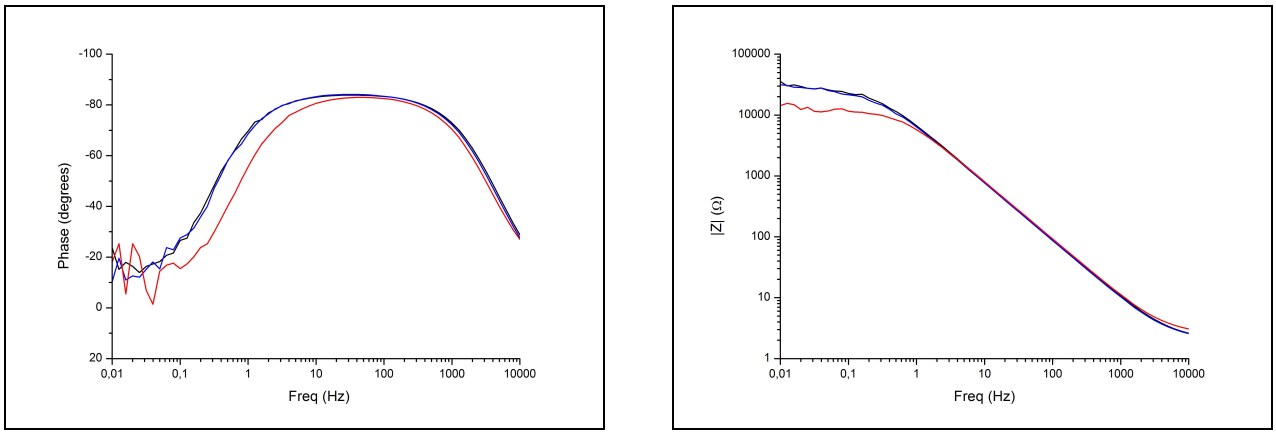

Figure 61: Bode plots of “as received" 347HFG SS at +720 mV vs SCE

K-K transform confirm that dataset is appreciable for frequencies higher than 1 Hz.

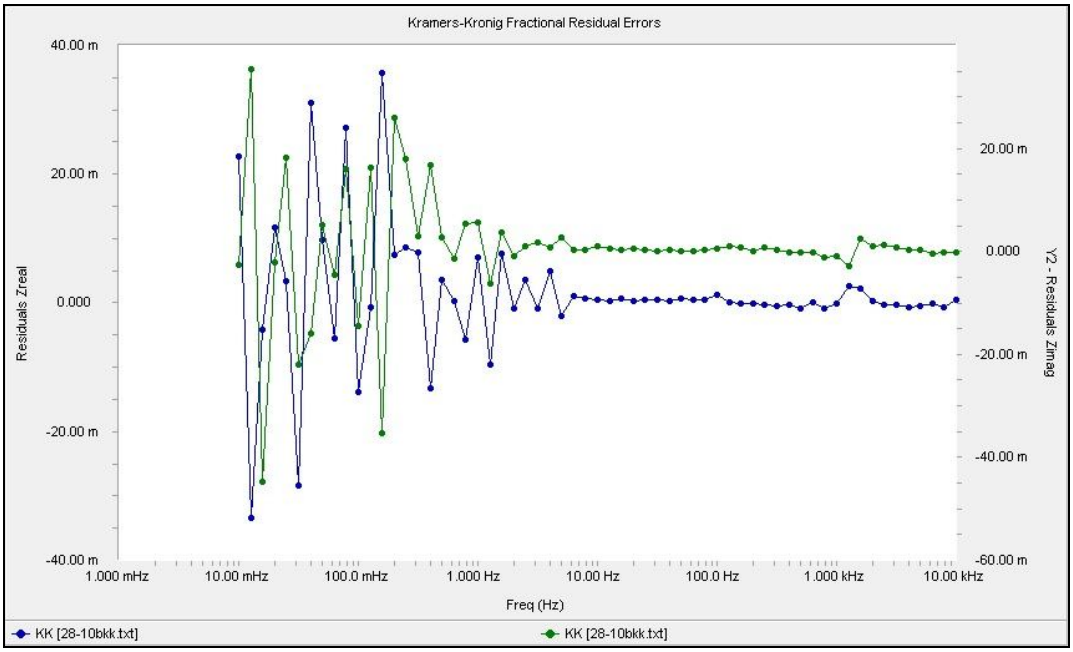

Figure 62: Kramers-Kroenig residual errors from "as received" 347HFG EIS spectra at +720 mV vs SCE

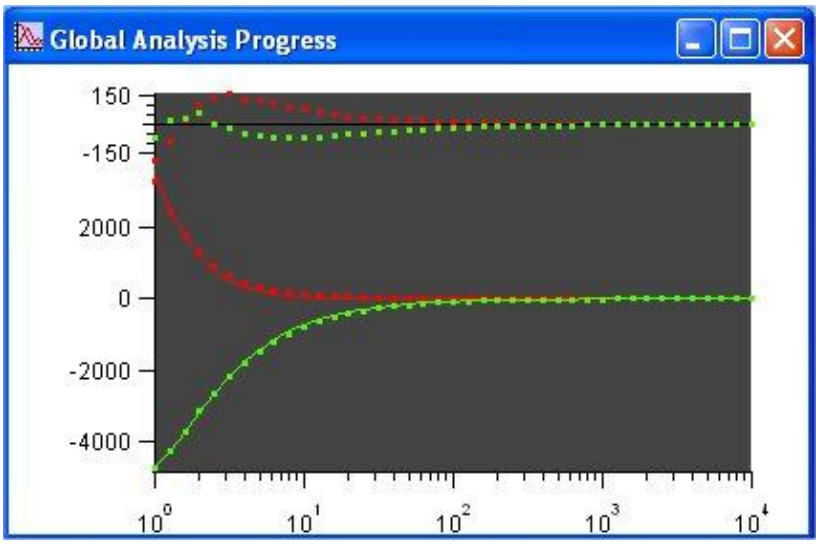

Figure 63: Data fitting and error graph monitor corresponding to the optimization at +720mV vs SCE

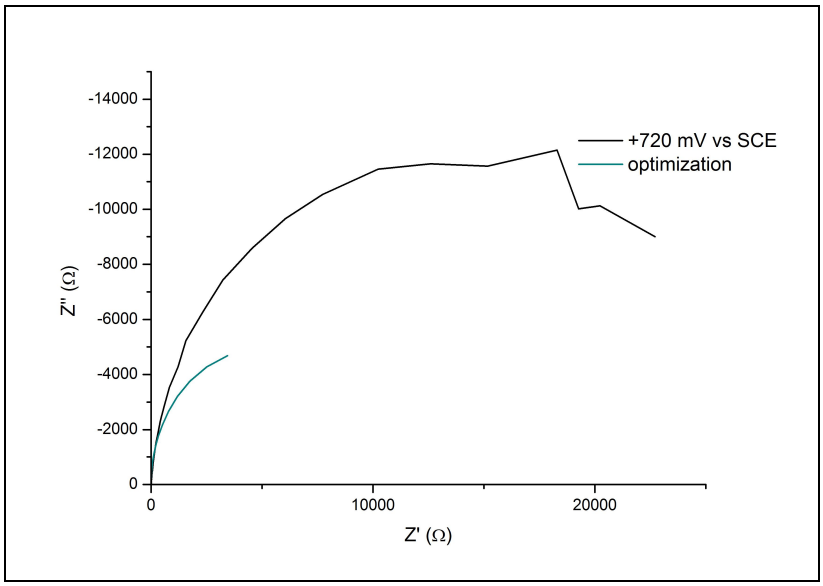

Figure 64: Optimized Nyquist plot for "as received" 347HFG SS at +720mV vs SCE

Parameter	Value	Parameter	Value
R_s (Ω/cm^2)	2,99(up limit: 3)	k_2^{00} (mol/cm^2s)	1,27e-16
R_{ct} (Ω/cm^2)	3,32e17	k_3^{00} (mol/cm^2s)	4,86e-10
C_{dl} (F/cm^2)	2,36e-5	k_5^0 (cm/s)	6,46e-8
Thickness (cm)	4,91e-8	k_7^0 (cm/s)	3,16e-11
α	0,724 (fix)	Ω (cm^3/mol)	14,59 (fix)
α_2	0,775	ε (V/cm)	3e6 (fix)
α_3	0,148	ϕ^0	0 (fix)
α_5	0,531	pH	-0,6 (fix)
α_7	0,634	T (K)	298 (fix)
n	0,5 (fix)	V (V vs NHE)	0,94 (fix)
d	3 (fix)	I (A/cm^2)	0 (fix)
χ	3 (fix)	β	-0,01
k_2 (mol/cm^2s)	6,0e-74	k_3 (mol/cm^2s)	5,01e-11
k_5 (cm/s)	6,46e-8	k_7 (cm/s)	3,16e-11

Table 5: Optimized values for "as received" 347HFG SS at +720 mV vs SCE

Spectra obtained at +1,05 V vs SCE show an apparently more stable dataset, the passive equivalent circuit is also confirmed.

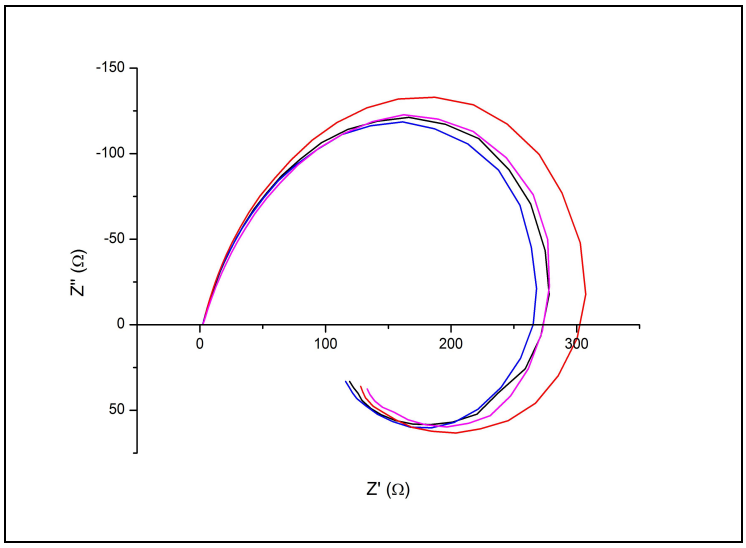

Figure 65: Nyquist plot of "as received" 347HFG SS at +1,05V vs SCE

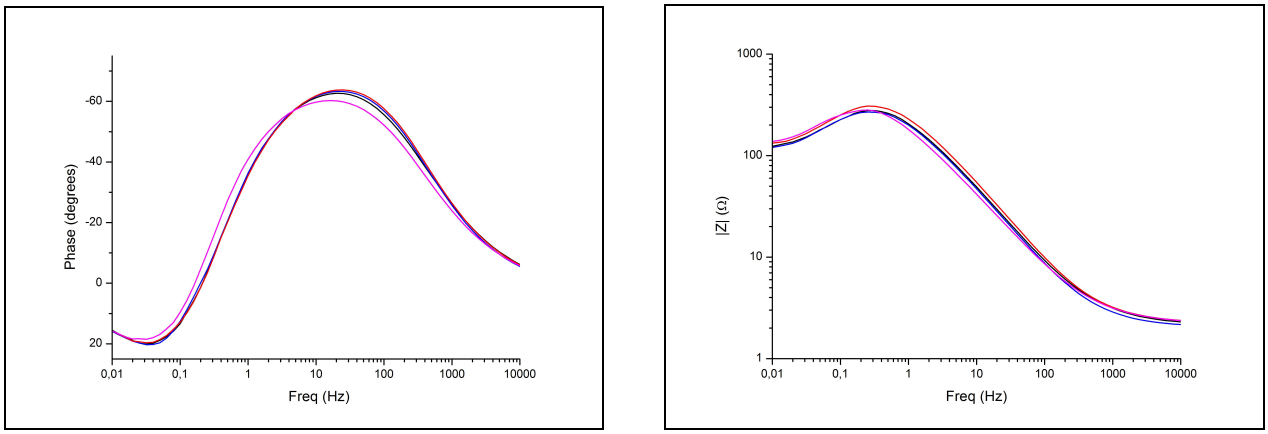

Figure 66: Bode plots of “as received" 347HFG SS at +1,05 V vs SCE

K-K transform confirm that data are coherent for frequencies higher than 0,5-1 Hz so, as in the case at open circuit potential, inductor can’t be modeled.

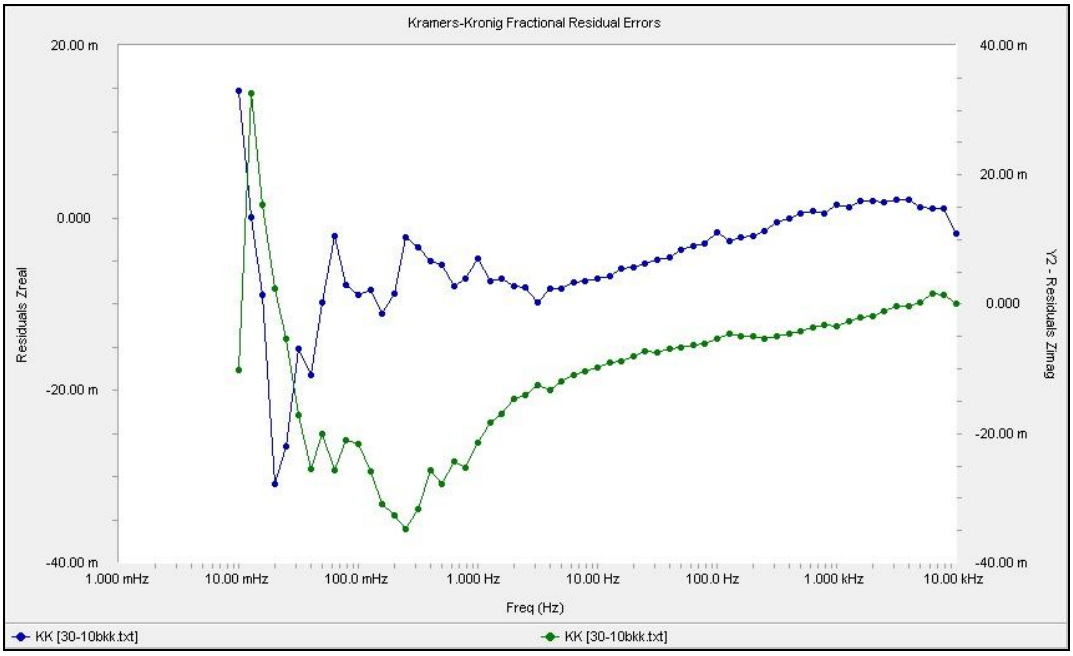

Figure 67: Kramers-Kroenig residual errors from "as received" 347HFG EIS spectra at +1,05 V vs SCE

Data were optimized, as previous, considering the passive film as a n-type semiconductor.

Is reported that applying anodic potentials [25] is possible to have an inversion from n- type to p-type semiconduction of the passive film.

As prove of that, Mott Shottky plot can be drawn.

For the Mott-Shottky theory, an n-type semiconductor, the following rule is valid:

$$\frac{1}{C^2} = \frac{2}{\varepsilon\varepsilon_0 e N_D}\left(V - V_{fb} - \frac{kt}{e}\right)$$

while for a p-type

$$\frac{1}{C^2} = \frac{-2}{\varepsilon\varepsilon_0 e N_A}\left(V - V_{fb} - \frac{kt}{e}\right)$$

where C is the semiconductor capacitance, ε the semiconductor dielectric constant, ε_0 the vacuum permittivity (8,85e-14 F/cm), *e* the electron charge (1,60e-19 C), V the applied potential, V_{fb} the flat band potential, $N_{D\ (A)}$ the donor (acceptor) density, k the Boltzmann constant, the term kt/e has a value about 0,025 V at 25°C.

So, plotting the thickness normalized C^{-2} values obtained from optimizations as function of potential, a positive slope should be obtained for points related to an n-type semiconductor while a

negative one is expected for a p-type semiconduction. Doesn't matter if plots are made considering the wrong semiconductive type, capacitance is not so strictly related to the semiconductive nature.

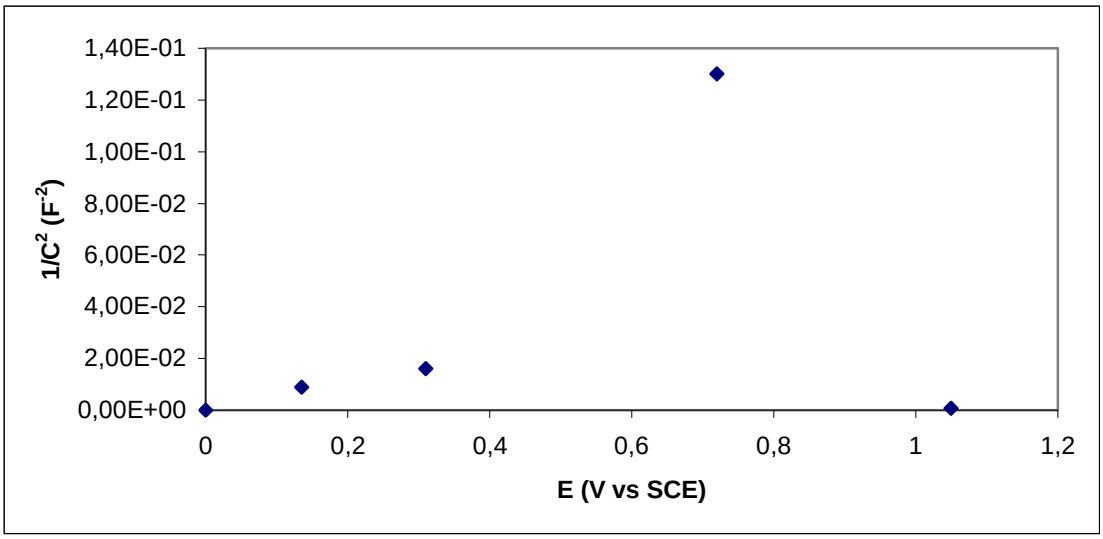

Figure 68: Mott-Shottky plots from optimized capacitance values

Mott-Shottky plots shows a n-type semiconduction at potentials up to +310 mV vs SCE and p-type semiconduction at +1,05 V vs SCE. Point corresponding to +720 mV vs SCE is in doubt, optimization using the whole PDM (considering both equations for n-type than p-type semiconduction) was applied confirming the n-type semiconduction at +720 mV vs SCE as can be seen in *figure 69* where optimizations result are completely overlayed.

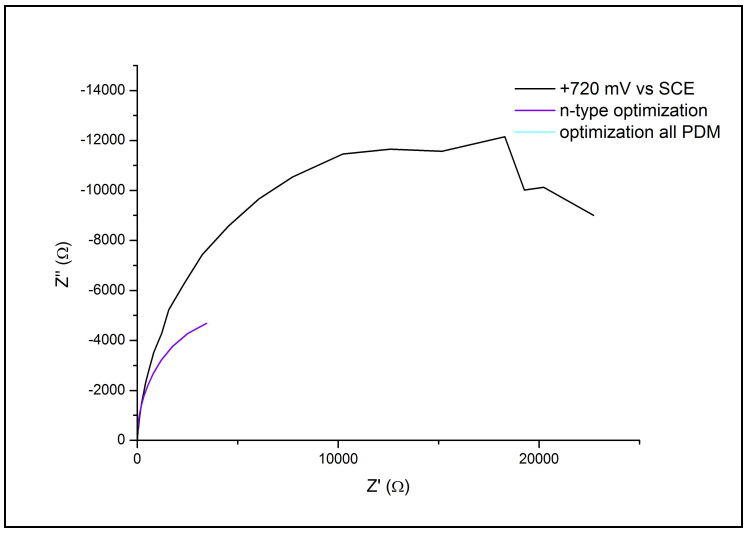

Figure 69: Optimized Nyquist plot for "as received" 347HFG SS at +720mV vs SCE using both n-type than complete optimizing code

Dataset obtained at +1,05 V vs SCE were also optimized using both code involving the whole PDM and the simplified for p-type semiconduction (reported in *appendix 3*).
New parameters that define the total impedance of the system are:

$$DD = \Omega \cdot (b_3 k_3) \cdot R_{ct}$$

$$EE = \omega\left[k_1 + C_{dl} \cdot R_{ct} \cdot \Omega \cdot (b_3 k_3) \cdot k_1 + R_{ct} \cdot I_V \cdot k_1 + R_{ct} \cdot I_M \cdot k_4 \cdot (a_4 - a_1)\right]$$

$$FF = \Omega \cdot (b_3 k_3) \cdot k_1 - \omega^2 \cdot C_{dl} \cdot R_{ct} \cdot k_1 + \\ + R_{ct} \cdot \begin{bmatrix} \Omega \cdot (k_3 b_3) \cdot I_v \cdot k_1 + I_L \cdot \Omega \cdot (a_3 \cdot k_3 - a_7 \cdot k_7 \cdot C_H^n) \cdot k_1 + \\ + \Omega \cdot (k_3 b_3) \cdot I_M \cdot k_4 \cdot (a_4 - a_1) + k_4 \cdot b_1 \cdot I_M \cdot \Omega \cdot (a_3 \cdot k_3 - a_7 \cdot k_7 \cdot C_H^n) \end{bmatrix}$$

$$GG = \omega \cdot R_{ct} \cdot k_1$$

Optimization error at +1,05 V vs SCE using the whole PDM equations was appreciable with a peak error closed to 30%.

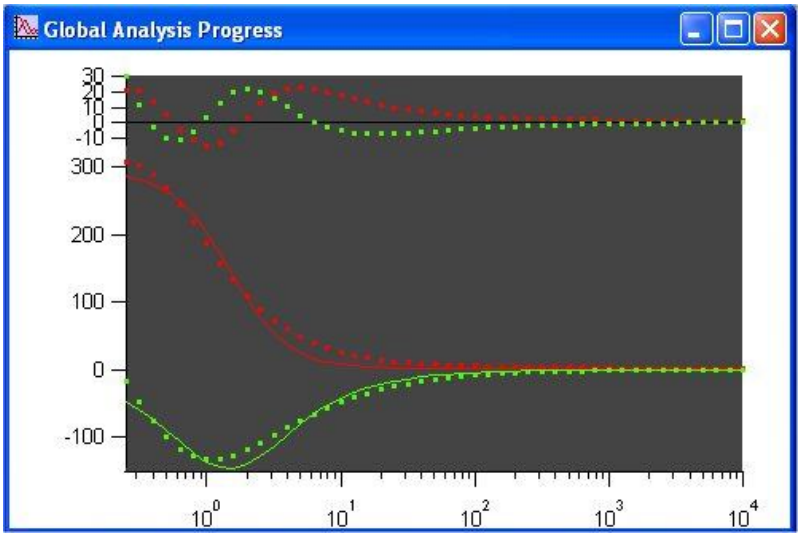

Figure 70: Data fitting and error graph monitor corresponding to the optimization at +1,05 V vs SCE

Looking to the *figure 71*, the overlay between complete and p-type optimization confirm that at 1,05 V vs SCE, a switch from an n-type to a p-type semiconduction has been obtained.

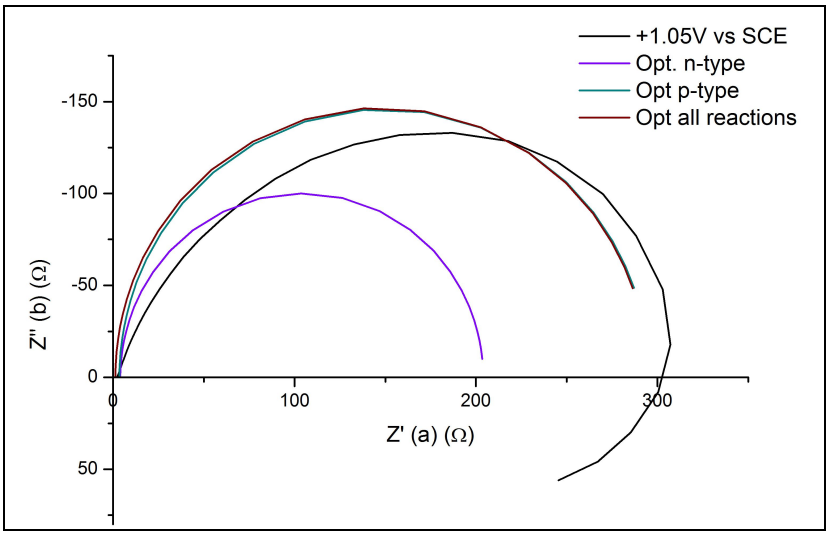

Figure 71: Optimized Nyquist plot for "as received" 347HFG SS at +1,05 V vs SCE using all optimizing codes

Optimized parameters obtained starting from impedance data obtained at +1,05 V vs SCE are reported here:

Parameter	Value	Parameter	Value
R_s (Ω/cm^2)	1,85(up limit: 3)	k_1^{00} (s^{-1})	3,19e-10
R_{ct} (Ω/cm^2)	7,02e16	k_2^{00} (mol/cm^2s)	2,96e-10
C_{dl} (F/cm^2)	3,7e-4	k_3^{00} (mol/cm^2s)	1,16e-14
Thickness (cm)	3,03e-7	k_4^{00} (mol/cm^2s)	4,97e-11
α	0,724 (fix)	k_5^0 (cm/s)	2,16e-8
α_1	0,220	k_7^0 (cm/s)	5,03e-10
α_2	0,413	Ω (cm^3/mol)	14,59 (fix)
α_3	0,296	ε (V/cm)	3e6 (fix)
α_4	0,878	ϕ^0	0 (fix)
α_5	0,716	pH	-0,6 (fix)
α_7	0,509	T (K)	298 (fix)
n	0,5 (fix)	V (V vs NHE)	1,29(fix)
d	3 (fix)	I (A/cm^2)	0,000157 (fix)
χ	3 (fix)	β	-0,01 (fix)
k_1 (s^{-1})	3,40e-20	k_2 (mol/cm^2s)	5,64e-29

k_3 (mol/cm^{2}s)	4,45e-28	k_4 (mol/cm^{2}s)	2,68e-11
k_5 (cm/s)	2,16e-8	k_7 (cm/s)	5,03e-10

Table 6: Optimized values for "as received" 347HFG SS at +1,05 mV vs SCE

So, by applying the Point Defect Model, numbers able to quantify passivity involved reactions are obtained. We are still working on this topic in order to have a comparison between “as received” and oxidized specimens.

FINAL REMARKS

Summarizing, in the present doctorate thesis, the following aspects regarding behaviour of alloy for high temperature applications were investigated:

- Microstructural characterization of solution annealed AISI 310N, 347HFG and 304 HCu (the latter supplied also in the shoot peened condition) was carried out. An homogeneous austenitic fine grain structure accompanied with Nb segregation was observed for 347HFG and 304HCu. In the case of 310N the grains were coarser and the presence of Si segregation were randomly detected beside Nb.
- Microhardness profiles (HV_{50}) were conducted to evaluate the penetration effects of shoot peening treatment at depths as high as 150-200 μm.
- Discontinuous oxidation testing were performed at temperatures in the range of 700-900°C under 15 Nm^3/h flowing moist air atmosphere for 7 days. The preliminary results seem to confirm an oxidation susceptibility in the following order: 310N<347HFG<304HCu.
- Oxidation kinetic study (thermogravimetric tests) of as received AISI 310N, 347HFG, 304HCu and Alloy 617 in oxygen atmosphere at 900°C; 310N, 347HFG and Alloy 617 show a protective oxidation kinetic, while 304HCu suffers from spalling.
- Investigation of grown oxide layer nature of all SS by microscopic techniques revealed an average oxide thickness in the range of 5 – 15 μm for 347HFG; about 5 μm until spallation for 304HCu and less than 5 μm for 310N. In the case of 347HFG a three layer oxide was clearly detected consisting of a first layer of Cr oxides followed by a mixed Fe and Cr oxide and finally an external layer of FeO_x. For 310N only a Cr oxide layer was detectable; for 304HCu the layer being essentially Fe-Cr oxides. Result confirmed also by GDOES.
- Study of the electrochemical behaviour of as received and oxidized SS specimens by means of polarization curves. All “as received” specimens exhibit a similar passive behaviour in terms of both potentials and current densities, apart the point corresponding at the critical passive current (i_{cr}) On oxidized samples, secondary passivations are weaker.
- New electrochemical approaches were tested during a period spent following Dr. Digby Macdonald's research labs at The Pennsylvania State University focusing on the passivity study of 347HFG stainless steel. Starting from the results of the potentiodynamic studies, an electrochemical impedance spectroscopy procedure was setted up; results were optimized by applying the “point defect model” developed by the same Dr. Macdonald revealing kinetic parameters of the passive layer and is semiconductive nature that is essentially n-type for all anodic potential values except near the breakdown in which assume a p-type character.

We are still working on electrochemical impedance studies in order to complete the alloys characterization also in oxidized status in order to obtain a complete description of the system evolution from the passive state at room temperature to conditions after working cycles at high temperature.

BIBLIOGRAPHY

1. Bregani F., *Corrosione in impianti di potenza*, ENEL/CRTN (1988)
2. Kofstad P., *High temperature Corrosion*, Elsevier applied science (1988)
3. Bianchi G., Mazza F., *Corrosione e protezione dei metalli*, AIM (2005)
4. Viswanathan R., Sarver J. et al., *J. Mat. Eng. Perf.*, 15 (2006) p. 255-274
5. Quaddakers W.J., Zurek J. et al., *JOM*, 61 (2009) p. 44-50
6. Matsuo H., Nishiama Y., *Adv. Mat. Tech. for Fossil Power Plants*, ASM int. (1992)
7. Osgerby S., Fry A., *Adv. Mat. Tech. for Fossil Power Plants*, ASM int. (1992)
8. Otsuka N., Fujikawa H., *Corrosion*, 47 (1991) p.240-248
9. Osgerby S., Fry R.T., *Mater. Res.*, 7 (2004) p.141-146
10. Meetham G. W., *J. Mat. Sci.*, 26 (1991) p.853-860
11. ASM Handbooks vol.9, Metallography and Microstructures 9th ed., ASM int. (1992)
12. Wu Q., Vasudevan V. et al., *Metallurg. Mat. Trans. A*, 39A (2008) p.2569-2585
13. Sourmail T., *Mat. Sci. Tech.*, 17 (2001) p.1-14
14. Cabrera A. L., *J. Vac. Sci. Tech. A*, 7 (1989) p.2681-2687
15. Mascanzoni A., Trucco U., *Metallurgia Italiana*, 4 (1967) p.277-282
16. Grabke H.J., Auer W. et al., *Werk. Und Korr.*, 44(1993) p.345-350
17. Trindade V.B., Krupp U., *Mat. And Corr.*, 56 (2005) p.785-790
18. Asteman H., Svensson J.E., *J. Electrochem. Soc.*, 151 (2004) p.B141-B150
19. Hussain N., Schanz G., *Ox. of Met.*, 32 (1989) p.405-431
20. Schweinsberg D.P., Sun B., *J. Appl. Electrochem.*, 23 (1993) p.1097-1101
21. Schweinsberg D.P., Sun B., *J. Appl. Electrochem.*, 24 (1994) p.803-807
22. Orazem M., Tribollet B., E*lectrochemical Impedance Spectroscopy*, Wiley (2008)
23. Macdonald D.D., Sun A., *Electrochim. Acta*, 51 (2006) p.1767-1779
24. Rosas Camacho O., *PhD Thesis*, (2010)
25. Macdonald D.D., Sun A. et al., *J. Electroanal. Chem.*, 572 (2004) p.421-431

26. Fattah-Alhosseini A., Soltani F. et al., *Coor. Sci.*, 53 (2011) p.3186-3192

27. Olsson C., Landolt D., *Electrochim. Acta,* 48 (2003) p.1093-1104

APPENDIX 1

Designation: E 112 – 96$^{\epsilon 3}$

Standard Test Methods for Determining Average Grain Size[1]

This standard is issued under the fixed designation E 112; the number immediately following the designation indicates the year of original adoption or, in the case of revision, the year of last revision. A number in parentheses indicates the year of last reapproval. A superscript epsilon (ε) indicates an editorial change since the last revision or reapproval.

This standard has been approved for use by agencies of the Department of Defense.

ε[1] NOTE—Equations A1.4, A1.5 and A1.6 were editorially revised in April 2000.
ε[2] NOTE—New numbers were assigned to the adjuncts in February 2003.
ε[3] NOTE—Footnotes 4, 5 and 9 were editorially corrected and footnote 8 was editorially removed in May 2004.

INTRODUCTION

These test methods of determination of average grain size in metallic materials are primarily measuring procedures and, because of their purely geometric basis, are independent of the metal or alloy concerned. In fact, the basic procedures may also be used for the estimation of average grain, crystal, or cell size in nonmetallic materials. The comparison method may be used if the structure of the material approaches the appearance of one of the standard comparison charts. The intercept and planimetric methods are always applicable for determining average grain size. However, the comparison charts cannot be used for measurement of individual grains.

1. Scope

1.1 These test methods cover the measurement of average grain size and include the comparison procedure, the planimetric (or Jeffries) procedure, and the intercept procedures. These test methods may also be applied to nonmetallic materials with structures having appearances similar to those of the metallic structures shown in the comparison charts. These test methods apply chiefly to single phase grain structures but they can be applied to determine the average size of a particular type of grain structure in a multiphase or multiconstituent specimen.

1.2 These test methods are used to determine the average grain size of specimens with a unimodal distribution of grain areas, diameters, or intercept lengths. These distributions are approximately log normal. These test methods do not cover methods to characterize the nature of these distributions. Characterization of grain size in specimens with duplex grain size distributions is described in Test Methods E 1181. Measurement of individual, very coarse grains in a fine grained matrix is described in Test Methods E 930.

1.3 These test methods deal only with determination of planar grain size, that is, characterization of the two-dimensional grain sections revealed by the sectioning plane. Determination of spatial grain size, that is, measurement of the size of the three-dimensional grains in the specimen volume, is beyond the scope of these test methods.

1.4 These test methods describe techniques performed manually using either a standard series of graded chart images for the comparison method or simple templates for the manual counting methods. Utilization of semi-automatic digitizing tablets or automatic image analyzers to measure grain size is described in Test Methods E 1382.

1.5 These test methods deal only with the recommended test methods and nothing in them should be construed as defining or establishing limits of acceptability or fitness of purpose of the materials tested.

1.6 The measured values are stated in SI units, which are regarded as standard. Equivalent inch-pound values, when listed, are in parentheses and may be approximate.

1.7 *This standard does not purport to address all of the safety concerns, if any, associated with its use. It is the responsibility of the user of this standard to establish appropriate safety and health practices and determine the applicability of regulatory limitations prior to use.*

1.8 The paragraphs appear in the following order:

[1] These test methods are under the jurisdiction of ASTM Committee E-4 on Metallography and are the direct responsibility of Subcommittee E04.08 on Grain Size.

Current edition approved May 10, 1996. Published July 1996. Originally published as E 112 – 55 T. Last previous edition E 112 – 95.

Copyright © ASTM International, 100 Barr Harbor Drive, PO Box C700, West Conshohocken, PA 19428-2959, United States.

Remaining part of the ATSM E112 standard is reported only in the author’s personal copy

Remaining part of the ATSM E112 standard is reported only in the author’s personal copy

Remaining part of the ATSM E112 standard is reported only in the author’s personal copy

Remaining part of the ATSM E112 standard is reported only in the author’s personal copy

Remaining part of the ATSM E112 standard is reported only in the author’s personal copy

Remaining part of the ATSM E112 standard is reported only in the author’s personal copy

Remaining part of the ATSM E112 standard is reported only in the author’s personal copy

Remaining part of the ATSM E112 standard is reported only in the author’s personal copy

Remaining part of the ATSM E112 standard is reported only in the author’s personal copy

Remaining part of the ATSM E112 standard is reported only in the author’s personal copy

Remaining part of the ATSM E112 standard is reported only in the author’s personal copy

Remaining part of the ATSM E112 standard is reported only in the author’s personal copy

Remaining part of the ATSM E112 standard is reported only in the author’s personal copy

Remaining part of the ATSM E112 standard is reported only in the author’s personal copy

Remaining part of the ATSM E112 standard is reported only in the author’s personal copy

Remaining part of the ATSM E112 standard is reported only in the author’s personal copy

Remaining part of the ATSM E112 standard is reported only in the author’s personal copy

Remaining part of the ATSM E112 standard is reported only in the author’s personal copy

Remaining part of the ATSM E112 standard is reported only in the author’s personal copy

Remaining part of the ATSM E112 standard is reported only in the author’s personal copy

Remaining part of the ATSM E112 standard is reported only in the author’s personal copy

Remaining part of the ATSM E112 standard is reported only in the author’s personal copy

Remaining part of the ATSM E112 standard is reported only in the author’s personal copy

Remaining part of the ATSM E112 standard is reported only in the author’s personal copy

Remaining part of the ATSM E112 standard is reported only in the author’s personal copy

APPENDIX 2

IMPEDANCE MODELS

Models are made to understand a physical phenomenon; they're often a mathematical representation of what is known as reality.

In electrochemistry, the target of a model is identifying processes at the interfaces or finding out some parameters that could be useful for obtaining information about certain processes. The best model that describes reaction happening at the interfaces of a passive metal is the Point Defect Model (PDM). Point defects are responsible for properties exhibited by films which include the early stages of film formation to the steady state measurements of thick films. Underlying mechanisms for describing currents, thickness, impedances and structures are based on the defects chemistry of the layers [25].

DEVELOPMENT OF THE POINT DEFECT MODEL IN IMPEDANCE

Experimentally has been demonstrated that there's always one predominant defect that accounts for charge transfer in a oxide layer; that defect can be cations interstitials, anions vacancies or metal vacancies where each one gives to the film a semiconductive character: metal vacancies give a p-type semiconduction while cation interstitials and anions vacancies an n-type; anion interstitials are negligible.

Mott-Shottky analysis determines the semiconductive character of a semiconductive film considering his capacitance at different potentials; a n-type semiconductor respect the following rule:

$$\frac{1}{C^2} = \frac{2}{\varepsilon\varepsilon_0 e N_D}\left(V - V_{fb} - \frac{kt}{e}\right)$$

while a p-type

$$\frac{1}{C^2} = \frac{-2}{\varepsilon\varepsilon_0 e N_A}\left(V - V_{fb} - \frac{kt}{e}\right)$$

where C is the semiconductor capacitance, ε the semiconductor dielectric constant, ε_0 the vacuum permittivity (8,85e-14 F/cm), *e* the electron charge (1,60e-19 C), V the applied potential, V_{fb} the flat

band potential, $N_{D\ (A)}$ the donor (acceptor) density, k the Boltzmann constant, the term kt/e has a value about 0,025 V at 25°C.

So, from slopes of C^{-2} as function of potentials, is clearly seeable the semiconductive nature.

On a passive or anodic film, interfacial defects generation/annihilation reactions are postulated to occur at the passive film interfaces as reported in *figure A 2.1* where, according to the Kroeger-Vink notation, m = metal atom, $V_M^{\chi'}$ = cation vacancy in the barrier layer, $M_i^{\chi+}$ = interstitial cation in the barrier layer, M_M = metal cation on the metal sublattice of the barrier layer, $V_O^{\bullet\bullet}$ = oxygen vacancy on the oxygen sublattice of the barrier layer, O_O = oxygen anion on the oxygen sublattice of the barrier layer, $M^{\delta+}$ = metal cation in solution, $MO_{\chi/2}$ = oxide barrier layer, χ = cation oxidation state into the barrier layer, δ = cation oxidation state in solution, k_i = reaction rates and L = barrier layer thickness.

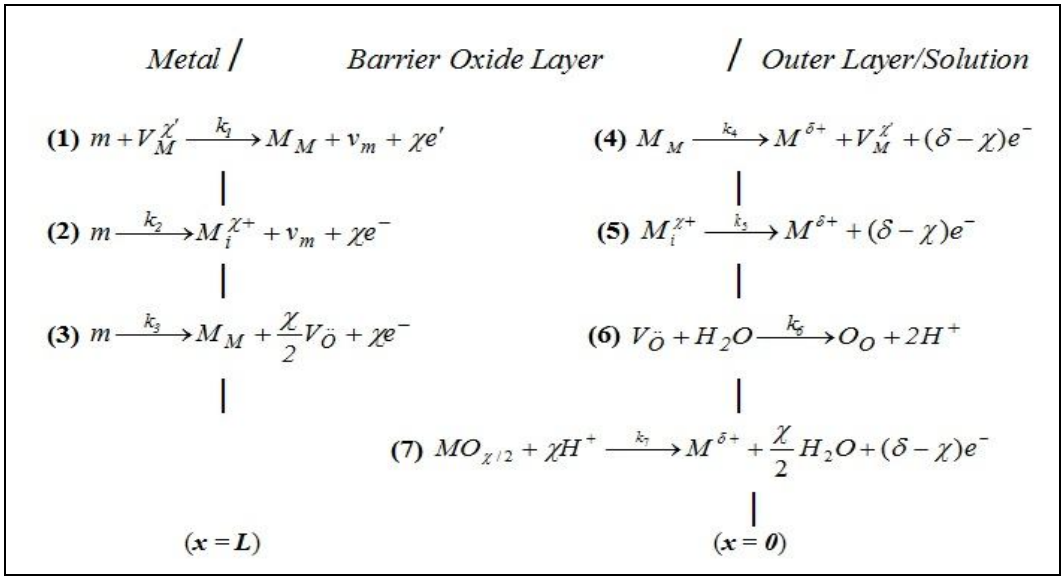

Figure A 2. 1: Interfacial defects generation/annhilation according to the Point Defect Model

According to PDM theory, an external porous layer could be present as result of corrosion products reprecipitation.

Reaction rate constants are function of the potential drops across the interfaces and may be function of potential across the layers which implies that rate constant can be function of the layer thickness (L) and pH.

The applied potential at the barrier layer/outer layer interface (BL/OL) is related to the potential applied to the entire system (V) and the potential drop across the outer layer (IR_{ol}, where I is the

total current density and R_{ol} the specific resistance of the outer layer). R_{ol} is dependant to physical properties of precipitated layer such as porosity, tortuosity, thickness, pores shape etc.

The potential drop IR_{ol} hasn't to be underevaluated during calculation of the barrier layer steady state thickness.

Rate constants for reactions reported in *figure A 2.1*, are written as follows according to PDM theory [24]:

$$k_i = k_i^0 e^{a_i (V - IR_{ol})} e^{-b_i L} e^{c_i pH}$$

where here *i* is related to reactions 1, 2 and 3 of PDM.

And

$$k_i = k_i^0 e^{a_i (V - IR_{ol})} e^{c_i pH}$$

where here *i* is related to reactions 4, 5, 6 and 7 of PDM.

Parameters of the rate constant definition are reported in *table A 2.1* where α_i are the transfer coefficients, γ the value F/RT (F is the Faraday constant, R the gas constant and T the absolute temperature), α the dependence of potential drop across the BL/OL interface on the applied potential V and is calculated as $\alpha = d\phi/dV$ with ϕ the potential drop across BL/OL interface, β the polarizability of BL/OL interface calculated as $\beta = d\phi/dpH$ and ε the dielectric constant.

Reaction	a_i (V^{-1})	b_i (cm^{-1})	c_i
$m + V_M^{\chi'} \xrightarrow{k_1} M_M + v_m + \chi e'$	$\chi\alpha_1(1-\alpha)\gamma$	$\chi\alpha_1\gamma\varepsilon$	$-\chi\alpha_1\gamma\beta$
$m \xrightarrow{k_2} M_i^{\chi+} + v_m + \chi e^-$	$\chi\alpha_2(1-\alpha)\gamma$	$\chi\alpha_2\gamma\varepsilon$	$-\chi\alpha_2\gamma\beta$
$m \xrightarrow{k_3} M_M + \frac{\chi}{2} V_{\ddot{O}} + \chi e^-$	$\chi\alpha_3(1-\alpha)\gamma$	$\chi\alpha_3\gamma\varepsilon$	$-\chi\alpha_3\gamma\beta$
$M_M \xrightarrow{k_4} M^{\delta+} + V_M^{\chi'} + (\delta - \chi)e^-$	$(\delta-\chi)\alpha_4\alpha\gamma$	0	$(\delta-\chi)\alpha_4\gamma\beta$
$M_i^{\chi+} \xrightarrow{k_5} M^{\delta+} + (\delta - \chi)e^-$	$(\delta-\chi)\alpha_5\alpha\gamma$	0	$(\delta-\chi)\alpha_5\gamma\beta$
$V_{\ddot{O}} + H_2O \xrightarrow{k_6} O_O + 2H^+$	$2\alpha_6\alpha\gamma$	0	$2\alpha_6\gamma\beta$
$MO_{\chi/2} + \chi H^+ \xrightarrow{k_7} M^{\delta+} + \frac{\chi}{2} H_2O + (\delta - \chi)e^-$	$(\delta-\chi)\alpha_7\alpha\gamma$	0	$(\delta-\chi)\alpha_7\gamma\beta$

Table A 2. 1: Parameters in the rate constants for interfacial reactions for PDM [24]

According to the *figure A 2.1*, the total current density of the system is related to reactions that produce or consume electrons, so reactions 1, 2, 3, 4, 5 and 7. The expression of the total current density is:

$$I = F\left\{\chi k_1 C_v^L + \chi k_2 + \chi k_3 + (\delta-\chi)k_4 + (\delta-\chi)k_5 C_i^0 + (\delta-\chi)k_7 \frac{c_{H^*}^L}{c_{H^+}^0}\right\}$$

where C_v^L are the concentration of cation vacancies at the metal/barrier layer (M/BL) interface, C_i^0 the concentration of cation interstitials at the BL/OL and $C_{H+}{}^L/C_{H+}{}^0$ is the report between H^+ concentration at the two interphases.

In order to simplify the rate constants introduce into the total current expression, pH at BL/OL interface is taken as constant (experimentally is used to work in buffered solutions), introducing parameters e^{cipH} into k_i^0; so pH becomes independent from potential. The new expressions of rate constants are:

$$k_i = k_i^0 e^{a_i(V-IR_{ol})} e^{-b_i L}$$

and

$$k_i = k_i^0 e^{a_i(V-IR_{ol})}$$

The expressions of k_i^0 are reported in *table A 2.2*

Reaction	k_i^0
$m + V_M^{\chi'} \xrightarrow{k_1} M_M + v_m + \chi e'$	$k_1{}^{00}\exp[-\chi\alpha_1\gamma(\phi+\beta pH)]$ [s^{-1}]
$m \xrightarrow{k_2} M_i^{\chi+} + v_m + \chi e^-$	$k_2{}^{00}\exp[-\chi\alpha_2\gamma(\phi+\beta pH)]$ [mol cm^{-2} s^{-1}]
$m \xrightarrow{k_3} M_M + \frac{\chi}{2}V_{\ddot{O}} + \chi e^-$	$k_3{}^{00}\exp[-\chi\alpha_3\gamma(\phi+\beta pH)]$ [mol cm^{-2} s^{-1}]
$M_M \xrightarrow{k_4} M^{\delta+} + V_M^{\chi'} + (\delta-\chi)e^-$	$k_4{}^{00}\exp[(\delta-\chi)\alpha_4\gamma(\phi+\beta pH)]$ [mol cm^{-2} s^{-1}]
$M_i^{\chi+} \xrightarrow{k_5} M^{\delta+} + (\delta-\chi)e^-$	$k_5{}^{00}\exp[(\delta-\chi)\alpha_5\gamma(\phi+\beta pH)]$ [cm s^{-1}]
$V_{\ddot{O}} + H_2O \xrightarrow{k_6} O_O + 2H^+$	$k_6{}^{00}\exp[2\alpha_6\gamma(\phi+\beta pH)]$ [cm s^{-1}]
$MO_{\chi/2} + \chi H^+ \xrightarrow{k_7} M^{\delta+} + \frac{\chi}{2}H_2O + (\delta-\chi)e^-$	$k_7{}^{00}\exp[(\delta-\chi)\alpha_7\gamma(\phi+\beta pH)]$ [mol cm^{-2} s^{-1}]

Table A 2. 2:Values for k_i^0 for rate constants of interfacial reactions for PDM [24]

Renaming the concentrations of cation vacancies, cation interstitials and hydrogen concentration as:

$$C_{V_M^{\chi'}} = C_M^L$$
$$C_{M_i^{\chi+}} = C_i^0$$
$$\frac{c_{H^+}^L}{c_{H^+}^\circ} = C_{H^+}$$

The total current of the system became expressed by the following equation:

$$I = F\left\{\chi k_1 C_M^L + \chi k_2 + \chi k_3 + (\delta - \chi)k_4 + (\delta - \chi)k_5 C_i^0 + (\delta - \chi)k_7 C_{H^+}^n\right\}$$

where n is the reaction order.

Here, I, k_i, L, $C_M{}^L$, $C_i{}^0$ and C_{H+} are function of potential, however, making pH constant, the differential of the total current is:

$$\delta I = \left(\frac{\vartheta I}{\vartheta V}\right)\delta V + \left(\frac{\vartheta I}{\vartheta I}\right)\delta I + \left(\frac{\vartheta I}{\vartheta L}\right)\delta L + \left(\frac{\vartheta I}{\vartheta C_M^L}\right)\delta C_M^L + \left(\frac{\vartheta I}{\vartheta C_i^0}\right)\delta C_i^0$$

that can be expressed as:

$$\delta I = I_V \delta V + I_I \delta I + I_L \delta L + I_M^L \delta C_M^L + I_i^0 C_i^0$$

where

$$I_V = \left(\frac{\vartheta I}{\vartheta V}\right) = F\left\{\chi k_1 a_1 C_M^L + \chi k_2 a_2 + \chi k_3 a_3 + (\delta - \chi)k_4 a_4 + (\delta - \chi)k_5 a_5 C_i^0 + (\delta - \chi)k_7 a_7 C_{H^+}^n\right\}$$

$$I_I = \left(\frac{\vartheta I}{\vartheta I}\right) = -I_V R_{ol}$$

$$I_L = \left(\frac{\vartheta I}{\vartheta L}\right) = -F\left\{\chi k_1 b_1 C_M^L + \chi k_2 b_2 + \chi k_3 b_3\right\}$$

$$I_M^L = \left(\frac{\vartheta I}{\vartheta C_M^L}\right) = F\left\{\chi k_1\right\}$$

$$I_i^0 = \left(\frac{\vartheta I}{\vartheta C_i^0}\right) = F\left\{(\delta - \chi)k_5\right\}$$

Derivation of the total current is now written as:

$$\Delta I = I_V \Delta V + I_I \Delta I + I_L \Delta L + I_M^L \Delta C_M^L + I_i^0 \Delta C_i^0$$

Dividing by ΔV, expression of the admittance is obtained:

$$Y = \frac{\Delta I}{\Delta V} = I_V + I_I \frac{\Delta I}{\Delta V} + I_L \frac{\Delta L}{\Delta V} + I_M^L \frac{\Delta C_M^L}{\Delta V} + I_i^0 \frac{\Delta C_i^0}{\Delta V}$$

The laborious task is to get the variations of these parameters as function of potential. As first instance, growth and dissolution of the film is obtained by balance of reactions 3 and 7:

$$\frac{dL}{dt} = -\frac{2}{\chi}\Omega J_0 - \Omega k_7 C_{H^+}^n = \Omega k_3 - \Omega k_7 C_{H^+}^n$$

where Ω is the volume per mole of cations in the barrier layer and J_0 the flux of oxygen vacancies.

If δI=ΔIexp(jωt) with ω angular frequency of the current and j the square root of -1, equation became

$$\frac{d\delta L}{dt} = \Omega k_3 a_3 \delta V - \Omega k_3 a_3 R_{ol} \delta I - \Omega k_3 b_3 \delta L - \Omega k_7 a_7 C_{H^+}^n \delta V + \Omega k_7 a_7 C_{H^+}^n R_{ol} \delta I$$

so

$$j\omega \Delta L = \Omega\left(k_3 a_3 - k_7 a_7 C_{H^+}^n\right)\Delta V - \Omega\left(k_3 a_3 R_{ol} - k_7 a_7 R_{ol} C_{H^+}^n\right)\Delta I - \Omega k_3 b_3 \Delta L$$

and

$$\frac{\Delta L}{\Delta V} = \frac{\Omega\left(k_3 a_3 - k_7 a_7 C_{H^+}^n\right)}{j\omega + \Omega k_3 b_3} - \frac{\Omega\left(k_3 a_3 R_{ol} - k_7 a_7 R_{ol} C_{H^+}^n\right)}{j\omega + \Omega k_3 b_3} \frac{\Delta I}{\Delta V}$$

Variation of the thickness of the barrier layer as a function of rate constants can be written as

$$\frac{\Delta L}{\Delta V} = L_V + L_I \frac{\Delta I}{\Delta V}$$

with

$$L_V = \frac{\Omega\left(k_3 a_3 - k_7 a_7 C_{H^+}^n\right)}{j\omega + \Omega k_3 b_3}$$

and

$$L_I = \frac{\Omega\left(k_3 a_3 R_{ol} - k_7 a_7 R_{ol} C_{H^+}^n\right)}{j\omega + \Omega k_3 b_3}$$

C_M^L and C_i^0 can be known considering that steady state has been reached so their expression can be obtained directly from chemical reactions:

$$C_M^L = \frac{k_4}{k_1}$$

$$C_i^0 = \frac{k_2}{k_5}$$

Expanding the rate constant equation for C_M^L:

$$C_M^L = \left\{\frac{k_4^0}{k_1^0} e^{(a_4 - a_1)(V - IR_{ol})} e^{b_1 L}\right\}$$

by deriving for the potential

$$\frac{dC_M^L}{dV} = \left\{\frac{k_4^0}{k_1^0}\right\}(a_4 - a_1)\left(1 - \frac{dI}{dV} R_{ol}\right) e^{(a_4 - a_1)(V - IR_{ol})} e^{b_1 L} + \frac{k_4^0}{k_1^0} e^{(a_4 - a_1)(V - IR_{ol})} e^{b_1 L} \frac{dL}{dV}$$

$$\frac{\Delta C_M^L}{\Delta V} = \frac{k_4}{k_1}(a_4 - a_1) - \frac{k_4}{k_1}(a_4 - a_1) R_{ol} \frac{\Delta I}{\Delta V} + \frac{k_4}{k_1} b_1 \frac{\Delta L}{\Delta V}$$

naming groups of variables respectively as C_{MV}^L, C_{MI}^L and C_{ML}^L, the dependency of C_M^L from the potential is:

$$\frac{\Delta C_M^0}{\Delta V} = C_{MV}^L + C_{MI}^L \frac{\Delta I}{\Delta V} + C_{ML}^L \frac{\Delta L}{\Delta V}$$

Following the same procedure for C_i^0, the derived equation is:

$$\frac{\Delta C_i^0}{\Delta V} = C_{iV}^0 + C_{iI}^0 \frac{\Delta I}{\Delta V} + C_{iL}^0 \frac{\Delta L}{\Delta V}$$

with

$$C_{iV}^0 = \frac{k_2}{k_5}(a_2 - a_5) \qquad C_{iI}^0 = -\frac{k_2}{k_5}(a_2 - a_5) R_{ol} \qquad C_{iL}^0 = -\frac{k_2}{k_5} b_2$$

After substitutions and solving for ΔI/ΔV, he expression of the total admittance becomes:

$$Y_f = \frac{\Delta I}{\Delta V} = \frac{I_V + I_L + I_M^L\left[C_{MV}^L + C_{ML}^L L_V\right] + I_i^0\left[C_{iV}^0 + C_{iL}^L L_V\right]}{1 - \left\{I_I + I_L L_I + I_M^L\left[C_{MI}^L + C_{ML}^L L_I\right] + I_i^0\left[C_{iI}^0 + C_{iL}^0 L_I\right]\right\}}$$

That is the faradaic admittance of the system. The inverse of the faradaic admittance is the faradaic impedance.

$$Z_f = \frac{1}{Y_f}$$

Faradaic impedance (Z_f) is, by definition, an active element that includes rate transfer of electroactive species to an electrode surface.

On the Y_f expression, simplifications are possible.

The system considered in the present work regards passivity of a stainless steel so the involved cation is Cr^{3+} and the reactions are the followings:

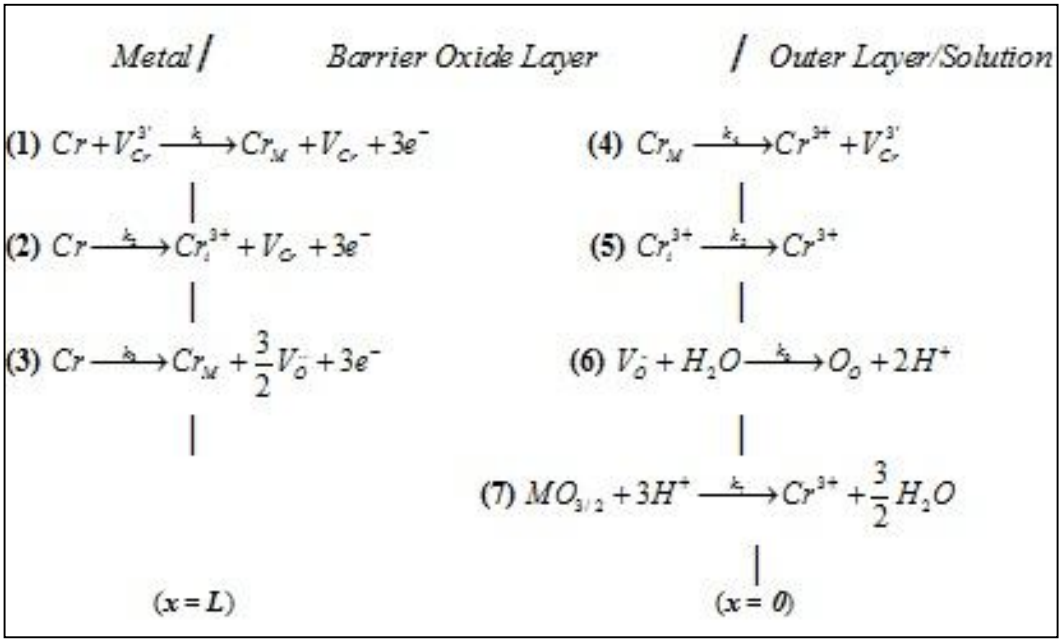

Figure A 2. 2: Interfacial defects generation/annihilation on a stainless steel surface according to the PDM

In the considered system there's no presence of any outer layer so R_{ol} is equal to zero. Being an n-type semiconductor, reactions to be considered in the current definition are 2, 3, 5 and 7 giving the followings final equations:

$$I_V = F \cdot (3a_2k_2 + 3a_3k_3)$$

$$I_L = -F(3b_2k_2 + 3b_3k_3)$$

$$Y_f = I_V + I_L \frac{\Omega k_3 a_3 - k_7 a_7 C_H^n}{j\omega + \Omega \cdot k_3 b_3}$$

When the system is switched to a p-type semiconduction, reaction to be considered are 1, 4 and 7 giving the followings equations of current components and admittance:

$$I_V = F \cdot \left(3k_1 a_1 \frac{k_4}{k_1} \right)$$

$$I_L = -F\left(3k_1 b_1 \frac{k_4}{k_1} \right)$$

$$I_M = F3k_1$$

$$Y_f = I_V + \frac{I_L \Omega (a_1 k_1 - a_7 k_7 C_H^n)}{j\omega + \Omega(b_1 k_1)} + \frac{I_M k_4 (a_4 - a_1 + b_1 L_v)}{k_1}$$

From that expression of the faradaic admittance, faradaic impedance is obtained and that has to be summed with impedance of the passive elements of the circuit (resistances, capacitances, inductance, Warburg elements etc.), elaborated to obtain the impedance equation in the form of $Z_{tot}=Z'+jZ''$.

Once obtained the expression of Z_{tot}, parameters are obtained with the aim of a curfe fitting program which accept as input data experimental Z' and Z'' as function of frequency obtained by electrochemical impedance spectroscopy.

APPENDIX 3.a

OPTIMIZATION CODE FOR n-TYPE SEMICONDUCTION CODE FOR IGOR © DATA FITTING SOFTWARE


```
#pragma rtGlobals=1        // Use modern global access method.

Function ZrealAllinc(w,frequency) : FitFunc
      Wave w
      Variable frequency
      Variable g,a2,a3,a5,a7,b2,b3,Sp,k2,k3,k5,k7,IU,IL,Zt,Zre,Zim,wangular,Ch,F,R,K02,K03,AA,BB,DD,EE,FF,GG


      //CurveFitDialog/ These comments were created by the Curve Fitting dialog. Altering them will
      //CurveFitDialog/ make the function less convenient to work with in the Curve Fitting dialog.
      //CurveFitDialog/ Equation:
      //CurveFitDialog/ f(frequency) = COMPLICATED
      //CurveFitDialog/ End of Equation
      //CurveFitDialog/ Independent Variables 1
      //CurveFitDialog/ frequency
      //CurveFitDialog/ Coefficients 24
      //CurveFitDialog/ w[0] = alpha
      //CurveFitDialog/ w[1] = alpha2
      //CurveFitDialog/ w[2] = alpha3
      //CurveFitDialog/ w[3] = alpha5
      //CurveFitDialog/ w[4] = alpha7
      //CurveFitDialog/ w[5] = n
      //CurveFitDialog/ w[6] = d
      //CurveFitDialog/ w[7] = chi
      //CurveFitDialog/ w[8] = k2oo
      //CurveFitDialog/ w[9] = k3oo
      //CurveFitDialog/ w[10] = k7o
      //CurveFitDialog/ w[11] = omega
      //CurveFitDialog/ w[12] = Cdl
      //CurveFitDialog/ w[13] = Rct
      //CurveFitDialog/ w[14] = V
      //CurveFitDialog/ w[15] = I
      //CurveFitDialog/ w[16] = T
      //CurveFitDialog/ w[17] = pH
      //CurveFitDialog/ w[18] = epsilon
      //CurveFitDialog/ w[19] = Rs
      //CurveFitDialog/ w[20] = k5o
      //CurveFitDialog/ w[21] = phio
      //CurveFitDialog/ w[22] = bet
      //CurveFitDialog/ w[23] = L


// This optimization program is for a n-type bilayer film when only oxygen vacancies
// and metal interstitials are the main charge carriers.

//             |                                        |
//            k2       x+                              |
//         M ---|--> Mi   + xe'                    x+    k5    d+
//             |                                  Mi -------|------> M  + (d-x)e'
//            k3                  ..                      |
//         M ---|--> Mm +(x/2)Vo + xe      ..            k6             +
//             |                              Vo + H2O ---|--> Oo + 2H
//             |                                        |
//             |                                     +  k7    d+
//             |                          MO(x/2) + xH ---|--> M  + (x/2) H2O + (d-x)e'
//             |                                        |
//             |                                        |
//           X=0                                      X=Sp
```

```
//  Equivalent circuit used in this optimization procedure
//
//          _____
//         |     |            |
//      ---|  Zf |------------|    |
//      |  |_____|          |    |
//      |                   |    |
//      |      |      |     |    |
//   -------------| Cdl |-------|----|----Rs---
//      |      |      |     |    |
//      |                   |    |
//      |---------Rct---------|    |
//                            |
//                            |
//  BARRIER LAYER       |       SOLUTION

      R=8.314472 //Gas Constant [J/mol*K] or [C*Volt/mol K]
      F=96485.34 // Faraday's Constant [J/mol]

      wangular=2*Pi*frequency // Angular frequency
      Ch=10^(-w[17]) // [mol/cm^3] Protons concentration in the bulk
      g=F/(R*w[16]) // Gama=F/(RT)


      a2=w[1]*(1-w[0])*g*w[7]   // [V^-1]
      a3=w[2]*(1-w[0])*g*w[7]   // [V^-1]
      a5=w[3]*w[0]*g*(w[6]-w[7])   // [V^-1]
      a7=w[4]*w[0]*g*(w[6]-w[7])   // [V^-1]

      b2=w[7]*w[1]*g*w[18]  // [cm^-1]
      b3=w[7]*w[2]*g*w[18]  // [cm^-1]

      K02=w[8]*exp(-w[7]*w[1]*g*(w[21]+w[22]*w[17]))   // Standard rate constant reaction 2
      K03=w[9]*exp(-w[7]*w[2]*g*(w[21]+w[22]*w[17]))   //Standard rate constant reaction 3

      Sp=(-1/b3)*ln((w[10]/K03)*10^(-w[5]*w[17]))-(a7-a3)*w[14]/b3       // Steady-state thickness [cm]


      k2=K02*exp(a2*w[14]-b2*Sp)
      k3=K03*exp(a3*w[14]-b3*Sp)
      k5=w[20]*exp(a5*w[14])
      k7=w[10]*exp(a7*w[14])


      IU=F*(w[7]*a2*k2+w[7]*a3*k3)
      IL=-F*(w[7]*b2*k2+w[7]*b3*k3)

      AA=w[11]*(k3*a3+k7*a7*Ch^w[5])
      BB=w[11]*(k3*b3)

      DD=BB*w[13]
      EE=wangular*w[13]*BB*w[12]+wangular+wangular*w[13]*IU
      FF=BB+IL*AA*w[13]+BB*IU*w[13]-wangular^2*w[12]*w[13]
      GG=wangular*w[13]

      Zre=w[19]+(FF*DD+EE*GG)/(FF^2+EE^2)

      return Zre
```

```
End


Function ZimagAllinc(w,frequency) : FitFunc
	Wave w
	Variable frequency
	Variable g,a2,a3,a5,a7,b2,b3,Sp,k2,k3,k5,k7,IU,IL,Zt,Zre,Zim,wangular,Ch,F,R,K02,K03,AA,BB,DD,EE,FF,GG

//CurveFitDialog/ These comments were created by the Curve Fitting dialog. Altering them will
	//CurveFitDialog/ make the function less convenient to work with in the Curve Fitting dialog.
	//CurveFitDialog/ Equation:
	//CurveFitDialog/ f(frequency) = COMPLICATED
	//CurveFitDialog/ End of Equation
	//CurveFitDialog/ Independent Variables 1
	//CurveFitDialog/ frequency
	//CurveFitDialog/ Coefficients 24
	//CurveFitDialog/ w[0] = alpha
	//CurveFitDialog/ w[1] = alpha2
	//CurveFitDialog/ w[2] = alpha3
	//CurveFitDialog/ w[3] = alpha5
	//CurveFitDialog/ w[4] = alpha7
	//CurveFitDialog/ w[5] = n
	//CurveFitDialog/ w[6] = d
	//CurveFitDialog/ w[7] = chi
	//CurveFitDialog/ w[8] = k2oo
	//CurveFitDialog/ w[9] = k3oo
	//CurveFitDialog/ w[10] = k7o
	//CurveFitDialog/ w[11] = omega
	//CurveFitDialog/ w[12] = Cdl
	//CurveFitDialog/ w[13] = Rct
	//CurveFitDialog/ w[14] = V
	//CurveFitDialog/ w[15] = I
	//CurveFitDialog/ w[16] = T
	//CurveFitDialog/ w[17] = pH
	//CurveFitDialog/ w[18] = epsilon
	//CurveFitDialog/ w[19] = Rs
	//CurveFitDialog/ w[20] = k5o
	//CurveFitDialog/ w[21] = phio
	//CurveFitDialog/ w[22] = bet
	//CurveFitDialog/ w[23] = L

	// This optimization program is for a n-type bilayer film when only oxygen vacancies
	//and metal interstitials are the main charge carriers.

//              |                                        |
//            k2       x+                               |
//         M ---|--> Mi   + xe'                    x+    k5    d+
//              |                                 Mi -------|------> M  + (d-x)e'
//             k3                ..                       |
//         M ---|--> Mm +(x/2)Vo + xe       ..             k6              +
//              |                              Vo + H2O ---|--> Oo + 2H
//              |                                         |
//              |                                       +  k7    d+
//              |                          MO(x/2) + xH ---|--> M  + (x/2) H2O + (d-x)e'
//              |                                         |
//              |                                         |
//            X=0                                      X=Sp
```

```
//  Equivalent circuit used in this optimization procedure
//
//          _____
//         |     |             |
//       ----|  Zf |-----------|    |
//       |   |_____|         |     |
//       |                   |    |
//       |       |      |    |    |
//    -------------| Cdl |-------|----|----Rs---
//       |       |      |    |    |
//       |                  |    |
//       |---------Rct---------|    |
//                             |
//                             |
//  BARRIER LAYER       |       SOLUTION

      R=8.314472 //Gas Constant [J/mol*K] or [C*Volt/mol K]
      F=96485.34 // Faraday's Constant [J/mol]

      wangular=2*Pi*frequency // Angular frequency
      Ch=10^(-w[17]) // [mol/cm^3] Protons concentration in the bulk
      g=F/(R*w[16]) // Gama=F/(RT)


      a2=w[1]*(1-w[0])*g*w[7]   // [V^-1]
      a3=w[2]*(1-w[0])*g*w[7]   // [V^-1]
      a5=w[3]*w[0]*g*(w[6]-w[7])   // [V^-1]
      a7=w[4]*w[0]*g*(w[6]-w[7])   // [V^-1]

      b2=w[7]*w[1]*g*w[18]  // [cm^-1]
      b3=w[7]*w[2]*g*w[18]  // [cm^-1]

      K02=w[8]*exp(-w[7]*w[1]*g*(w[21]+w[22]*w[17]))   // Standard rate constant reaction 2
      K03=w[9]*exp(-w[7]*w[2]*g*(w[21]+w[22]*w[17]))   //Standard rate constant reaction 3

      Sp=(-1/b3)*ln((w[10]/K03)*10^(-w[5]*w[17]))-(a7-a3)*w[14]/b3       // Steady-state thickness [cm]


      k2=K02*exp(a2*w[14]-b2*Sp)
      k3=K03*exp(a3*w[14]-b3*Sp)
      k5=w[20]*exp(a5*w[14])
      k7=w[10]*exp(a7*w[14])


      lU=F*(w[7]*a2*k2+w[7]*a3*k3)
      lL=-F*(w[7]*b2*k2+w[7]*b3*k3)

      AA=w[11]*(k3*a3+k7*a7*Ch^w[5])
      BB=w[11]*(k3*b3)

      DD=BB*w[13]
      EE=wangular*w[13]*BB*w[12]+wangular+wangular*w[13]*lU
      FF=BB+lL*AA*w[13]+BB*lU*w[13]-wangular^2*w[12]*w[13]
      GG=wangular*w[13]

      Zim=(GG*FF-EE*DD)/(FF^2+EE^2)

      return Zim

End
```

APPENDIX 3.b

OPTIMIZATION CODE FOR p-TYPE SEMICONDUCTION CODE FOR IGOR © DATA FITTING SOFTWARE


```
#pragma rtGlobals=1		// Use modern global access method.

Function ZrealAllinc(w,frequency) : FitFunc
	Wave w
	Variable frequency
	Variable g,a1,a4,a7,b1,Sp,k1,k4,k7,IU,IL,IM,Zt,Zre,Zim,wangular,Ch,F,R,K01,K04,AA,BB,DD,EE,FF,GG


	//CurveFitDialog/ These comments were created by the Curve Fitting dialog. Altering them will
	//CurveFitDialog/ make the function less convenient to work with in the Curve Fitting dialog.
	//CurveFitDialog/ Equation:
	//CurveFitDialog/ f(frequency) = COMPLICATED
	//CurveFitDialog/ End of Equation
	//CurveFitDialog/ Independent Variables 1
	//CurveFitDialog/ frequency
	//CurveFitDialog/ Coefficients 21
	//CurveFitDialog/ w[0] = alpha
	//CurveFitDialog/ w[1] = alpha1
	//CurveFitDialog/ w[2] = alpha4
	//CurveFitDialog/ w[3] = alpha7
	//CurveFitDialog/ w[4] = n
	//CurveFitDialog/ w[5] = d
	//CurveFitDialog/ w[6] = chi
	//CurveFitDialog/ w[7] = k1oo
	//CurveFitDialog/ w[8] = k4oo
	//CurveFitDialog/ w[9] = k7o
	//CurveFitDialog/ w[10] = omega
	//CurveFitDialog/ w[11] = epsilon
	//CurveFitDialog/ w[12] = Cdl
	//CurveFitDialog/ w[13] = Rct
	//CurveFitDialog/ w[14] = V
	//CurveFitDialog/ w[15] = I
	//CurveFitDialog/ w[16] = T
	//CurveFitDialog/ w[17] = pH
	//CurveFitDialog/ w[18] = phio
	//CurveFitDialog/ w[19] = Rs
	//CurveFitDialog/ w[20] = bet



// This optimization program is for a p-type monolayer film when only oxygen vacancies
//and metal interstitials are the main charge carriers.

//                  |                                  |
//              x'  k1                                 |
//        M  +Vm---|--> Mi   + xe'                     k4        d+
//                  |                          Mm -------|------> M  + (d-x)e'
//                 k3                                  |
//                  |                                 ..          k6             +
//                  |                          Vo + H2O ---|--> Oo + 2H
//                  |                                  |
//                  |                                +  k7     d+
//                  |                  MO(x/2) + xH ---|--> M  + (x/2) H2O + (d-x)e'
//                  |                                  |
//                  |                                  |
//                X=0                                X=Sp


//  Equivalent circuit used in this optimization procedure
```

```
//          ____
//         |    |          |
//      ---| Zf |----------|    |
//      |  |____|         |    |
//      |                 |    |
//      |      |     |    |    |
//   -----------| Cdl |-------|----|----Rs---
//      |      |     |    |    |
//      |               |    |
//      |--------Rct--------|    |
//                        |
//                        |
//  BARRIER LAYER       |       SOLUTION
```

```
	R=8.314472 //Gas Constant [J/mol*K] or [C*Volt/mol K]
	F=96485.34 // Faraday's Constant [J/mol]

	wangular=2*Pi*frequency // Angular frequency
	Ch=10^(-w[17]) // [mol/cm^3] Protons concentration in the bulk
	g=F/(R*w[16]) // Gama=F/(RT)


	a1=w[1]*(1-w[0])*g*w[6]   // [V^-1]
	a4=w[2]*w[0]*g*(w[5]-w[6])   // [V^-1]
	a7=w[3]*w[0]*g*(w[5]-w[6])   // [V^-1]

	b1=w[6]*w[1]*g*w[11]  // [cm^-1]

	K01=w[7]*exp(-w[6]*w[1]*g*(w[18]+w[20]*w[17]))   // Standard rate constant reaction 1
	K04=w[8]*exp((w[5]-w[6])*w[2]*g*(w[18]+w[20]*w[17]))   //Standard rate constant reaction 4

	Sp=(-1/b1)*ln((w[9]/K01)*10^(-w[4]*w[17]))-(a7-a1)*w[14]/b1       // Steady-state thickness [cm]


	k1=K01*exp(a1*w[14]-b1*Sp)
	k4=K04*exp(a4*w[14])
	k7=w[9]*exp(a7*w[14])


	IU=F*w[6]*a1*k1*(k4/k1)
	IL=-F*w[6]*b1*k1*(k4/k1)
	IM=F*w[6]*k1

	AA=w[10]*(k1*a1-k7*a7*Ch^w[4])
	BB=w[10]*(k1*b1)

	DD=BB*w[13]
	EE=wangular*w[13]*BB*w[12]+wangular+wangular*w[13]*IU
	FF=BB+IL*AA*w[13]+BB*IU*w[13]-wangular^2*w[12]*w[13]+IM*AA*w[13]
	GG=wangular*w[13]

	Zre=w[19]+(FF*DD+EE*GG)/(FF^2+EE^2)

	return Zre

End
```

```
Function ZimagAllinc(w,frequency) : FitFunc
	Wave w
	Variable frequency
	Variable g,a1,a4,a7,b1,Sp,k1,k4,k7,IU,IL,IM,Zt,Zre,Zim,wangular,Ch,F,R,K01,K04,AA,BB,DD,EE,FF,GG


	//CurveFitDialog/ These comments were created by the Curve Fitting dialog. Altering them will
	//CurveFitDialog/ make the function less convenient to work with in the Curve Fitting dialog.
	//CurveFitDialog/ Equation:
	//CurveFitDialog/ f(frequency) = COMPLICATED
	//CurveFitDialog/ End of Equation
	//CurveFitDialog/ Independent Variables 1
	//CurveFitDialog/ frequency
	//CurveFitDialog/ Coefficients 21
	//CurveFitDialog/ w[0] = alpha
	//CurveFitDialog/ w[1] = alpha1
	//CurveFitDialog/ w[2] = alpha4
	//CurveFitDialog/ w[3] = alpha7
	//CurveFitDialog/ w[4] = n
	//CurveFitDialog/ w[5] = d
	//CurveFitDialog/ w[6] = chi
	//CurveFitDialog/ w[7] = k1oo
	//CurveFitDialog/ w[8] = k4oo
	//CurveFitDialog/ w[9] = k7o
	//CurveFitDialog/ w[10] = omega
	//CurveFitDialog/ w[11] = epsilon
	//CurveFitDialog/ w[12] = Cdl
	//CurveFitDialog/ w[13] = Rct
	//CurveFitDialog/ w[14] = V
	//CurveFitDialog/ w[15] = I
	//CurveFitDialog/ w[16] = T
	//CurveFitDialog/ w[17] = pH
	//CurveFitDialog/ w[18] = phio
	//CurveFitDialog/ w[19] = Rs
	//CurveFitDialog/ w[20] = bet



// This optimization program is for a p-type monolayer film when only oxygen vacancies
//and metal interstitials are the main charge carriers.

//                 |                                |
//              x'  k1                              |
//        M  +Vm---|--> Mi   + xe'                   k4        d+
//                 |                          Mm -------|------> M  + (d-x)e'
//                 k3                                 |
//                 |                            ..    k6            +
//                 |                         Vo + H2O ---|--> Oo + 2H
//                 |                                    |
//                 |                                 +  k7    d+
//                 |                       MO(x/2) + xH ---|--> M  + (x/2) H2O + (d-x)e'
//                 |                                    |
//                 |                                    |
//               X=0                                  X=Sp


//  Equivalent circuit used in this optimization procedure
//
//         ____
//        |    |            |
```

```
//        ----|   Zf  |----------|     |
//        |   |_____ |          |     |
//        |                      |    |
//        |       |      |       |    |
//     -------------| Cdl |-------|----|----Rs---
//        |       |      |       |    |
//        |                      |    |
//        |---------Rct----------|    |
//                                |
//                                |
//   BARRIER LAYER        |        SOLUTION

      R=8.314472 //Gas Constant [J/mol*K] or [C*Volt/mol K]
      F=96485.34 // Faraday's Constant [J/mol]

      wangular=2*Pi*frequency // Angular frequency
      Ch=10^(-w[17]) // [mol/cm^3] Protons concentration in the bulk
      g=F/(R*w[16]) // Gama=F/(RT)


      a1=w[1]*(1-w[0])*g*w[6]   // [V^-1]
      a4=w[2]*w[0]*g*(w[5]-w[6])   // [V^-1]
      a7=w[3]*w[0]*g*(w[5]-w[6])   // [V^-1]

      b1=w[6]*w[1]*g*w[11]  // [cm^-1]

      K01=w[7]*exp(-w[6]*w[1]*g*(w[18]+w[20]*w[17]))   // Standard rate constant reaction 1
      K04=w[8]*exp((w[5]-w[6])*w[2]*g*(w[18]+w[20]*w[17]))   //Standard rate constant reaction 4

      Sp=(-1/b1)*ln((w[9]/K01)*10^(-w[4]*w[17]))-(a7-a1)*w[14]/b1       // Steady-state thickness [cm]


      k1=K01*exp(a1*w[14]-b1*Sp)
      k4=K04*exp(a4*w[14])
      k7=w[9]*exp(a7*w[14])


      IU=F*w[6]*a1*k1*(k4/k1)
      IL=-F*w[6]*b1*k1*(k4/k1)
      IM=F*w[6]*k1

      AA=w[10]*(k1*a1-k7*a7*Ch^w[4])
      BB=w[10]*(k1*b1)

      DD=BB*w[13]
      EE=wangular*w[13]*BB*w[12]+wangular+wangular*w[13]*IU
      FF=BB+IL*AA*w[13]+BB*IU*w[13]-wangular^2*w[12]*w[13]+IM*AA*w[13]
      GG=wangular*w[13]

      Zim=(GG*FF-EE*DD)/(FF^2+EE^2)

      return Zim

End
```

APPENDIX 3.c

OPTIMIZATION CODE FOR p-TYPE SEMICONDUCTION CODE FOR IGOR © DATA FITTING SOFTWARE


```
#pragma rtGlobals=1        // Use modern global access method.

Function ZrealAllinc(w,frequency) : FitFunc
      Wave w
      Variable frequency
      Variable g,a1,a2,a3,a4,a5,a7,b1,b2,b3,Sp,k1,k2,k3,k4,k5,k7,IU,IL,IM,Zt,Zre,Zim,
               wangular,Ch,F,R,K01,k02,k03,K04,AA,BB,DD,EE,FF,GG,PP,TT,SS


      //CurveFitDialog/ These comments were created by the Curve Fitting dialog. Altering them will
      //CurveFitDialog/ make the function less convenient to work with in the Curve Fitting dialog.
      //CurveFitDialog/ Equation:
      //CurveFitDialog/ f(frequency) = COMPLICATED
      //CurveFitDialog/ End of Equation
      //CurveFitDialog/ Independent Variables 1
      //CurveFitDialog/ frequency
      //CurveFitDialog/ Coefficients 27
      //CurveFitDialog/ w[0] = alpha
      //CurveFitDialog/ w[1] = alpha1
      //CurveFitDialog/ w[2] = alpha2
      //CurveFitDialog/ w[3] = alpha3
      //CurveFitDialog/ w[4] = alpha4
      //CurveFitDialog/ w[5] = alpha5
      //CurveFitDialog/ w[6] = alpha7
      //CurveFitDialog/ w[7] = n
      //CurveFitDialog/ w[8] = d
      //CurveFitDialog/ w[9] = chi
      //CurveFitDialog/ w[10] = k1oo
      //CurveFitDialog/ w[11] = k2oo
      //CurveFitDialog/ w[12] = k3oo
      //CurveFitDialog/ w[13] = k4oo
      //CurveFitDialog/ w[14] = k7o
      //CurveFitDialog/ w[15] = omega
      //CurveFitDialog/ w[16] = epsilon
      //CurveFitDialog/ w[17] = Cdl
      //CurveFitDialog/ w[18] = Rct
      //CurveFitDialog/ w[19] = V
      //CurveFitDialog/ w[20] = I
      //CurveFitDialog/ w[21] = T
      //CurveFitDialog/ w[22] = pH
      //CurveFitDialog/ w[23] = phio
      //CurveFitDialog/ w[24] = Rs
      //CurveFitDialog/ w[25] = bet
      //CurveFitDialog/ w[26] = k5o


// This optimization program is for a n-p-type monolayer film when
//metal and oxygen vacancies and metal interstitials are the main charge carriers.

//                  |                                  |
//              x'   k1                                |
//        M  +Vm-----> Mi   + xe'                       k4        d+
//                  |                              Mm ----------> M  + (d-x)e'
//                  |                                x+      k5   d+
//                 k2    x+                          Mi ----------> M  + (d-x)e'
//             M ------> Mi   + xe'                ..          k6            +
//                  |                          Vo + H2O ---|--> Oo + 2H
//                 k3                  ..                    |
//        M ---|--> Mm +(x/2)Vo + xe                         |
```

```
//                  |                                  |
//                  |                                + k7    d+
//                  |                  MO(x/2) + xH ---|--> M  + (x/2) H2O + (d-x)e'
//                  |                                  |
//                X=0                                X=Sp

//  Equivalent circuit used in this optimization procedure
//          _____
//         |     |            |
//       ----|  Zf |-----------|    |
//       |   |_____|         |    |
//       |                   |    |
//       |       |     |     |    |
//    -------------| Cdl |-------|----|----Rs---
//       |       |     |     |    |
//       |                   |    |
//       |---------Rct---------|    |
//                             |
//                             |
//  BARRIER LAYER        |       SOLUTION
```

```
R=8.314472 //Gas Constant [J/mol*K] or [C*Volt/mol K]
F=96485.34 // Faraday's Constant [J/mol]

wangular=2*Pi*frequency // Angular frequency
Ch=10^(-w[22]) // [mol/cm^3] Protons concentration in the bulk
g=F/(R*w[21]) // Gama=F/(RT)


a1=w[1]*(1-w[0])*g*w[9]   // [V^-1]
a4=w[4]*w[0]*g*(w[8]-w[9])   // [V^-1]
a7=w[3]*w[0]*g*(w[8]-w[9])   // [V^-1]
a2=w[2]*(1-w[0])*g*w[9]   // [V^-1]
a3=w[3]*(1-w[0])*g*w[9]   // [V^-1]
a5=w[5]*w[0]*g*(w[8]-w[9])   // [V^-1]

b1=w[9]*w[1]*g*w[16]  // [cm^-1]
b2=w[9]*w[2]*g*w[16]  // [cm^-1]
b3=w[9]*w[3]*g*w[16]  // [cm^-1]

K01=w[10]*exp(-w[9]*w[1]*g*(w[23]+w[25]*w[22]))   // Standard rate constant reaction 1
K04=w[13]*exp((w[8]-w[9])*w[4]*g*(w[23]+w[25]*w[22]))   //Standard rate constant reaction 4
K02=w[11]*exp(-w[2]*w[9]*g*(w[23]+w[25]*w[22]))   // Standard rate constant reaction 2
K03=w[12]*exp(-w[3]*w[9]*g*(w[23]+w[25]*w[22]))   //Standard rate constant reaction 3

Sp=(-1/b1)*ln((w[14]/K01)*10^(-w[7]*w[22]))-(a7-a1)*w[19]/b1+
+(-1/b3)*ln((w[14]/K03)*10^(-w[7]*w[22]))-(a7-a3)*w[19]/b3       // Steady-state thickness [cm]


k1=K01*exp(a1*w[19]-b1*Sp)
k4=K04*exp(a4*w[19])
k7=w[14]*exp(a7*w[19])
k2=K02*exp(a2*w[19]-b2*Sp)
k3=K03*exp(a3*w[19]-b3*Sp)
k5=w[26]*exp(a5*w[19])

IU=F*(w[9]*a1*k1*(k4/k1)+w[9]*k2*a2+w[9]*k3*a3)
IL=-F*(w[9]*b1*k1*(k4/k1)+w[9]*k2*b2+w[9]*k3*b3)
IM=F*w[9]*k1
```

```
	AA=w[15]*(k3*a3-k7*a7*Ch^w[7])
	BB=w[15]*(k3*b3)
	SS=IM*k4*(a4-a1)
	PP=BB*IU*k1+IL*AA*k1+BB*SS+k4*b1*AA*IM
	TT=k1*IU+SS

	DD=BB*k1*w[18]
	EE=wangular*w[17]*BB*w[18]*k1+wangular*k1+wangular*w[18]*TT
	FF=BB*k1+w[18]*PP-wangular^2*w[18]*w[17]*k1
	GG=wangular*w[18]*k1

	Zre=w[19]+(FF*DD+EE*GG)/(FF^2+EE^2)

	return Zre


End


Function ZimagAllinc(w,frequency) : FitFunc
	Wave w
	Variable frequency
	Variable g,a1,a2,a3,a4,a5,a7,b1,b2,b3,Sp,k1,k2,k3,k4,k5,k7,IU,IL,IM,Zt,Zre,Zim,
		wangular,Ch,F,R,K01,k02,k03,K04,AA,BB,DD,EE,FF,GG,PP,TT,SS

	//CurveFitDialog/ These comments were created by the Curve Fitting dialog. Altering them will
	//CurveFitDialog/ make the function less convenient to work with in the Curve Fitting dialog.
	//CurveFitDialog/ Equation:
	//CurveFitDialog/ f(frequency) = COMPLICATED
	//CurveFitDialog/ End of Equation
	//CurveFitDialog/ Independent Variables 1
	//CurveFitDialog/ frequency
	//CurveFitDialog/ Coefficients 27
	//CurveFitDialog/ w[0] = alpha
	//CurveFitDialog/ w[1] = alpha1
	//CurveFitDialog/ w[2] = alpha2
	//CurveFitDialog/ w[3] = alpha3
	//CurveFitDialog/ w[4] = alpha4
	//CurveFitDialog/ w[5] = alpha5
	//CurveFitDialog/ w[6] = alpha7
	//CurveFitDialog/ w[7] = n
	//CurveFitDialog/ w[8] = d
	//CurveFitDialog/ w[9] = chi
	//CurveFitDialog/ w[10] = k1oo
	//CurveFitDialog/ w[11] = k2oo
	//CurveFitDialog/ w[12] = k3oo
	//CurveFitDialog/ w[13] = k4oo
	//CurveFitDialog/ w[14] = k7o
	//CurveFitDialog/ w[15] = omega
	//CurveFitDialog/ w[16] = epsilon
	//CurveFitDialog/ w[17] = Cdl
	//CurveFitDialog/ w[18] = Rct
	//CurveFitDialog/ w[19] = V
	//CurveFitDialog/ w[20] = I
	//CurveFitDialog/ w[21] = T
	//CurveFitDialog/ w[22] = pH
	//CurveFitDialog/ w[23] = phio
	//CurveFitDialog/ w[24] = Rs
```

```
//CurveFitDialog/ w[25] = bet
//CurveFitDialog/ w[26] = k5o


// This optimization program is for a n-p-type monolayer film when
//metal and oxygen vacancies and metal interstitials are the main charge carriers.

//                    |                                  |
//              x'   k1                                  |
//        M  +Vm-----> Mi   + xe'                        k4        d+
//                    |                              Mm ----------> M  + (d-x)e'
//                    |                               x+      k5   d+
//                   k2     x+                        Mi ----------> M  + (d-x)e'
//              M ------> Mi   + xe'                   ..          k6             +
//                    |                          Vo + H2O ---|--> Oo + 2H
//                   k3                  ..                     |
//        M ---|--> Mm +(x/2)Vo + xe                            |
//                    |                                        |
//                    |                                    +  k7     d+
//                    |                      MO(x/2) + xH ---|--> M  + (x/2) H2O + (d-x)e'
//                    |                                        |
//                  X=0                                      X=Sp


//  Equivalent circuit used in this optimization procedure
//           ____
//          |    |              |
//       ---|  Zf  |-----------|    |
//       |  |____ |          |    |
//       |                   |    |
//       |       |     |     |    |
//    ------------| Cdl |-------|----|----Rs---
//       |       |     |     |    |
//       |                   |    |
//       |---------Rct---------|    |
//                             |
//                             |
//  BARRIER LAYER       |       SOLUTION

    R=8.314472 //Gas Constant [J/mol*K] or [C*Volt/mol K]
    F=96485.34 // Faraday's Constant [J/mol]

    wangular=2*Pi*frequency // Angular frequency
    Ch=10^(-w[22]) // [mol/cm^3] Protons concentration in the bulk
    g=F/(R*w[21]) // Gama=F/(RT)


    a1=w[1]*(1-w[0])*g*w[9]   // [V^-1]
    a4=w[4]*w[0]*g*(w[8]-w[9])   // [V^-1]
    a7=w[3]*w[0]*g*(w[8]-w[9])   // [V^-1]
    a2=w[2]*(1-w[0])*g*w[9]   // [V^-1]
    a3=w[3]*(1-w[0])*g*w[9]   // [V^-1]
    a5=w[5]*w[0]*g*(w[8]-w[9])   // [V^-1]

    b1=w[9]*w[1]*g*w[16]  // [cm^-1]
    b2=w[9]*w[2]*g*w[16]  // [cm^-1]
    b3=w[9]*w[3]*g*w[16]  // [cm^-1]

    K01=w[10]*exp(-w[9]*w[1]*g*(w[23]+w[25]*w[22]))   // Standard rate constant reaction 1
```

```
K04=w[13]*exp((w[8]-w[9])*w[4]*g*(w[23]+w[25]*w[22]))   //Standard rate constant reaction 4
K02=w[11]*exp(-w[2]*w[9]*g*(w[23]+w[25]*w[22]))   // Standard rate constant reaction 2
K03=w[12]*exp(-w[3]*w[9]*g*(w[23]+w[25]*w[22]))   //Standard rate constant reaction 3

Sp=(-1/b1)*ln((w[14]/K01)*10^(-w[7]*w[22]))-(a7-a1)*w[19]/b1+
+(-1/b3)*ln((w[14]/K03)*10^(-w[7]*w[22]))-(a7-a3)*w[19]/b3       // Steady-state thickness [cm]


k1=K01*exp(a1*w[19]-b1*Sp)
k4=K04*exp(a4*w[19])
k7=w[14]*exp(a7*w[19])
k2=K02*exp(a2*w[19]-b2*Sp)
k3=K03*exp(a3*w[19]-b3*Sp)
k5=w[26]*exp(a5*w[19])

IU=F*(w[9]*a1*k1*(k4/k1)+w[9]*k2*a2+w[9]*k3*a3)
IL=-F*(w[9]*b1*k1*(k4/k1)+w[9]*k2*b2+w[9]*k3*b3)
IM=F*w[9]*k1

AA=w[15]*(k3*a3-k7*a7*Ch^w[7])
BB=w[15]*(k3*b3)
SS=IM*k4*(a4-a1)
PP=BB*IU*k1+IL*AA*k1+BB*SS+k4*b1*AA*IM
TT=k1*IU+SS

DD=BB*k1*w[18]
EE=wangular*w[17]*BB*w[18]*k1+wangular*k1+wangular*w[18]*TT
FF=BB*k1+w[18]*PP-wangular^2*w[18]*w[17]*k1
GG=wangular*w[18]*k1


Zim=(GG*FF-EE*DD)/(FF^2+EE^2)

return Zim

End
```